THE GEOLOGICAL SOCIETY OF AMERICA®

Tectonic evolution of the Beishan orogen in central Asia: Subduction, accretion, and continent-continent collision during the closure of the Paleo-Asian Ocean

Jie Li[1,2,3], Chen Wu[2,†], Xuanhua Chen[3], Andrew V. Zuza[4], Peter J. Haproff[5], An Yin[6], and Zhaogang Shao[3]
[1]*School of Earth Sciences and Resources, China University of Geosciences (Beijing), Beijing 100083, China*
[2]*State Key Laboratory of Tibetan Plateau Earth System and Resources Environment, Institute of Tibetan Plateau Research, Chinese Academy of Sciences, Beijing 100101, China*
[3]*SinoProbe Center, Chinese Academy of Geological Sciences, Beijing 100037, China*
[4]*Nevada Bureau of Mines and Geology, University of Nevada, Reno, Nevada 89557, USA*
[5]*Department of Earth and Ocean Sciences, University of North Carolina, Wilmington, North Carolina 28403, USA*
[6]*Department of Earth and Space Sciences, University of California, Los Angeles, California 90095-156702, USA*

ABSTRACT

The Beishan orogen is part of the Neoproterozoic to early Mesozoic Central Asian Orogenic System in central Asia that exposes ophiolitic complexes, passive-margin strata, arc assemblages, and Precambrian basement rocks. To better constrain the tectonic evolution of the Beishan orogen, we conducted field mapping, U-Pb zircon dating, whole-rock geochemical analysis, and Sr-Nd isotopic analysis. The new results, when interpreted in the context of the known geological setting, show that the Beishan region had experienced five phases of arc magmatism at ca. 1450–1395 Ma, ca. 1071–867 Ma, ca. 542–395 Ma, ca. 468–212 Ma, and ca. 307–212 Ma. In order to explain the geological, geochemical, and geochronological data from the Beishan region, we present a tectonic model that involves the following five phases of deformation: (1) Proterozoic rifting that separated the North Beishan block from the Greater North China craton that led to the opening of the Beishan Ocean, (2) early Paleozoic north-dipping subduction (ca. 530–430 Ma) of the Beishan oceanic plate associated with back-arc extension followed by collision between the North and South Beishan microcontinental blocks, (3) northward slab rollback of the south-dipping subducting Paleo-Asian oceanic plate at ca. 450–440 Ma along the northern margin of the North Beishan block that led to the formation of a northward-younging extensional continental arc (ca. 470–280 Ma) associated with bimodal igneous activity, which indicates that the westward extension of the Solonker suture is located north of the Hongshishan-Pengboshan tectonic zone, (4) Late Carboniferous opening and Permian north-dipping subduction of the Liuyuan Ocean in the southern Beishan orogen, and (5) Mesozoic-Cenozoic intracontinental deformation induced by the final closure of the Paleo-Asian Ocean system in the north and the Tethyan Ocean system in the south.

1. INTRODUCTION

The Central Asian Orogenic System (Briggs et al., 2007, 2009; Zuza and Yin, 2017), also known as the Altai orogenic system (Şengör, 1984), the Central Asia Fold Belt (Zonenshain et al., 1990), or the Central Asian Orogenic Belt (Şengör, 1984; Jahn et al., 2000), is the largest Phanerozoic accretionary orogen in the world. Determining its tectonic history is key to better understanding the processes that govern continental deformation and crustal growth (Fig. 1) (e.g., Şengör et al., 1993; Şengör and Natal'in, 1996; Yin and Nie, 1996; Heubeck, 2001; Windley et al., 2007; Xiao et al., 2009b; Kröner et al., 2014; Wu et al., 2016a, 2016b; Chen et al., 2022). The tectonic assembly of central Asia occurred over ~800 m.y. from the Neoproterozoic to the Mesozoic through long-term ocean-closure event(s) and terrane/block collisions (e.g., Zonenshain et al., 1990; Şengör et al., 1993; Khain et al., 2002; Kröner et al., 2007; Windley et al., 2007; Xiao et al., 2009a, 2009b; Zuza and Yin, 2017; Chen et al., 2022). The construction of the Central Asian Orogenic System was associated with multiple phases and modes of deformation, metamorphism, magmatism, and basin formation associated with oceanic subduction, accretion of oceanic materials onto continental margins, continental-arc collision, and terminal continent-continent collision (Xiao et al., 1992; Şengör et al., 1993, 2018; Şengör and Natal'in, 1996; Hsü and Chen, 1999; Khain et al., 2002; Li, 2004; Charvet et al., 2007; Windley et al., 2007; Xiao et al., 2010a, 2013, 2014, 2018; Kröner et al., 2014; Yakubchuk, 2017; Zuza and Yin, 2017; Windley and Xiao, 2018; Huang et al., 2020; Xiao et al., 2020).

Despite its importance in understanding the geologic history of Asia, exactly where and when the Paleo-Asian Ocean domain was sutured against the Tarim-North China cratonal system in the south remains highly uncertain, especially in the south-central Central Asian Orogenic System (Şengör et al., 1993; Hsü and Chen, 1999; Windley et al., 2007; Xiao et al., 2009a, 2009b, 2010b, 2014; Wilhem et al., 2012; Eizenhöfer et al., 2014). The southern extent of the Central Asian Orogenic System and Paleo-Asian Ocean is relatively well constrained in the east, along the Solonker suture zone at the northern margin of the North China craton (e.g., Xiao et al., 2003; Eizenhöfer et al., 2014; Zhang et al., 2020a; Zhao et al., 2021), but how this suture zone projects to the west toward Tarim is contentious. One model postulates that this suture continues to the southern Beishan along the Liuyuan suture (Xiao et al., 2010b; Mao et al., 2012b;

Chen Wu https://orcid.org/0000-0003-0647-3530
†Corresponding author: wuchen@itpcas.ac.cn; wuchenlovegeology@gmail.com.

GSA Bulletin;
published online 6 July 2022
https://doi.org/10.1130/B36451.1; 17 figures; 2 tables; 1 supplemental file.

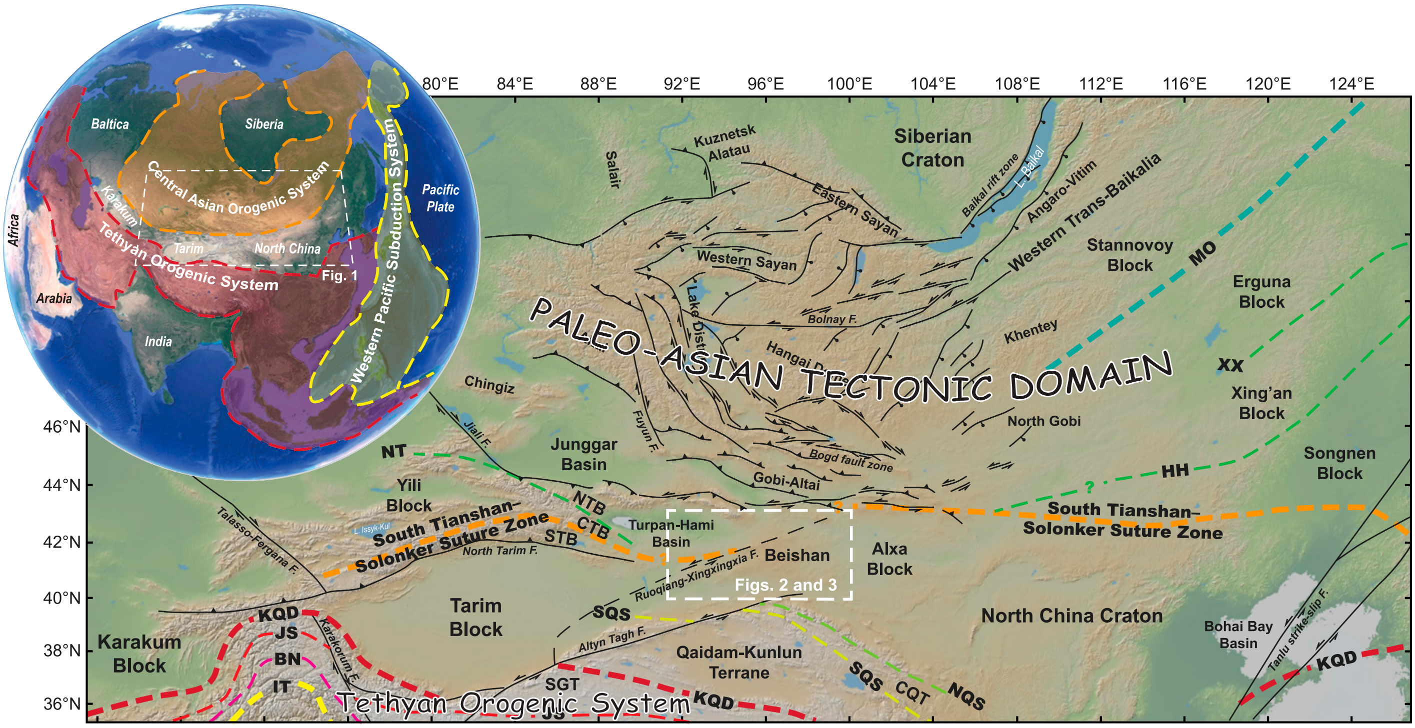

Figure 1. Tectonic division map of the Tethyan and Central Asian Orogenic System modified after Yin and Harrison (2000), Yin (2010), and Şengör et al. (1993). The top left inset shows the location of Figure 1 in the context of the Asian continent. The locations of Figures 2 and 3 are shown. IT—Indus-Tsangpo suture; BN—Bangong-Nujiang suture; JS—Jinsha suture; KQD—Kunlun-Qinling-Dabie suture; SQS—South Qilian suture; NQS—North Qilian suture; NT—North Tianshan suture; HH—Heihe-Hegenshan suture; XX—Xinlin-Xiguitu suture; MO—Mongol-Okhotsk suture; SGT—Songpan-Ganzi terrane; CQT—Central Qilian terrane; STB—South Tianshan belt; CTB—Middle Tianshan block; NTB—North Tianshan belt; F.—fault.

Guo et al., 2017; Zheng et al., 2020), whereas another model suggests this tectonic boundary projects to the northern margin of the Beishan region along the Hongshishan suture (Fig. 2) (Liu and Wang, 1995; Saktura et al., 2017; He et al., 2018). The two competing models make specific predictions on the spatial and temporal distribution and evolution of arc magmatic belts and the location of the major suture zone(s) across the Beishan region.

To test the above models for the Central Asian Orogenic System evolution, we conducted an integrated field, geochemical, and geochronologic investigation and a synthesis of existing work across the Beishan orogen. The main purpose of this study is to determine the distribution of arc magmatism in space and time and the nature of suture zones and their relationships to the tectonic evolution of the Central Asian Orogenic System.

2. REGIONAL GEOLOGY

Interpreting the newly collected geochronological and geochemical data from this study depends on the current understanding of the geologic framework and geologic history of the Beishan region, which is briefly outlined below. The Beishan region exposes east-trending mountain ranges that reach elevations of 2–2.5 km (Figs. 2 and 3). The region is bounded by the Mesozoic left-slip Xingxingxia fault to the west, the southern Mongolian collage system to the north, the Dunhuang block to the south, and the Cenozoic Ruoshui fault and Alxa block to the east (Figs. 2 and 3) (Zuo et al., 1991; Yue and Liou, 1999; Wang et al., 2010; Xiao et al., 2010b; Zuo and Li, 2011). Mesozoic intracontinental shortening, expressed as a mixed-mode of thrusting and strike-slip faulting (Zheng et al., 1996; Zuo et al., 2011; Zhang and Cunningham, 2012), may have deformed the

169—Guo et al., 2020; 170—Gao et al., 2020; 171—Fu et al., 2020b; 172—Duan et al., 2020; 173—Cheng et al., 2020; 174—Chen et al., 2020c; 175—Tian et al., 2020c; 176—Zhu et al., 2019; 177—Zhao et al., 2019a; 178—Zhao et al., 2019b; 179—Yang et al., 2019b; 180—Li et al., 2019b; 181—Guan et al., 2019; 182—Chen et al., 2019; 183—Yu et al., 2018; 184—Xu et al., 2018a; 185—Xu et al., 2018b; 186—Xie et al., 2018a; 187—Xie et al., 2018b; 188—Liu and Zhu, 2018; 189—Gao et al., 2018a; 190—Gao et al., 2018b; 191—Cheng et al., 2018; 192—Yi et al., 2017; 193—Yang et al., 2017; 194—Wang et al., 2017b; 195—Qi et al., 2017; 196—Liang et al., 2017; 197—Chen et al., 2017c; 198—Ding et al., 2017; 199—Yang et al., 2016b; 200—Zhu et al., 2015; 201—Xie et al., 2015; 202—Niu et al., 2014; 203—Qu et al., 2013; 204—Niu et al., 2013; 205—Hui et al., 2013; 206—Chen et al., 2013; 207—Hou et al., 2013; 208—Zhang et al., 2012d; 209—Yan et al., 2012; 210—Wu et al., 2012; 211—Li, et al., 2012c; 212—Yang et al., 2010b; 213—Xiao et al., 2010c; 214—Wang et al., 2009a; 215—Wang et al., 2009b; 216—Liu et al., 2006; 217—Zhang, 2014; 218—This study. DQ F.—Daquan fault; XXX F.—Xingxingxia fault; GBQ-HLY F.—Gubaoquan-Hongliuyuan fault; LBQ-YMJ DSZ—Lebaquan-Yemajing ductile shear zone; SBJ DSZ—Shibanjing ductile shear zone; GLJ-SGJ DSZ—Gonglujing-Sangejing ductile shear zone.

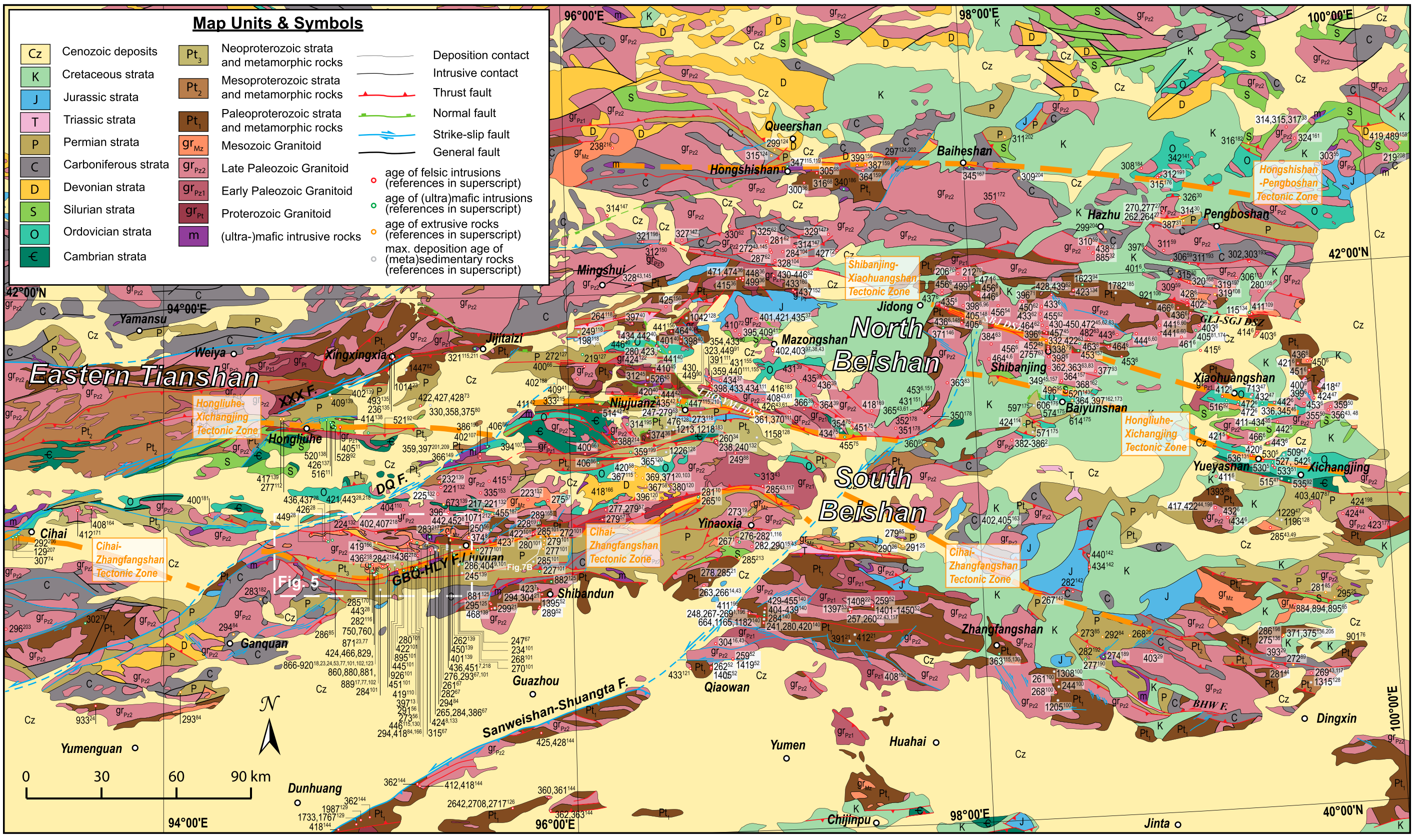

Figure 2. Overview geologic map of the Beishan orogen of central Asia showing age constraints of magmatism and sedimentary deposition. The geology was compiled from Gansu BGMR (1989), Hsü and Chen (1999), and our geologic interpretation. The white box indicates the location of the composite map in Figure 5, and the location of Figure 7B is marked with white arrow. Data are from: 1—Zheng et al., 2020; 2—Zhao et al., 2020c; 3—Chen et al., 2017a; 4—Xiu et al., 2018; 5—Hu et al., 2015; 6—Li et al., 2020a; 7—Zhao et al., 2007; 8—Mao et al., 2012a; 9—Mao et al., 2012b; 10—Zheng et al., 2014; 11—Zhang and Guo, 2008; 12—Li et al., 2009; 13—Li et al., 2011; 14—Zhang et al., 2010; 15—Zhang et al., 2011a; 16—Feng et al., 2012; 17—Qu et al., 2011; 18—Liu et al., 2011; 19—Zheng et al., 2016a; 20—Guo et al., 2014; 21—Song et al., 2016; 22—He et al., 2015; 23—Liu et al., 2015; 24—Yuan et al., 2015; 25—Xu et al., 2018c; 26—Xu et al., 2019a; 27—Li et al., 2020b; 28—Li et al., 2015; 29—Xu et al., 2019b; 30—Ren et al., 2019a; 31—Ren et al., 2019b; 32—Niu et al., 2019; 33—Li et al., 2019a; 34—Bu et al., 2019; 35—Zheng et al., 2019; 36—Song et al., 2013a; 37—Zheng et al., 2018b; 38—Zheng et al., 2012; 39—Li, 2013; 40—Song et al., 2015; 41—Wang et al., 2018b; 42—Tian et al., 2014; 43—Zhang, 2013; 44—Ding et al., 2015; 45—Song et al., 2013b; 46—Zheng et al., 2013; 47—Ao et al., 2016; 48—Zhang et al., 2012a; 49—Zhang et al., 2012b; 50—Yang et al., 2013; 51—Ao et al., 2012; 52—Yuan et al., 2019; 53—Zong et al., 2017; 54—Zhuan et al., 2018; 55—Zhao et al., 2018; 56—Zhang et al., 2011b; 57—Li et al., 2013; 58—Li et al., 2011b; 59—Li et al., 2018a; 60—Dong et al., 2018; 61—Zhang et al., 2018a; 62—Y. Yuan et al., 2018; 63—Wang et al., 2014a; 64—Wang et al., 2021b; 65—Wang et al., 2021e; 66—Tian et al., 2021; 67—Niu et al., 2021b; 68—Yang et al., 2020; 69—Sun et al., 2020a; 70—Li et al., 2020c; 71—Chen et al., 2020a; 72—Bai et al., 2020; 73—Yu et al., 2020; 74—Wang et al., 2020b; 75—Wang et al., 2020a; 76—Wang et al., 2021a; 77—Soldner et al., 2020a; 78—Kang et al., 2020; 79—Fu et al., 2020a; 80—Chen et al., 2020b; 81—Liu et al., 2019; 82—Zhou et al., 2018; 83—Wang et al., 2018c; 84—Niu et al., 2018a; 85—Niu et al., 2018b; 86—Ma et al., 2018; 87—Li et al., 2018b; 88—Guo et al., 2018; 89—An, 2018; 90—Wang et al., 2018a; 91—Wang et al., 2018d; 92—Shi et al., 2018; 93—Zhao et al., 2017a; 94—Zhang et al., 2017b; 95—Sun et al., 2017; 96—Pan et al., 2017a; 97—Pan et al., 2017b; 98—Cheng et al., 2017; 99—C. Chen et al., 2017b; 100—Zheng et al., 2018a; 101—Wang et al., 2017a; 102—Saktura et al., 2017; 103—Guo et al., 2017; 104—Zheng et al., 2016b; 105—Zhao et al., 2016; 106—Yang et al., 2016a; 107—Wang et al., 2016; 108—Jia et al., 2016; 109—Gao et al., 2016; 110—Zhu et al., 2016; 111—Yu et al., 2016; 112—Chen et al., 2016; 113—Zhao et al., 2015; 114—Yang et al., 2015; 115—Wang, 2015; 116—Zhang et al., 2015a; 117—Zhang et al., 2015b; 118—Tian et al., 2015; 119—Wang et al., 2014b; 120—Liang et al., 2014; 121—He et al., 2014; 122—Song et al., 2014; 123—Ye et al., 2013; 124—Lu et al., 2013; 125—Jiang et al., 2013; 126—Zong et al., 2013; 127—Tian et al., 2013; 128—Song et al., 2013c; 129—He et al., 2013; 130—Yu et al., 2012; 131—Hou et al., 2012; 132—Li et al., 2012a; 133—Mao et al., 2010; 134—Liu et al., 2010; 135—Wang et al., 2010; 136—Shan et al., 2013; 137—Yu et al., 2006; 138—Cleven et al., 2015a; 139—Cleven et al., 2018; 140—Zheng et al., 2021; 141—Zhang et al., 2020b; 142—Jin et al., 2020; 143—Tian et al., 2020a; 144—Zhao et al., 2017b; 145—Zhang et al., 2017a; 146—Zhang et al., 2012c; 147—Zhang, 2017; 148—Zhang et al., 2021; 149—Yu et al., 2021; 150—Yang et al., 2021b; 151—Wang et al., 2021c; 152—Wang et al., 2021d; 153—Sun et al., 2021; 154—Meng et al., 2021; 155—Lv et al., 2021; 156—Huang et al., 2021; 157—Zhao et al., 2020a; 158—Zhang et al., 2020c; 159—Yan et al., 2020; 160—Wang et al., 2020d; 161—Tian et al., 2020d; 162—Tian et al., 2020b; 163—Tao et al., 2022; 164—Sun et al., 2020c; 165—Sun et al., 2020b; 166—Niu et al., 2020a; 167—Niu et al., 2020b; 168—Hao et al., 2020;

configurations of a Paleozoic orogen as part of the south-central Central Asian Orogenic System that includes the Beishan area (Figs. 2 and 3) (Şengör et al., 1993; Yin and Harrison, 2000; Windley et al., 2007; Xiao et al., 2010b; Zuza and Yin, 2017).

The Beishan region exposes Neoproterozoic–Phanerozoic magmatic arc rocks, (ultra-)mafic intrusions, and ophiolitic mélange belts (Fig. 2) (Zuo et al., 1991; Liu and Wang, 1995; Xiao et al., 2010b; Ao et al., 2012; Li et al., 2012a; Tian et al., 2014; Cleven et al., 2015a, 2015b; He et al., 2018). The main Paleozoic orogenic event was followed by Mesozoic-Cenozoic intracontinental deformation due to the far-field effects of collisional tectonic processes responsible for the closure of the Meso- and Neo-Tethys oceans to the south (Zheng et al., 1996; Yin and Harrison, 2000; Guo et al., 2008; Yin, 2010; Zhang and Cunningham, 2012; Cunningham, 2013, 2017; Gillespie et al., 2017; Yang et al., 2021a; Yun et al., 2021). Understanding the Paleozoic tectonic evolution of the Beishan orogen not only provides a new constraint for the evolution of the Central Asian Orogenic System but also provides strain markers for better quantifying the magnitude of Mesozoic-Cenozoic tectonic deformation (e.g., Yin and Nie, 1996).

2.1. Paleozoic Tectonics

The Paleozoic Beishan orogen records the opening and subsequent closure of several oceans of the Paleo-Asian domain as multiple terranes collided with the northern margin of the Tarim-North China cratons, resembling that of the Mesozoic–Cenozoic subduction-accretion system in the western Pacific Ocean tectonic domain (Hsü and Chen, 1999; Xiao et al., 2010b; Song et al., 2015). Paleozoic Beishan orogenesis involved the development of four tectonic zones (Figs. 2 and 3) that feature ophiolite blocks and (ultra-)mafic rocks, including the: (1) Hongshishan-Baiheshan-Pengboshan; (2) Shibanjing-Xiaohuangshan; (3) Hongliuhe-Niujuanzi-Baiyunshan-Yueyashan-Xichangjing; and (4) Cihai-Liuyuan-Zhangfangshan tectonic zones from north to south (Zuo et al., 1991; Liu and Wang, 1995; Wei et al., 2004; Ao et al., 2010, 2012, 2016; Xiao et al., 2010b; Yang et al., 2010a; Zuo and Li, 2011; Wang et al., 2017a; He et al., 2018; Wang et al., 2018a). These four tectonic zones separate the following tectonic units of the Beishan orogen from north to south: the Queershan arc, Heiyingshan-Hanshan arc, Mazongshan arc, Shuangyingshan-Huaniushan arc, and Shibanshan arc from north to south, respectively (Fig. 2) (Xiao et al., 2010b). These tectonic units variably contain flysch, arc-type assemblages, ophiolites, and low- to high-grade metamorphic rocks (Gansu BGMR, 1989, 1996). Each of the four tectonic zones exposed in the Beishan contains at least one block or tectonic slice of (ultra-)mafic or ophiolitic material (Fig. 2) generated and emplaced during Cambrian, Silurian–Devonian, and Carboniferous–Permian oceanic subduction or rifting (e.g., Gansu BGMR, 1989, 1996; Cleven et al., 2015a, 2015b; Shi et al., 2018; Zhang et al., 2020b).

Several important first-order questions regarding the formation of the Beishan orogen remain controversial. These questions include: (1) How many and which type of magmatic arcs (i.e., oceanic, continental, or transitional) were involved in orogeny (e.g., Zuo et al., 1991; Liu and Wang, 1995; Xiao et al., 2010b; Liu et al., 2011; Zheng et al., 2012, 2014, 2016a, 2019, 2021; Saktura et al., 2017; He et al., 2018)?

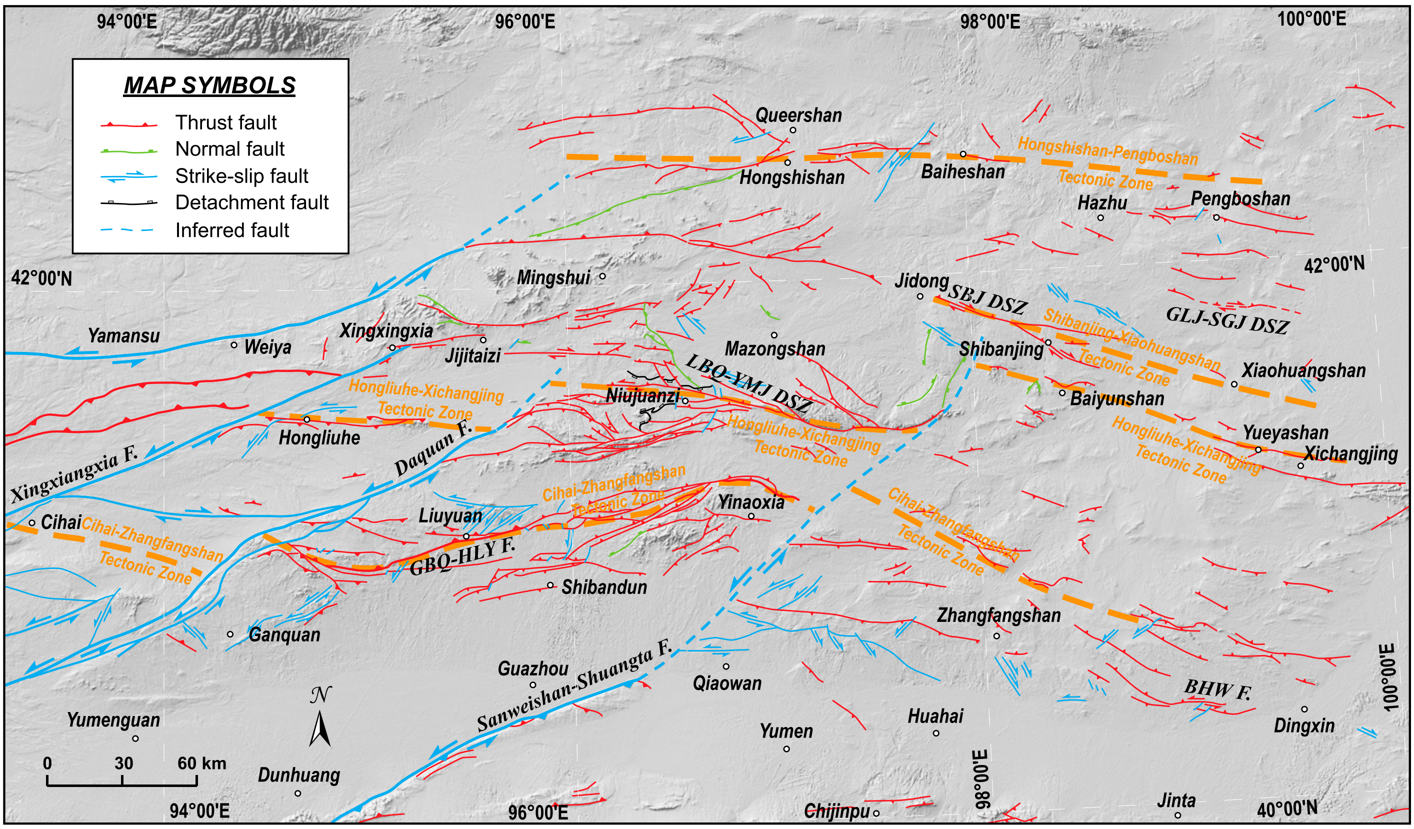

Figure 3. Regional tectonic map of the Beishan orogen of central Asia from Gansu BGMR (1989), Guo et al. (2008), Xiao et al. (2010b), Yang et al. (2021a), Yun et al. (2021), and our structural interpretation. BHW F.—Beihewan fault; GBQ-HLY F.—Gubaoquan-Hongliuyuan fault; LBQ-YMJ DSZ—Lebaquan-Yemajing ductile shear zone; SBJ DSZ—Shibanjing ductile shear zone; GLJ-SGJ DSZ—Gonglujing-Sangejing ductile shear zone.

(2) Was the subduction polarity north- and/or south-dipping (e.g., Xiao et al., 2010b; Song et al., 2015; Ao et al., 2016; Cleven et al., 2018; Zhang et al., 2018a; Li et al., 2020a; Wang et al., 2020a; Zheng et al., 2021)? (3) How many separate sutures are present and in which type of tectonic setting did they originate from (i.e., mature ocean or back-arc basin/rift) (e.g., Wei et al., 2004; Jiang et al., 2006, 2007; Zhang and Guo, 2008; Xiao et al., 2010b; Yang et al., 2010a; Ao et al., 2012; Hou et al., 2012; Mao et al., 2012b; Hu et al., 2015; Wang et al., 2018a; Niu et al., 2020a; Tian et al., 2020a; Niu et al., 2021a)? and (4) When and where did the final assembly of the Beishan orogen occur (i.e., Devonian or Permian; i.e., Liuyuan region, Niujuanzi tectonic zone, or further north) (e.g., Zuo et al.., 1991; Liu and Wang, 1995; Xiao et al., 2010b; Mao et al., 2012b; Wang et al., 2017; Zheng et al., 2020, 2021)?

2.1.1. Tectonic Models for the Development of the Beishan Orogen

Despite many uncertainties, previous studies have proposed the following general models for the tectonic evolution of the Beishan orogen. (1) At least four open oceans/rifts/back-arc basins existed from the Cambrian–Permian, evidenced by the presence of ophiolite or (ultra-)mafic rock fragments (Zuo et al., 1991; Xiao et al., 2010b; Yang et al., 2010a; Zheng et al., 2013; Cleven et al., 2015a; Shi et al., 2018). (2) Arc magmatism, subduction, and collision occurred from the Ordovician to Permian, evidenced by the presence of arc-related and syn-collisional plutons (Zhao et al., 2007; Li et al., 2009, 2011a, 2012a, 2013; Wang et al., 2009a; Mao et al., 2010, 2012a; Zhang et al., 2010, 2011a, 2012a, 2012b, 2017a, 2018a; Li et al., 2011a; Ao et al., 2012; Feng et al., 2012; Lu et al., 2013; Yang et al., 2013; Guo et al., 2014; Zheng et al., 2014, 2018b, 2019, 2020; Wang et al., 2014a; Song et al., 2015; Zhu et al., 2016; Li et al., 2020a). (3) High-pressure eclogite-facies metamorphism occurred in the Ordovician, evidenced by eclogite exposed in the southern Beishan with peak metamorphic ages ranging from ca. 467 Ma to ca. 452 Ma (Liu et al., 2011; Qu et al., 2011; Saktura et al., 2017; Soldner et al., 2020b). The Paleozoic Beishan orogen exposes high-pressure metamorphic rocks (e.g., Mei et al., 1999; Liu et al., 2011; Soldner et al., 2020b), Paleozoic arc-related granitoids and volcanic rocks, Paleozoic ophiolitic mélange materials, and late Paleozoic sedimentary rocks (Fig. 2) (e.g., Xiao et al., 2010b; Zheng et al., 2012, 2016a, 2019, 2020, 2021; Cleven et al., 2015a, 2015b; Niu et al., 2018a, 2018b, 2021b; Shi et al., 2018).

These models for the tectonic evolution of the Beishan orogen differ in the number of terranes/blocks involved, the basement upon which the arc(s) was formed, subduction polarity, and the timing of subduction and ocean closure (Fig. 4). These general models include (Fig. 4): (1) the accretionary terranes/blocks model of Xiao et al. (2010b), which requires several continental and island arcs to have developed above south- and north-dipping subduction zones since the Ordovician and a long-lived continental arc to have developed above the bidirectional Liuyuan subduction zone from the Ordovician to Permian (Fig. 4A); (2) closure of multiple oceans and accretion of island arcs at the end of the Silurian (Liu et al., 2011), which emphasizes the high-pressure metamorphism and emplacement along the Liuyuan Ocean suture (Fig. 4B); (3) the early Paleozoic closure of multiple oceans/back-arc basins and accretion of island arcs (Zuo et al., 1991), which emphasizes that the Shibanjing-Xiaohuangshan tectonic zone is the main suture between the Tarim plate and Mingshui-Hanshan microplate and more southerly tectonic zones represent back-arc extensional products (Fig. 4C); (4) the continent-continent collision model of He et al. (2018), which requires that the Beishan orogen contains comparable basement and the Hongshishan-Pengboshan tectonic zone developed as a south-dipping subduction zone since the Cambrian and generated the other tectonic zones (Fig. 4D); (5) the one terrane and two oceans model of Saktura et al. (2017), which emphasizes that high-pressure metamorphism is the result of the Liuyuan oceanic subduction and requires continuous subduction of the Paleo-Asian oceanic lithosphere between the Queershan and Mazongshan-Hanshan regions in the Ordovician–Permian (Fig. 4E); and (6) southward subduction of the Paleo-Asian oceanic lithosphere and subsequent completion of Wilson cycles (Fig. 4F) (Liu and Wang, 1995), which contrasts the continent-continent collision models shown in Figures 4D and 4E.

2.2. Mesozoic Tectonics of the Beishan Region

Due to limited investigations of the Mesozoic rocks exposed in the Beishan, the tectonic evolution of this period is not well constrained. The northeast-striking Xingxingxia fault, located north of the Altyn Tagh fault, separates the eastern Tianshan orogen in the west from the Beishan orogen in the east (Figs. 2 and 3) (Yue and Liou, 1999; Wang et al., 2010). Variable left-slip faulting along the Xingxingxia fault initiated at 240–235 Ma, which was coeval with the initiation of the Altyn Tagh fault determined from $^{40}Ar/^{39}Ar$ thermochronology (Wang et al., 2010). The estimated left-slip displacement along the Xingxingxia fault is ~30–35 km, which has been constrained by offset of the eastern Tianshan orogen (Wang et al., 2010). Stratigraphic and sedimentologic studies have led to interpretations that the Beishan experienced Jurassic north-south-oriented contraction (Zheng et al., 1996), possibly related to collision between Asia and a terrane separated from Gondwana (Yin and Harrison, 2000). Jurassic regional contraction affected much of the Beishan and surrounding area, including the Alxa Block, Gobi Altai area, Eastern Tianshan Range, Hexi Corridor, and Longshoushan (Zheng et al., 1996; Zuo et al., 2011; Zhang and Cunningham, 2012; Gillespie et al., 2017; Zhang et al., 2018b). This contraction was expressed by the development of extensive north-directed thrusts placing Proterozoic and Paleozoic rocks atop strongly folded and faulted Jurassic strata (Zheng et al., 1996; Zuo et al., 2011; Zhang and Cunningham, 2012; Tian et al., 2013, 2015, 2016). Although the minimum displacement of late Middle Jurassic intracontinental thrusting is estimated to be ~120–180 km by Zheng et al. (1996), we consider that the magnitude of shortening is still unconstrained because of the limited exposure of Jurassic strata and unclear contact relationships in the Beishan. Furthermore, our field observations of pre-Cretaceous and Cretaceous strata record subsequent Late Jurassic–Early Cretaceous extension event. Robust estimates of Mesozoic exhumation determined by Late Triassic–Early Jurassic apatite fission-track cooling ages from pre-Mesozoic strata and granitoids is relatively small at <4–5 km (Tian et al., 2016; Gillespie et al., 2017). The cause of the contractional deformation may be closures of the Tethyan oceans along the southern edge of Asia or Mongol-Okhotsk oceans to the north of the North China craton (Zheng et al., 1996; Gillespie et al., 2017).

2.3. Cenozoic Tectonics of the Beishan Region

The Beishan region has previously been identified as a stable Cenozoic crustal fragment due to its relative lack of seismicity, low mountain relief, and minimal tilt of subhorizontal Cenozoic strata, which contrasts strongly to adjacent regions such as the Qilian and Tianshan mountains that are within the field of the Cenozoic India-Asian collision-related deformation (Guo et al., 2008; Cunningham, D., 2013; Tian et al., 2016; Zuza et al., 2016, 2018; Jia et al., 2020; Wu et al., 2021; Yang et al., 2021a). Nevertheless, recent studies have documented Cenozoic reactivation or active deformation in the Beishan region along their southern margin (Fig. 3) (Gillespie et al., 2017; Yang et al., 2019a, 2021a; Yun et al., 2021). Late Cretaceous–early Paleocene (70–60 Ma) accelerated exhumation of southern Beishan is recorded by apatite fission-track

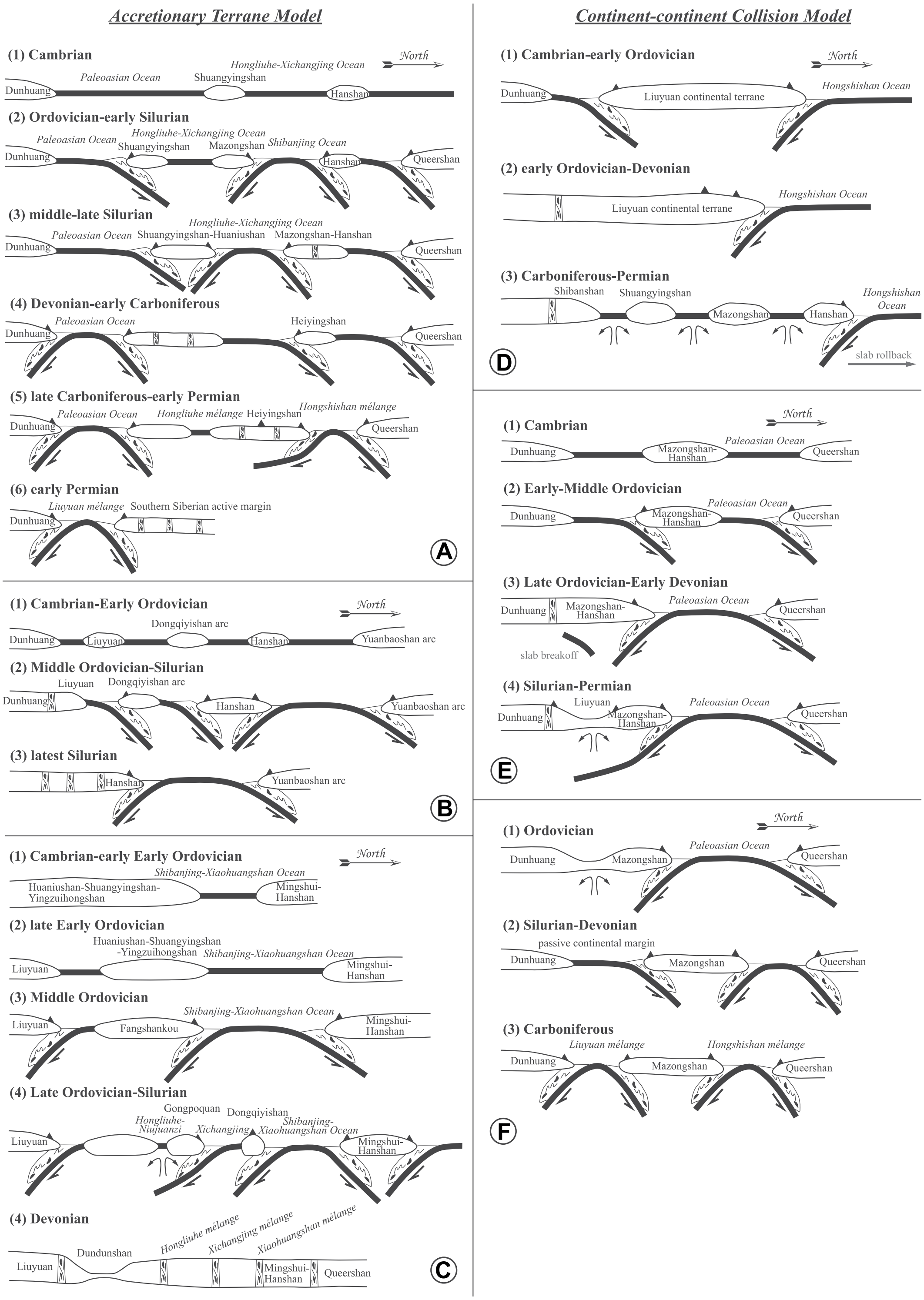

Figure 4. Major tectonic models proposed for the evolution of the Paleozoic Beishan orogen in the southern Central Asian Orogenic System. Note that the north arrow points to the north in the present-day coordinate system.

and apatite helium thermochronology (Gillespie et al., 2017). The left-slip Sanweishan-Shuangta and Daquan faults are thought to have formed in the late Pliocene and early Pleistocene, respectively, based on depositional ages of sediments in fault-formed valleys and electron spin resonance dating of fault gouge (Fig. 3) (Guo et al., 2008). In response to the activity of Altyn Tagh fault, several left-slip faults with reverse- or normal-slip components (e.g., Jiujing-Bantan fault, Ebomiao fault, Beihewan fault, and Liuyuan transpressional duplex) may have initiated in the late Quaternary along the south margin of the Beishan, although displacements are small (Fig. 3) (Yang et al., 2019a, 2021a; Yun et al., 2021). Far-field stress induced by the India-Asian collision to the south is thought to have caused these pulses of faulting and rock exhumation in the southern Beishan (Guo et al., 2008; Yin, 2010; Gillespie et al., 2017). The southern Beishan have experienced <2 km uplift and related erosional denudation since the Neogene as indicated by published thermochronological data (Tian et al., 2016; Gillespie et al., 2017).

3. STRUCTURAL GEOLOGY AND LITHOLOGY OF THE STUDY AREA

The Beishan orogen, located in the central-southern Central Asian Orogenic System, makes it an ideal place to determine when and how the closure of this ocean was been accomplished and whether this closure process can be correlated with the formation of the Solonker suture to the east (Fig. 1) (Xiao et al., 2010b). Early geological investigation in the Beishan orogen emphasized lithologic distributions, whereas our field investigation focused on the tectonic origin of lithologic assemblages, fault geometry, deformation kinematics, and temporal relationships among major structures. Our study area in the southern Beishan orogen is dominated by east-trending structures including foliations, distribution of mappable units, and a series of east-striking thrusts, folds, and ductile shear zones (Fig. 5).

3.1. Ductile Shear Deformation

Mei et al. (1999) and Yu et al. (1999) first documented the ductilely deformed Neoproterozoic granitoid in the Liuyuan area in the hanging wall of the Gubaoquan-Hongliuyuan fault (Figs. 5B). Later, Qu et al. (2011) documented the right-slip and top-to-south shear zone (labeled here as F1 in Fig. 5B). This 5–8-km-wide shear zone is developed in Precambrian rocks with N25°E striking, subvertical foliations, and a mineral lineation that plunges steeply (75°) to N25°W. The shear zone is composed of strongly deformed granitoid and high-pressure eclogite facies-amphibolite facies metamorphic rocks. Kinematic indicators such as asymmetric folds and rotated clasts show top-to-south and right-lateral sense of shear. The shear zone moved prior to the Silurian (ca. 438 Ma) based on the undeformed granitoid crystallization age (Fig. 5B) (Liu et al., 2011).

3.2. Thrust Faults

The Gubaoquan-Hongliuyuan fault is northwest-striking in the western part of the study area and northeast-striking in the eastern part of the study area, which exhibits arc-shaped convex southward in ground surface that indicate dipping to the north (labeled as F2 in Figs. 5B and 6). It juxtaposes Carboniferous-Permian sedimentary strata in the eastmost part of the study area and Precambrian gneiss complex over Carboniferous-Permian rift-related rocks. The fault zone is defined by a cataclastic zone ∼50–200 m wide with dominantly downdip striations (Figs. 7C and 7D).

The gneiss complex consists of augen mylonitic granitoid, schist, mylonitic quartzofeldspathic gneiss, amphibolite, eclogite, and Silurian-Devonian (ca. 446–402 Ma) arc-related granitoids and (ultra-)mafic intrusions that intruded into the above units (Figs. 7A, 7E, and 7F) (Liu et al., 2011; Mao et al., 2012a; Li et al., 2015; Wang et al., 2017a). Meanwhile, the units in the hanging wall were intruded by Early Permian (ca. 285–280 Ma) arc-related granitoid and mafic dikes (Fig. 7A) (Gao et al., 2020). The deformed and metamorphized rocks in the hanging wall were previously assigned a Pre-Paleoproterozoic age (Gansu BGMR, 1996; Shaanxi IGS, 2014). However, updated dating of the mylonitic granitoid and high-pressure metamorphic rock components in the complex yielded demonstrably igneous/protolith ages of ca. 933–868 Ma, which may be the response of peri-Rodinian subduction system in the Beishan region (Liu et al., 2015; Yuan et al., 2015; Zong et al., 2017; Soldner et al., 2020a). The Carboniferous-Permian sedimentary strata in the hanging wall of the Gubaoquan-Hongliuyuan fault consists of basaltic layer, tuffaceous siltstone, sandstone, and conglomerate intercalations and mudstone, which suggest that sedimentary setting transition from alluvial fan to delta-front facies in rift setting (Figs. 7G and 8) (Niu et al., 2021b). The hanging wall sedimentary units tightly folded into pairs of NE-trending anticlines and synclines (Fig. 6). Axial planes dip NW and subhorizontal hinge lines suggest southeast-directed thrusting (Figs. 7I and 7J).

The Carboniferous-Permian rift-related rocks in the footwall of the Gubaoquan-Hongliuyuan fault consist of gabbro, basalt, chert, andesite, conglomerate, sandstone, and slate, which suggest a rifted basin setting (Figs. 5B, 7B, and 8) (Chen et al., 2016; Wang et al., 2017a). The unit in the footwall are slightly folded into a pair of NE-trending antiform and synform adjacent to Gubaoquan (Fig. 5B) and are penetratively foliated in the clastic rocks (Fig. 7H). The fault may have moved in the Permian based on the undeformed Late Permian volcanic deposits, which is the response of the north-dipping subduction of the Liuyuan Ocean.

The left-lateral oblique F6 thrust is NNE-striking and NW-dipping in the eastern portion of the study area, and structurally merged with F2 in the south and F3 in the north (Fig. 6). It places Devonian-Permian (volcanic)sedimentary rocks over Carboniferous-Permian rocks. Both hanging wall and footwall units are folded. The hanging wall is also imbricated by north-dipping thrusts that merges with F3 in the north. The F7 fault is a décollement fault between crystallized rocks and supracrustal sedimentary covers, which accommodate the differences of deformation styles and shortening amount in hanging wall and footwall rocks (Fig. 6).

The left-lateral oblique F3 thrust is E-striking and N-dipping in the northern portion of the study area, and structurally merged with F2 further to the east (Figs. 5B and 6). It juxtaposes a crystallized complex over the Devonian-Permian sedimentary sequence described above in the eastern portion of the study area, and extends into the crystallized complex in the west. The crystallized complex consists of gneiss, amphibolite, and schist assigned a Precambrian age based on regional lithologic correlations by Shaanxi IGS (2014), although recently some Ordovician ages (ca. 466 Ma and 450 Ma) were reported in this unit (Wang et al., 2017a; Cleven et al., 2018). The above complex unit was intruded by a lot of Ordovician-Devonian magmatic intrusions and Early Permian mafic intrusions (Li et al., 2011a; Zhang, 2014; Zhu et al., 2016; this study). These faults' (F2, F3, F6, and F7) characteristics suggest the thick-skinned structure in the Huitongshan-Hongliuyuan area (Fig. 6).

3.3. Cenozoic Structures

Cenozoic northeast-striking left-slip faulting currently dominates the Beishan orogen, which crosscut the Paleozoic arc magmatic belts and sutures (Figs. 2 and 3). The most prominent Cenozoic structure in the study area is the left-slip Daquan fault (labeled as F4 in the west portion of Fig. 5B) that cut across all the Pre-Cenozoic structures and parallel to the Xingxingxia fault and Sanweishan-Shuangta fault (Fig. 3). However, the offset along the fault is still unclear due to limited studies. To the north, the fault terminates into an east-trending fault zone in the Hongyanjing-Huoshishan area, where to the south it connects with the northeast-striking Shulehe left-slip fault in the northern Kumtagh sand sea (Figs. 1 and 3). Guo et al. (2008) interpreted the Daquan fault to have moved in the Pleistocene (ca. 1.5–1.2 Ma) based on the electron spin resonance ages of fault gouge. The F5 left-slip fault, which strikes northeast and has lenticular fault pattern, is a branch of the Daquan fault (Fig. 5B). The fault zone is defined by a cataclastic zone ∼100 m wide with dominantly near-horizontal striations. Estimated fault horizontal offset on the fault is 5–6 km as indicated by the misplaced Triassic granitoid in our study area.

4. DATA AND METHODS

The findings of this paper are based on multiple types of data, including field, stratigraphic,

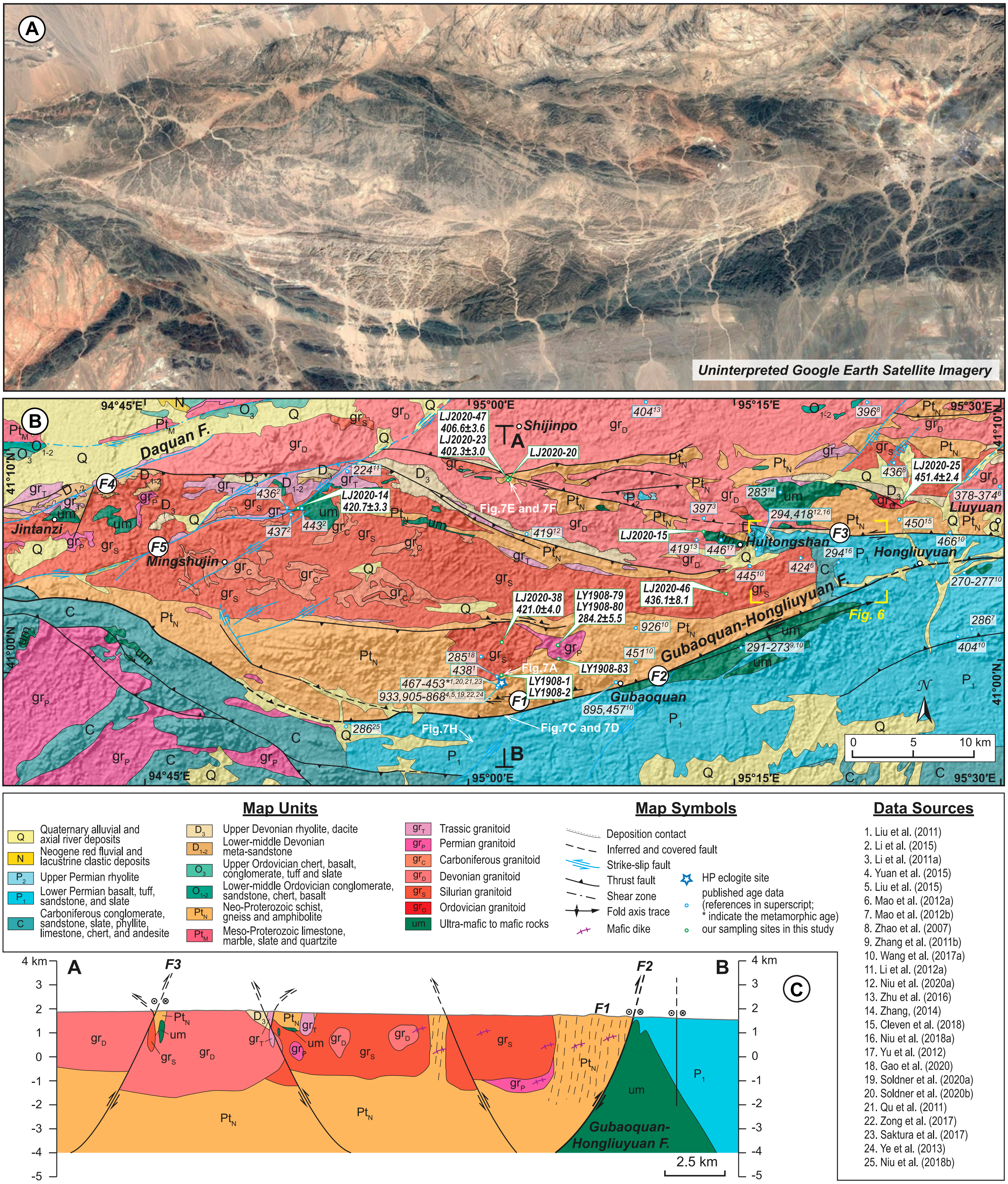

Figure 5. (A) Uninterpreted Google Earth-based satellite image of the western Liuyuan region, southern Beishan orogen of central Asia. (B) Geologic map of the western Liuyuan region. The map is based on a compilation of Shaanxi IGS (2014) and our own geologic mapping and structural interpretations. The locations and zircon U-Pb ages of samples from this study are shown. Location of Figure 6 and photos (Figs. 7A, 7C, 7F, and 7H) also shown. (C) Simplified geologic cross section of the western Liuyuan region. F.—fault; HP—high pressure.

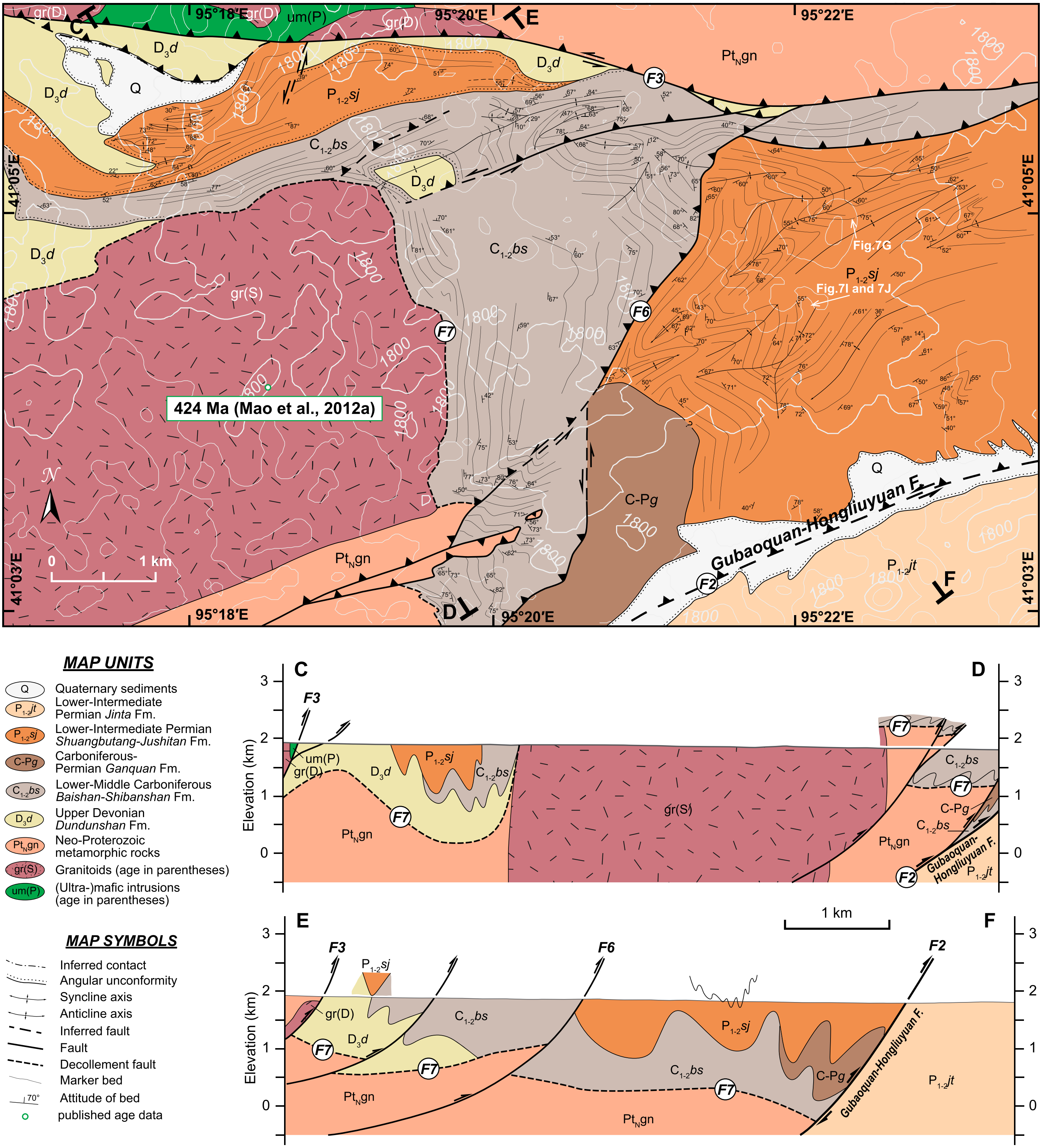

Figure 6. Geologic map and two cross sections of the Huitongshan-Hongliuyuan region of southern Beishan orogen, after Shaanxi IGS (2014) and our own observations. Location of photos (Figs. 7G, 7I, and 7J) also shown. F.—fault; Fm.—Formation.

geochronologic, and geochemical data sets across the Beishan region. Our geochronology and geochemistry data were combined with published zircon U-Pb ages and geochemical data of magmatic rocks in the area. We also conducted stratigraphical analyses of key stages and detrital zircon chronology analysis. The integrated data sets allow for a tectonic reconstruction of the Beishan region.

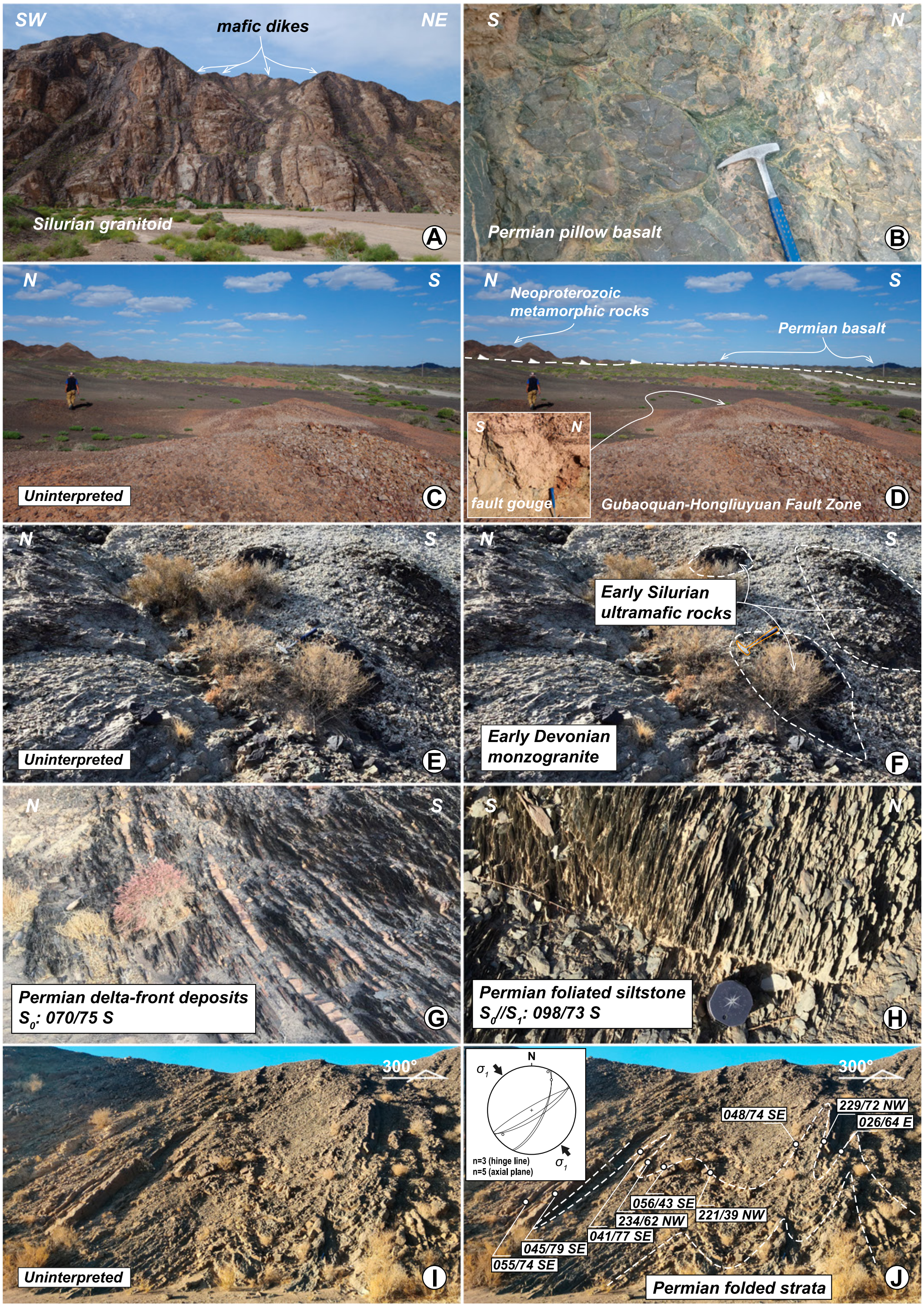

Figure 7. Field photographs from the southern Beishan orogen of central Asia displaying important geologic relationships discussed in text. Photograph locations are shown in Figures 2, 5, and 6. (A) undeformed Silurian granitoid are intruded by Early Permian mafic dikes in Gubaoquan. (B) Early Permian pillow basalt east of Liuyuan town. (C and D) Gubaoquan-Hongliuyuan cataclastic fault zone is ~50–200 m wide. Neoproterozoic metamorphic rocks thrust over Early Permian basalt from the north to the south in the Gubaoquan. (E and F) Early Silurian Huitongshan (ultra-) mafic intrusions intruded by Devonian granitoid. (G) Permian delta-front deposits consist of thin-bedded sandstone, siltstone, and mudstone. (H) Permian foliated siltstone in the footwall of the Gubaoquan-Hongliuyuan fault. (I and J) Folded Permian sedimentary strata with NE-trending and dipping to the north, which indicate a south tectonic vergence, in the hanging wall of the Gubaoquan-Hongliuyuan fault. Note that the format of the attitudes of bedding or foliations is strike, dip, and dip quadrant.

4.1. Laser Ablation–Inductively Coupled Plasma–Mass Spectrometry (LA-ICP-MS) Zircon U-Pb Dating

Zircon grains selected for U-Pb dating to determine their crystallization ages were separated by traditional methods at the Institute of the Hebei Regional Geology and Mineral Survey in Langfang, China, and mounted in epoxy with standard zircons GJ1 ($^{238}U/^{206}Pb$ age of 604.4 ± 4.7 Ma) (Jackson et al., 2004) and 91500 ($^{238}U/^{206}Pb$ age of 1064 Ma). Cathodoluminescence imaging was performed using a scanning electron microscope at the Beijing Geoanalysis Co., Ltd. to select analytical targets and assess grain zonation. U-Pb dating was conducted using an Agilent 7500a ICP-MS coupled with a 193 nm excimer ArF laser-ablation system at the Key Laboratory of Continental Collision and Plateau Uplift, Institute of Tibetan Plateau Research, Chinese Academy of Sciences,

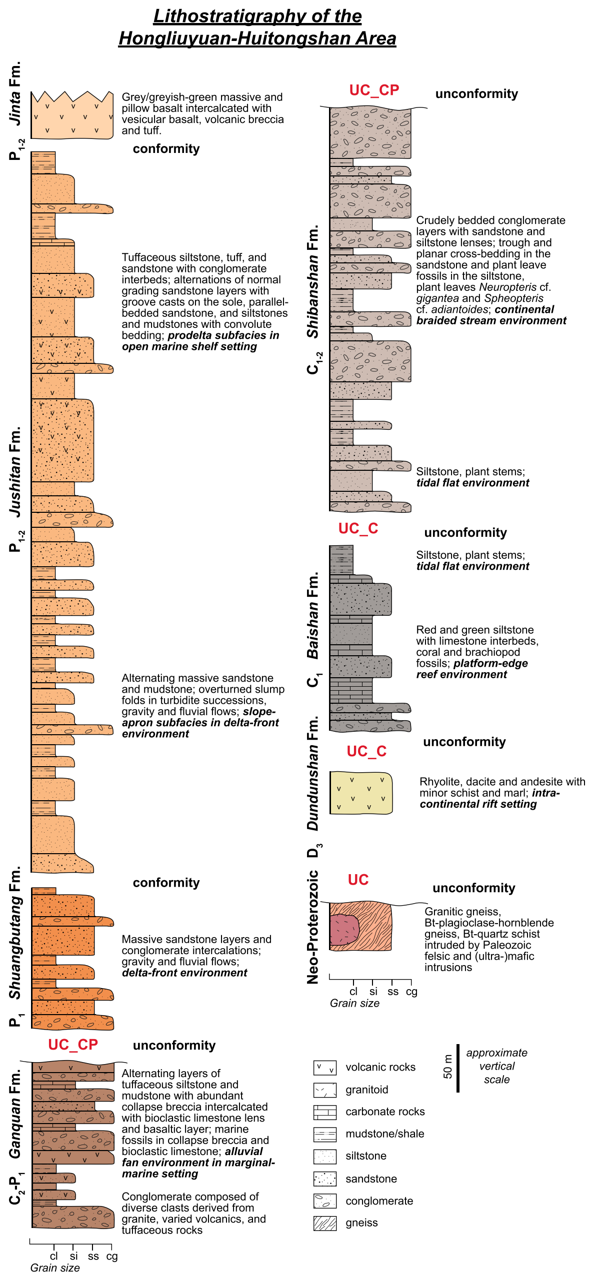

Figure 8. Lithostratigraphy of the Hongliuyuan-Huitongshan area of southern Beishan orogen compiled from Shaanxi IGS (2014) and Niu et al. (2021b). Fm.—Formation.

Beijing. Considering the size distribution of the zircon grains and signal stability, we used 30 μm ablation pits for all grains. The analytical procedure is similar to that of Xie et al. (2008).

U-Pb ages presented here are $^{206}Pb/^{238}U$ ages given that all grains are younger than ca. 1000 Ma (Ludwig, 2003). The fractionation correction and results were calculated using GLITTER 4.0. Common Pb was corrected following the method described by Andersen (2002). We analyzed ~20–35 grains per sample and included analyses with discordance of <10%. We focused on the dominant population of younger ages and interpreted the crystallization ages to be the weighted mean age of the youngest age cluster ($n \geq 3$) (Table 1). Distinctly older age populations were generally interpreted as inherited. Uncertainties of individual ages are 1σ and plotted at 2σ. All analytical and systematic uncertainties of the weighted mean ages are reported at the 95% confidence level. Age calculations and concordia plots were made using Isoplot 3.0 of Ludwig (2003). The geochronologic data are presented in Table S1[1].

4.2. Whole-Rock Geochemistry and Sr-Nd Isotopic Analysis

Igneous samples were analyzed for major and trace elements and Sr-Nd isotopes at the

[1]Supplemental Material. Table S1: LA-ICP-MS results for zircon U-Pb ages of igneous samples from this study. Table S2: Major and trace elements for magmatic intrusion samples from this study. Table S3: Summary of geochronology results of intrusive rocks of the Beishan region. Table S4: Summary of geochemistry data of intrusive rocks of the Beishan region. Table S5: Summary of whole-rock Sr-Nd isotopic geochemistry data of intrusive rocks of the Beishan region. Table S6: Summary of zircon Hf isotopic data of intrusive rocks of the Beishan region. Please visit https://doi.org/10.1130/GSAB.S.19694485 to access the supplemental material, and contact editing@geosociety.org with any questions.

TABLE 1. SUMMARY OF SAMPLE LOCATIONS AND ZIRCON GEOCHRONOLOGY RESULTS IN THE BEISHAN REGION, CENTRAL ASIA

Sample number	Rock type	Latitude (°N)	Longitude (°E)	Elevation (m)	Interpreted age (Ma)	MSWD	n	Method
LJ2020-20	Olivine pyroxenite	41°08′18.10″	95°01′58.92″	1970	-	-	-	Geochemistry
LJ2020-47	Monzogranite	41°08′18.03″	95°02′02.29″	1953	406.6 ± 3.6	2.9	24 out of 25	Geochemistry/U-Pb zircon/Sr-Nd isotope
LJ2020-23	Monzogranite	41°08′16.87″	95°01′56.45″	1982	402.3 ± 3.0	1.6	25 out of 25	Geochemistry/U-Pb zircon/Sr-Nd isotope
LJ2020-14	Hornblende gabbro	41°07′03.58″	94°49′13.10″	1915	420.7 ± 3.3	3.2	35 out of 35	Geochemistry/U-Pb zircon
LJ2020-25	Bt-monzogranite	41°07′00.85″	95°24′39.23″	1799	451.4 ± 2.4	0.86	25 out of 25	Geochemistry/U-Pb zircon/Sr-Nd isotope
LJ2020-15	K-feldspar granite	41°05′55.13″	95°13′09.51″	1839	-	-	-	Geochemistry
LJ2020-46	Diorite	41°03′02.75″	95°14′34.58″	1766	436.1 ± 8.1	6.3	16 out of 20	Geochemistry/U-Pb zircon/Sr-Nd isotope
LJ2020-38	Granite	41°01′10.79″	95°02′02.11″	1794	421.0 ± 4.0	2.3	20 out of 25	Geochemistry/U-Pb zircon/Sr-Nd isotope
LY1908-80	Granite	41°00′41.67″	95°04′25.75″	1812	284.2 ± 5.5	4.2	19 out of 25	Geochemistry/U-Pb zircon
LY1908-79	Granite	41°00′41.67″	95°04′25.75″	1812	-	-	-	Geochemistry/Sr-Nd isotope
LY1908-83	Granite	41°00′18.43″	95°04′31.64″	1790	-	-	-	Geochemistry
LY1908-1	Granite	40°59′25.29″	95°02′00.17″	1769	-	-	-	Geochemistry/Sr-Nd isotope
LY1908-2	Granite	40°59′25.29″	95°02′00.17″	1769	-	-	-	Geochemistry

Note: MSWD—mean square of weighted deviates; n—number of selective zircon grains for weighted mean age; Bt—biotite.

TABLE 2. WHOLE-ROCK Rb-Sr AND Sm-Nd ISOTOPE COMPOSITIONS OF GRANITOIDS IN OUR STUDY, BEISHAN REGION, CENTRAL ASIA

Sample number	Age (Ma)	Rb (ppm)	Sr (ppm)	$^{87}Rb/^{86}Sr$	$^{87}Sr/^{86}Sr$	Error (2σ)	$(^{87}Sr/^{86}Sr)_i$	Sm (ppm)	Nd (ppm)	$^{147}Sm/^{144}Nd$	$^{143}Nd/^{144}Nd$	Error (2σ)	$(^{143}Nd/^{144}Nd)_i$	$\varepsilon_{Nd}(t)$	$f_{Sm/Nd}$	T_{DM} (Ga)
LJ2020-47	406.6	95.60	83.30	3.421240	0.729439	0.00000843266	0.709629	6.15	42.85	0.086795	0.512197	0.00000445184	0.511966	–2.90	–0.56	1.15
LJ2020-23	402.3	83.81	296.67	0.842133	0.712410	0.00000838857	0.707585	2.23	11.16	0.120792	0.512609	0.00000493291	0.512291	3.34	–0.39	0.89
LJ2020-25	451.4	109.50	476.35	0.685243	0.714234	0.00000742121	0.709828	4.48	21.60	0.125537	0.512216	0.00000570677	0.511845	–4.13	–0.36	1.61
LJ2020-46	436.1	91.63	678.84	0.402369	0.709340	0.00000823688	0.706841	3.71	19.34	0.115862	0.512382	0.00000457190	0.512051	–0.49	–0.41	1.20
LJ2020-38	421.0	170.49	197.96	2.567295	0.726327	0.00000951727	0.710933	4.02	18.06	0.134602	0.512381	0.00000493635	0.512010	–1.68	–0.32	1.48
LY1908-79	284.2	30.03	206.47	0.433650	0.706786	0.00000904709	0.705032	1.86	8.52	0.132108	0.512786	0.00000612429	0.512540	5.23	–0.33	0.68
LY1908-1	421.0	85.53	260.66	0.978163	0.718074	0.00000922099	0.712209	5.00	24.80	0.121865	0.512259	0.00000518193	0.511923	–3.37	–0.38	1.48

Note: $(^{87}Sr/^{86}Sr)_i = (^{87}Sr/^{86}Sr)_s – (^{87}Rb/^{86}Sr)_s*(e^{\lambda t}–1)$, $\lambda = 1.42 \times 10^{-11}\ a^{-1}$, $\varepsilon_{Nd}(t)\quad [(^{143}Nd/^{144}Nd)_s/(^{143}Nd/^{144}Nd)_{CHUR}–1]\quad 10^4$, $f_{Sm/Nd} = (^{147}Sm/^{144}Nd)_s/(^{147}Sm/^{144}Nd)_{CHUR}–1$.
$T_{DM} = (1/\lambda)*\ln\{[0.51315–(^{143}Nd/^{144}Nd)_s]/[0.2137–(^{147}Sm/^{144}Nd)_s] + 1\}$ (Keto and Jacobsen, 1987), where T_{DM} = depleted mantle model age.
$(^{143}Nd/^{144}Nd)_{CHUR} = 0.512638$, $(^{147}Sm/^{144}Nd)_{CHUR} = 0.1967$, $\lambda = 0.654 \times 10^{-11}\ a^{-1}$, where s = sample.
CHUR—chondritic uniform reservoir.

State Key Laboratory of Geological Processes and Mineral Resources, China University of Geosciences (Wuhan). Weathered surfaces were removed from fresh samples and crushed. The crushed samples were ground into powder (>200 mesh) using a ball mill. Major element compositions were determined by X-ray fluorescence spectrometry with analytical accuracy better than 2%. Trace element compositions were measured by ICP-MS with analytical accuracy better than 5%. Sr-Nd isotope analyses were conducted using multicollector-ICP-MS with spectral analysis accuracy better than 0.002%. Sample dissolution was performed using acid digestion ($HF + HClO_4 + HNO_3$). Separation of Rb and Sr was performed using AG50W × 12 strongly acidic cation exchange resins. Isotope measurements of the background were conducted within the error range. Analytical results of standard samples BCR-2 and RGM-2 include: $^{143}Nd/^{144}Nd = 0.512634 \pm 5$ (2σ) and $^{87}Sr/^{86}Sr = 0.704993 \pm 9$ (2σ), and $^{143}Nd/^{144}Nd = 0.512801 \pm 5$ (2σ) and $^{87}Sr/^{86}Sr = 0.704150 \pm 8$ (2σ), respectively. Details of the analytical procedure are described in Liu et al. (2004) and Li et al. (2012b). The whole-rock geochemical and Sr-Nd isotopic data are presented in Table S2 (see footnote 1) and Table 2, respectively.

4.3. Spatial and Temporal Relations of Magmatic Rocks

The spatial and temporal distribution of arc magmatic rocks in relation to a subduction zone can be used to infer the polarity, style, timing, and duration of subduction (Ducea et al., 2015). Because the Hongliuhe-Xichangjing tectonic zone has been recognized by previous studies as a mature ocean setting (Ao et al., 2012; Song et al., 2014) and near-parallel geographic distribution of several tectonic zones in Beishan, we chose the Hongliuhe-Xichangjing tectonic zone as a reference line to measure the distance of variable magmatic rocks from subduction zone. The distance is the length perpendicular to the reference line from sample locations acquired from previous data sets and this study.

Although the Mesozoic and Cenozoic tectonics of the Beishan orogen remain incompletely understood, the impact of each new tectonic event on the older tectonic framework must be considered in order to obtain a more reasonable result. We divided the data into two domains to plot the age versus distance diagram to reduce the effect of unclear strike-slip faulting and lateral displacement: the west domain, which is bounded by the Daquan fault and Sanweishan-Shuangta fault, and the east domain, which is in eastern part of the Sanweishan-Shuangta fault. We use the Hongliuhe-Xichangjing tectonic zone and Hongshishan-Pengboshan tectonic zone as reference lines based on the following reasons: (1) one age cluster is distributed in the north of the Hongliuhe-Xichangjing tectonic zone, which show a trench-arc relation; (2) despite the age distribution of younging northward extended to the north of the Hongshishan-Pengboshan tectonic zone that has similar ages along the zone, the extreme lack of geologic and chronologic data adjacent to the China-Mongolia border region limits our understanding of farther north. The summarized geochronologic data are presented in Table S3 (footnote 1).

5. RESULTS

5.1. Sample Description

Eleven granitoid samples and two (ultra-) mafic rock samples were collected in the western Liuyuan region during 2019 and 2020 for U-Pb zircon dating and geochemical analysis. Sample locations are listed in Table 1 and shown in Figure 5B.

5.1.1. (Ultra-)Mafic Rocks

Our two (ultra-)mafic rock samples were collected from the Huitongshan (ultra-)mafic intrusion belt that is intruded by Silurian granitoid plutons (Fig. 5B). The olivine pyroxenite (sample LJ2020-20) contains semi-euhedral olivine (~30%–40%), pyroxene (50%–60%), and minor carbonate and metallic minerals (~10%–20%) (Fig. 9A). Large pyroxene grains (~1–2 mm in diameter) are surrounded by finer olivine grains (~0.01–0.12 mm in diameter). The hornblende gabbro (Sample LJ2020-14) consists mainly of plagioclase (~40%–50%), pyroxene (~25%–35%), amphibole (~10%–15%), and other minerals (~5%–10%) (Fig. 9B). Pyroxene and amphibole grains are distributed between crystalline grains of plagioclase.

5.1.2. Granitoids

Two samples were collected from gray- to white-colored, undeformed, medium- to coarse-grained monzogranite (LJ2020-47 and LJ2020-23) that intrudes the Huitongshan (ultra-)mafic rocks (Fig. 5B). The main minerals include plagioclase (~45%), quartz (~38%), and biotite + K-feldspar (~15%) (Figs. 9C and 9D). Plagioclase grains are characterized by light clay and sericitization. One sample was collected from biotite monzogranite (LJ2020-25) that is dark gray in color. The main minerals include quartz (~60%), plagioclase (~20%), and biotite (~15%). Feldspar grains are mostly plagioclase (~70%–75%) with polysynthetic twinning and perthite (~20%–25%) with typical gridiron

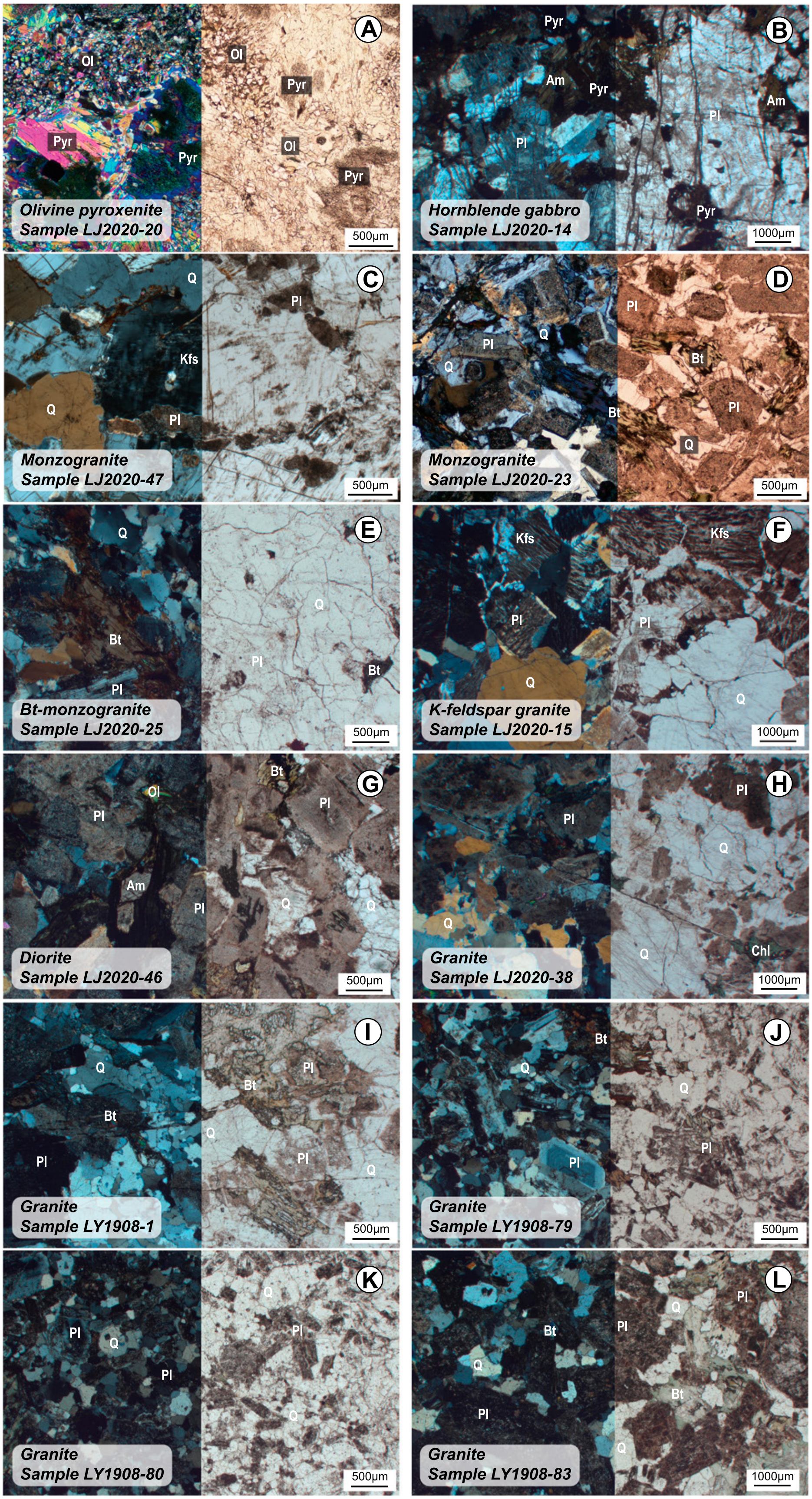

Figure 9. Photomicrographs of magmatic rocks collected as part of this study in southern Beishan orogen. (A) Silurian olivine pyroxenite (sample LJ2020-20). (B) Silurian altered hornblende gabbro (sample LJ2020-14). (C and D) Devonian monzogranites (samples LJ2020-47 and LJ2020-23). (E) Late Ordovician biotite monzogranite (sample LJ2020-25). (F) Devonian K-feldspar granite (sample LJ2020-15). (G–I) Silurian granitoids (samples LJ2020-38, LJ2020-46, and LY1908-1). (J–L) Early Permian granite (sample LY1908-79, LY1908-80, and LY1908-83). Left-side photomicrographs are in cross polarized light. Right-side photomicrographs are in plane polarized light. Q—quartz; Pl—plagioclase; Kfs—K-feldspar; Bt—biotite; Ol—olivine; Pyr—pyroxene; Am—amphibole; Chl—chlorite.

twinning. Quartz grains show deformation textures in the form of undulose extinction (Fig. 9E). One sample was collected from K-feldspar granite (LJ2020-15) that intrudes the Huitonghshan gabbro (Fig. 5B). The main minerals include quartz (~40%–50%), K-feldspar (~35%–40%), and plagioclase (~10%–15%) (Fig. 9F). One sample was collected from medium- to coarse-grained diorite (LJ2020-46) that is gray to white in color. Main mineral assemblages include quartz (~40%), plagioclase (~30%), amphibole (~10%), biotite (~15%), and minor olivine (<3%) (Fig. 9G). Six samples were collected from a granitic pluton (LJ2020-38, LY1908-80, LY1908-79, LY1908-83, LY1908-1, and LY1908-2) that intrudes Neoproterozoic metamorphic basement and is intruded by Early Permian doleritic dikes (Fig. 5B). These samples are characterized by main mineral assemblages of quartz (~40%–50%), plagioclase (~20%–35%), and biotite (~10%–15%). Plagioclase is characterized by light clayization and chloritization (Figs. 9H–9L).

5.2. Geochronological Results

Analytical results of igneous samples are shown in Figure 5B and Table 1. Twenty-five zircon grains of monzogranite sample LJ2020-47 were analyzed, yielding concordant ages between ca. 392 Ma and ca. 456 Ma. The zircon grains have clear oscillatory zoning and Th/U values of 0.416–0.887 (Fig. 10H). The weighted mean U-Pb age of twenty-four concordant zircon grains is 406.6 ± 3.6 Ma (mean square of weighted deviation [MSWD]   2.9) (Fig. 10A), which we interpret as the crystallization age of this granitoid sample. One spot

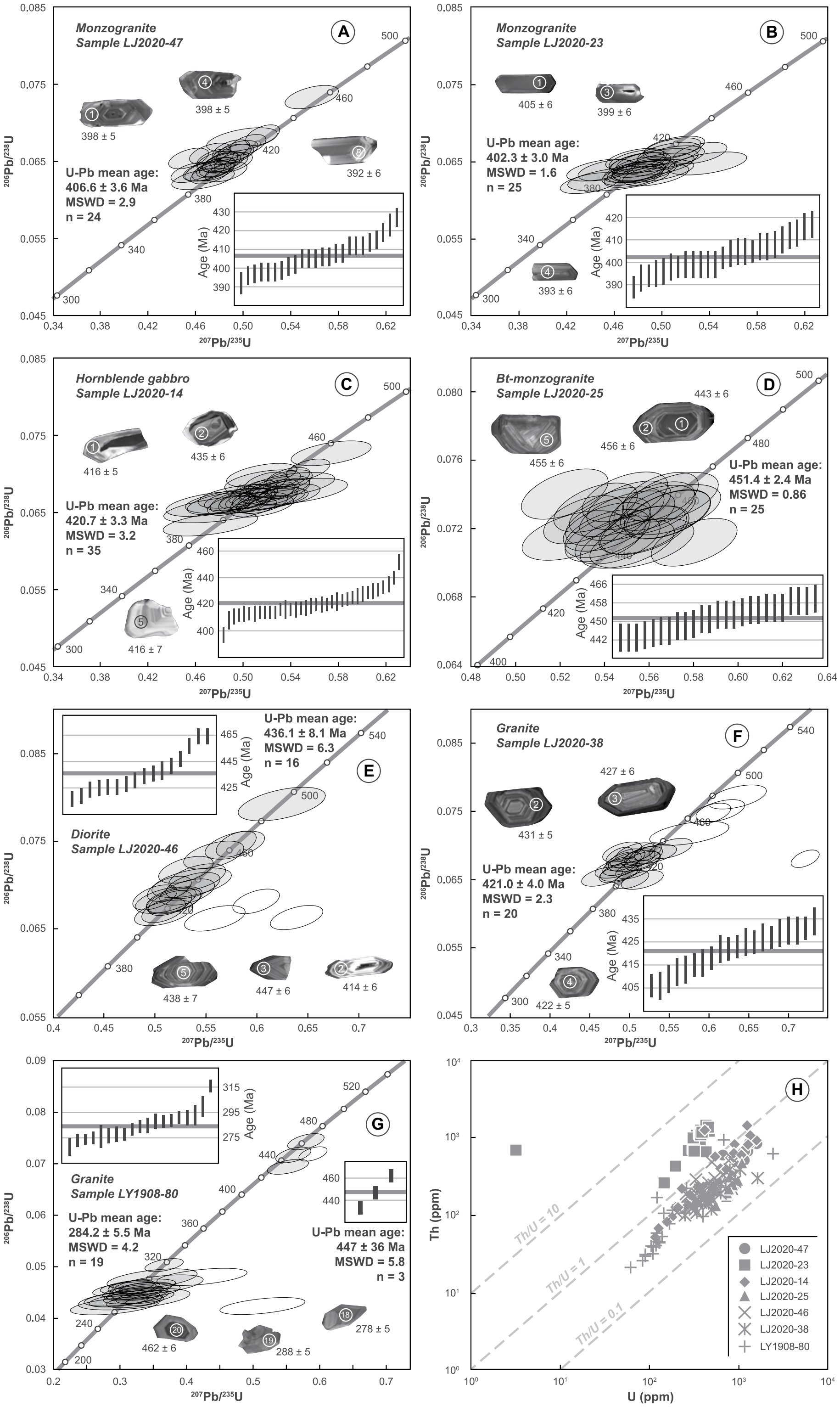

Figure 10. U-Pb concordia diagrams showing results of single shot zircon analyses and representative zircon cathodoluminescence images for each sample. (A) Monzogranite sample LJ2020-47; (B) Monzogranite sample LJ2020-23; (C) Hornblende gabbro sample LJ2020-14; (D) Bt-monzogranite sample LJ2020-25; (E) Diorite sample LJ2020-46; (F) Granite sample LJ2020-38; (G) Granite sample LY1908-80; (H) Th vs. U diagram. Error ellipses are 2σ. Discordant zircon ages shown by circle without filling are uninterpreted. White circles represent ~30 μm analyzed spots. MSWD—mean square of weighted deviates.

from this sample yields a concordant age of 456 ± 6 Ma (Fig. 10A), which may indicate an inherited grain.

Twenty-five zircon grains of monzogranite sample LJ2020-23 were analyzed, yielding concordant ages between ca. 389 Ma and ca. 417 Ma. The zircon grains have clear oscillatory zoning and Th/U values of 1.529–216.056 (Fig. 10H). The weighted mean U-Pb age of twenty-five concordant zircon grains is 402.3 ± 3.0 Ma (MSWD = 1.6) (Fig. 10B), which we interpret as the crystallization age of this granitoid sample.

Thirty-five zircon grains of hornblende gabbro sample LJ2020-14 were analyzed, yielding concordant ages between ca. 397 Ma and ca. 452 Ma. The zircon grains have clear oscillatory zoning and Th/U values of 0.317–2.923 (Fig. 10H). The weighted mean U-Pb age of thirty-five concordant zircon grains is 420.7 ± 3.3 Ma (MSWD = 3.2) (Fig. 10C), which we interpret as the crystallization age of this gabbro sample.

Twenty-five zircon grains of biotite monzogranite sample LJ2020-25 were analyzed, yielding concordant ages between ca. 443 Ma and ca. 460 Ma. The zircon grains have clear oscillatory zoning structure and Th/U values of 0.241–0.480 (Fig. 10H). The weighted mean U-Pb age of twenty-five concordant zircon grains is 451.4 ± 2.4 Ma (MSWD = 0.86) (Fig. 10D), which we interpret as the crystallization age of this granitoid sample.

Twenty zircon grains of diorite sample LJ2020-46 were analyzed, yielding concordant ages between ca. 417 Ma and ca. 492 Ma. The zircon grains have clear oscillatory zoning and Th/U values of 0.401–0.952 (Fig. 10H). The weighted mean U-Pb age of 16 concordant zircon grains is 436.1 ± 8.1 Ma (MSWD = 6.3) (Fig. 10E), which we interpret as the crystallization age of this granitoid sample. One spot from this sample yield concordant age of 492 ± 8 Ma (Fig. 10E), which may indicate an inherited zircon grain.

Twenty-five zircon grains of granite sample LJ2020-38 were analyzed, yielding concordant ages ranging from 406 Ma to 434 Ma. The zircon grains have a clear oscillatory zoning structure and Th/U values of 0.175–0.447 (Fig. 10H). The weighted mean U-Pb age of 20 concordant zircon grains is 421.0 ± 4.0 Ma (MSWD = 2.3) (Fig. 10F), which we interpret as the crystallization age of this granitoid sample.

Twenty-five zircon grains of granite sample LY1908-80 were analyzed, yielding diverse ages ranging from a U-Pb age of 268 Ma to 462 Ma. The zircon grains have a clear oscillatory zoning structure and Th/U values of 0.240–1.381 (Fig. 10H). The older population of concordant analyses are clustered at ca. 440 Ma with a weighted mean age of 447 ± 36 Ma (MSWD = 5.8, n = 3), and the younger population of concordant zircon grains yields a weighted mean age of 284.2 ± 5.5 Ma (MSWD = 4.2, n = 19) (Fig. 10G). We interpret the younger population as the crystallization age of this granitoid sample, and the older population as the inherited.

5.3. Whole-Rock Geochemistry and Sr-Nd Isotope Results

Major and trace element data for 13 representative samples of igneous intrusions are presented in Table S2. Here, we show the results of geochemical analyses in three groups: the (1) Late Ordovician–Early Devonian granitic plutons that are inferred to represent early Paleozoic magmatism (i.e., samples LJ2020-47, LJ2020-23, LJ2020-25, LJ2020-15, LJ2020-46, LJ2020-38, LY1908-1, and LY1908-2); (2) Silurian (ultra-)mafic intrusions that are inferred to represent early Paleozoic extension-related magmatism (i.e., samples LJ2020-20 and LJ2020-14); and (3) Early Permian granitoid samples inferred to be related to rift-related magmatism during the opening of the Liuyuan Ocean (i.e., samples LY1908-80, LY1908-79, and LY1908-83).

All granitoid samples are felsic (SiO_2 ~64–77 wt%; Table S2) with geochemical classifications spanning the granodiorite to granite fields based on their weight percentage of silica and alkaline elements ($Na_2O + K_2O$ versus SiO_2; Fig. 11A). These samples are mostly (high-K) calc-alkaline with the exception of three Early Permian samples (LY1908-80, LY1908-79, and LY1908-83) that are tholeiitic (Fig. 11B). In the A/NK versus A/CNK diagram (Maniar and Piccoli, 1989), these samples are metaluminous (Fig. 11C). Granitoid samples display relatively flat (La/Yb is ~2–30) rare earth element patterns (Fig. 11E) and are characterized by negative Ba, Nb, P, and Ti anomalies (Fig. 11D), which is indicative of an arc/subduction setting for the original melt. The Devonian (LJ2020-23) and three Early Permian (LY1908-80, LY1908-79, and LY1908-83) granitoid samples display no Eu anomalies, whereas the remaining seven granitic samples show negative Eu anomalies, indicating minor involvement of plagioclase in fractional melting (Fig. 11E). The Early Devonian sample LJ2020-15 is characterized by high Cs, Th, and Pb contents and negative Ba, Nb, Sr, Eu, and Ti anomalies, suggesting a thickened crust melt source related to the upwelling of mantle materials. In the Nb versus 10,000*Ga/Al diagram (Whalen et al., 1987), these samples plot mostly in the I- and S-type granite fields that are commonly associated with arc magmatism and/or crustal anataxis and partially overlap with the A-type granite field. The Early Devonian K-feldspar granite sample (LJ2020-15) plots in the A-type granite field, which is generally associated with extension regardless of the magma origin source (Fig. 11F) (e.g., Whalen et al., 1987; Eby, 1990, 1992; Turner et al., 1992). On the granite classification diagram (Pearce et al., 1984), these samples plot mostly in the volcanic arc field, whereas the sample LJ2020-15 plots in the within-plate granite field (Fig. 11G).

The two (ultra-)mafic samples have low silica concentrations (SiO_2 ~46 wt%; Table S2) and plot within the alkaline monzo-gabbro field for sample LJ2020-14 and subalkaline gabbro field for sample LJ2020-20 (Fig. 11A) (Middlemost, 1994). Sample LJ2020-20 has relatively lower concentrations of trace elements compared to sample LJ2020-14 (Figs. 11H and 11I; Table S2). Primitive-mantle-normalized trace element patterns of the (ultra-)mafic rocks show enrichment in large-ion lithophile elements (i.e., Ba, K, and Rb), but depletion in high-field-strength elements (i.e., Nb, Ta, P, Ti, and Zr; Fig. 11H). These two samples have similar primitive-mantle-normalized trace element patterns (Fig. 11H). However, sample LJ2020-20 shows enriched Pb and Sr and depleted Zr and Hf, whereas sample LJ2020-14 is enriched in Zr and Hf and depleted Pb. Chondrite-normalized rare earth element (REE) abundances are variable. Sample LJ2020-14 is light (L)REE enriched and has a flat heavy (H)REE pattern without distinct Ce anomaly, similar to the ocean island basalt-type pattern (Fig. 11I). Sample LJ2020-20 is LREE depleted and has a flat HREE pattern, similar to the normal-type mid-ocean ridge basalt pattern (Fig. 11I). In the Ti_2O-K_2O-P_2O_5 ternary diagram (Pearce et al., 1975), the two samples plot in the non-oceanic field (Fig. 11J). In the Hf/3-Th-Ta ternary diagram (Wood, 1980), the two samples plot in the calc-alkaline destructive plate-margin basalt field (Fig. 11K).

Sr-Nd isotopic data of the seven granitoids samples are shown in Table 2 and Figure 11L. All data and parameters are within normal ranges and do not contain abnormal values. For example, $^{87}Rb/^{86}Sr$ is not high (<3.5), so there is no abnormally low I_{Sr} value (<0.7000), which indicates that the data have geological significance. In addition, the average $f_{Sm/Nd}$ is between −0.6 and −0.3 (Table 2), indicating that differentiation of the granitoids is not obvious. It can be concluded that Sr-Nd isotopes of the rocks record the characteristics of their protoliths and thus, the model age T_{DM} is effective (Jahn et al., 2000). The five Late Ordovician to Early Devonian granitoid samples have negative $\varepsilon_{Nd}(t)$ values of −4.13 to −0.49, model ages of 1.15–1.61 Ga, and plot in the fourth quadrant in the $\varepsilon_{Nd}(t)$ versus $(^{87}Sr/^{86}Sr)_i$ diagram (Table 2; Fig. 11L). A second Early Permian granitoid sample (LY1908-79) has a positive $\varepsilon_{Nd}(t)$ value of 5.23 and a 0.68 Ga model age (Table 2; Fig. 11L). Both Early Devonian granitoid samples plot in the first quadrant (Table 2; Fig. 11L).

The geochemical data are consistent between the Late Ordovician–Early Devonian felsic plutonic samples except for the ca. 397 Ma K-feldspar granite, which is associated with syn/post-collisional extension. The Silurian Huitongshan (ultra-)mafic intrusions are related to magmatism during subduction slab rollback/breakoff. The Early Permian granitoids are related to magmatism during lithospheric extension/subduction slab breakoff. However, we note that more thorough geochemical analysis is required to draw more definitive conclusions.

Felsic rocks are an important and characteristic component of the continental crust, which involves crust anatexis of either a recycled source or a juvenile source (e.g., Huppert and Sparks, 1988; Clemens and Stevens, 2016). This study compiled all published geochemistry data, Sr-Nd isotopes and zircon Hf isotopic data of arc-related felsic rocks in the Beishan orogen (Tables S4–S6). The empirical fit defined by the La/Yb ratios of global intermediate rocks with crustal thickness (Profeta et al., 2016) is used to track the crustal thickness of the Beishan orogen. $(La/Yb)_N$ and calculated crustal thickness, following the method of Sundell et al. (2021), for the felsic rocks (55–72 wt% SiO_2) from the Beishan orogen are plotted against age in Figure 12A. A first-order observation is that calculated crustal thickness increases from ca. 540 to 450 Ma, decreases from ca. 450 to 310 Ma, and then increases again after ca. 310 Ma (Fig. 12A). For $\varepsilon_{Nd}(t)$ versus age and $\varepsilon_{Hf}(t)$ versus age diagrams, the same first-order observations are that $\varepsilon_{Nd}(t)/\varepsilon_{Hf}(t)$ decreases from ca. 540 to 450 Ma (becomes more juvenile), increases from ca. 450 to 310 Ma (becomes more evolved), and then decreases after ca. 310 Ma (becomes more juvenile) (Figs. 12B and 12C).

5.4. Geochronological and Geochemical Information of Tectonic Zones

In the following sections, the chronological and geochemical information of the four tectonic zones that controlled the Paleozoic evolution of the Beishan orogen are summarized based on the synthesis of our data and existing works (Fig. 2).

5.4.1. Hongshishan-Baiheshan-Pengboshan Tectonic Zone

Zircons from gabbro yield U-Pb crystallization ages of 347–345 Ma (Wang et al., 2014b; Niu et al., 2020b). Thus, the closure of an ocean and emplacement of the tectonic mélange must have postdated this time. Results of whole-rock

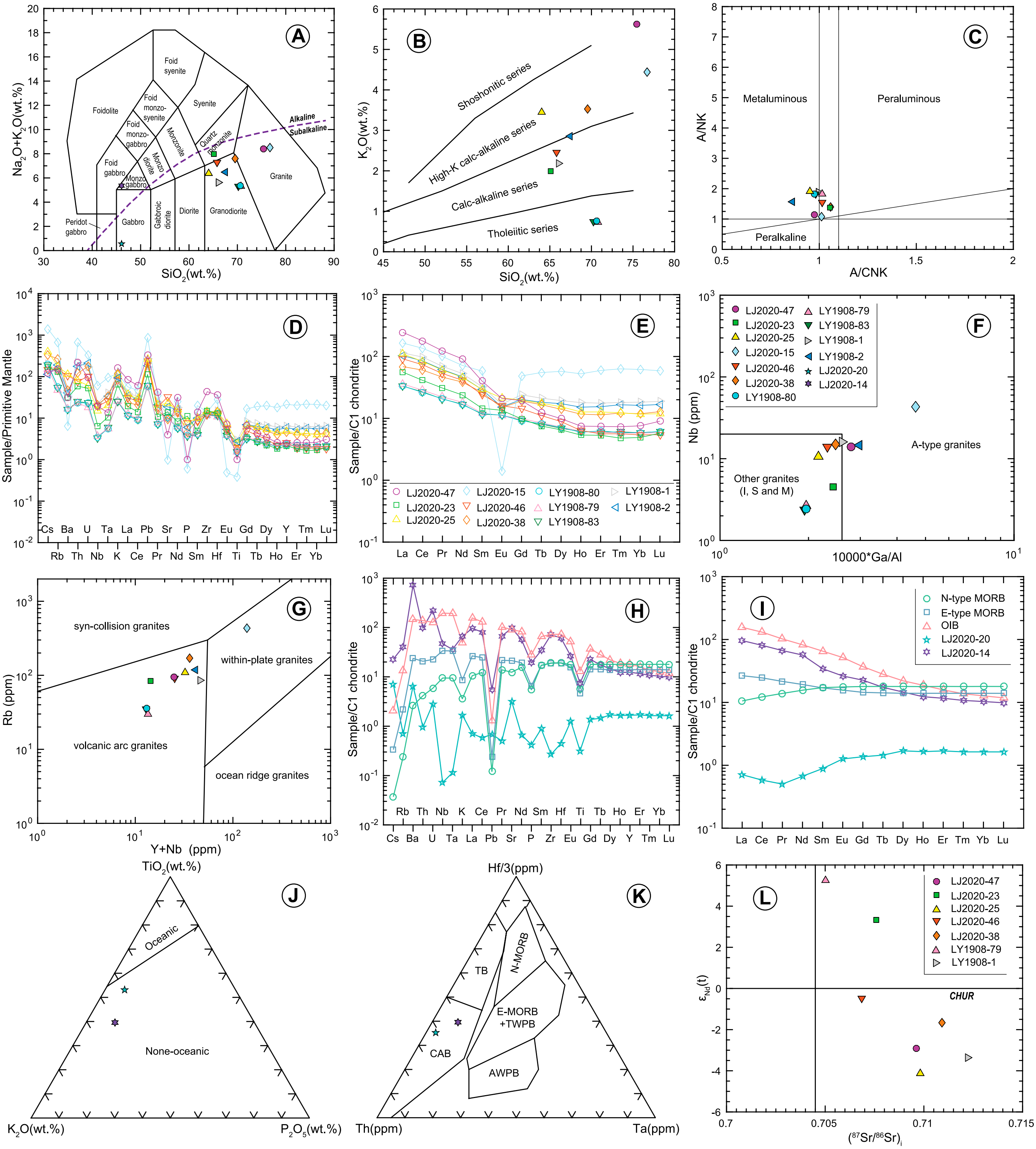

and isotopic geochemical analyses have been interpreted to reflect petrogenesis in embryonic ocean or mid-ocean ridge settings (Huang and Jin, 2006; Yang et al., 2010a; Wang et al., 2014b; Niu et al., 2020b). Zhang et al. (2020b) documented a northwest-trending tectonic mélange of the Hongshishan-Pengboshan tectonic zone in the Elegen region, adjacent to the Pengboshan region, which is composed of basalt, plagioclase granite, siliceous rock, and sandy slate. Zircons from plagioclase granite yield a U-Pb crystallization age of 342 ± 4.7 Ma, and results of whole-rock geochemical analyses are interpreted to reflect petrogenesis in a back-arc extensional setting (Zhang et al., 2020b).

Figure 11. Geochemical results of samples from the southern Beishan orogen in central Asia. (A) $Na_2O + K_2O$ versus SiO_2 diagram. Normalization values are from Middlemost (1994). (B) K_2O versus SiO_2 diagram for granitoids. Normalization values are from Le Maitre (1989). (C) A/NK versus A/CNK (A—Al_2O_3 content, NK—$Na_2O + K_2O$ content, CNK—$CaO + Na_2O + K_2O$ content) diagram for granitoids. Normalization values are from Maniar and Piccoli (1989). (D and E) Trace-element diagrams for granitoids. (D) Primitive mantle-normalized, multi-element spider diagrams. (E) Chondrite-normalized rare earth element patterns. Normalization values are from Sun and McDonough (1989). (F) Nb versus 10,000 × Ga/Al diagram for granitoid samples. Normalization values are from Whalen et al. (1987). (G) Rb versus Y + Nb diagram for the analyzed granitoid samples. Normalization values are from Pearce et al. (1984). (H and I) Trace-element diagrams for the Huitongshan (ultra-)mafic samples. Chondrite and primitive-mantle-normalizing values are from Sun and McDonough (1989). OIB, N-MORB, and E-MORB data are from Sun and McDonough (1989). (J) Ternary TiO_2-K_2O-P_2O_5 diagram for the Huitongshan (ultra-)mafic samples. Normalization values are from Pearce et al. (1975). (K) Ternary Hf/3-Th-Ta diagram for the (ultra-)mafic samples. Normalization values are from Wood (1980). N-MORB—normal mid-ocean ridge basalt; E-MORB—enriched mid-ocean ridge basalt; TWPB—tholeiitic within-plate basalt; AWPB—alkaline within-plate basalt; CAB—calc-alkaline plate-margin basalt; TB—tholeiitic plate-margin basalt. (L) $\varepsilon_{Nd}(t)$ versus $(^{87}Sr/^{86}Sr)_i$ diagram for granitoid samples.

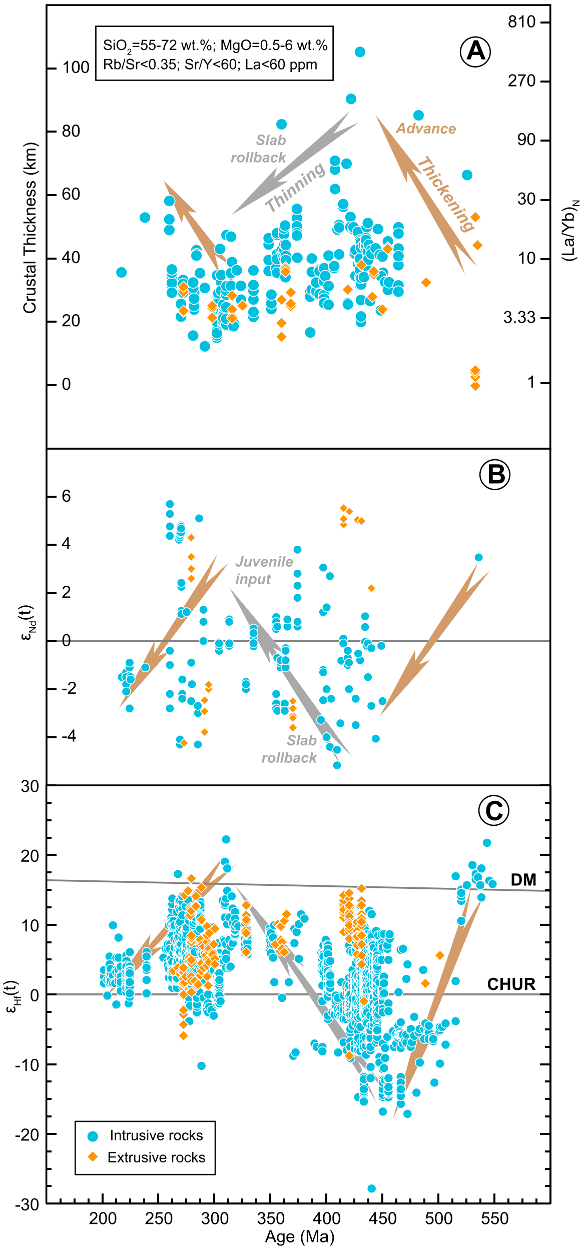

Figure 12. (A) Plot of crustal thickness versus crystallization age for rocks of the Beishan orogen in central Asia based on the $(La/Yb)_N$ calibration of Sundell et al. (2021). Data are listed in Table S4 (see text footnote 1). (B) Plot of $\varepsilon_{Nd}(t)$ values versus crystallization ages of magmatic rocks. Data are listed in Table S5. (C) Plot of zircon $\varepsilon_{Hf}(t)$ values versus crystallization ages of magmatic rocks. Data are listed in Table S6 (text footnote 1). DM—depleted mantle; CHUR—chondritic uniform reservoir.

5.4.2. Shibanjing-Xiaohuangshan Tectonic Zone

Zircons from (meta-)gabbro in the Shibanjing and Xiaohuangshan regions yield U-Pb crystallization ages of 499–453 Ma (Chen et al., 2017a; Meng et al., 2021) and 516 ± 8 Ma (Shi et al., 2018), respectively. Results of whole-rock geochemical analyses have been interpreted to reflect ophiolite petrogenesis in a back-arc or intra-plate extensional setting or supra-subduction zone (Yang et al., 2010a; Chen et al., 2017a; Shi et al., 2018; Meng et al., 2021). Otherwise, ca. 345–336 Ma for basalt and gabbro in the Xiaohuangshan region have been reported, which are much younger than previous crystallization age records, and results of whole-rock geochemical analyses show a supra-subduction zone signature (Zheng et al., 2013). In the Jijitaizi region located west of the Shibanjing region, large exposures of (ultra-)mafic rocks including meta-peridotite, cumulate gabbro, and volcanic rocks have been reported (Xiao et al., 2010b; Li et al., 2012c; Wang, 2015). Gabbro yields a U-Pb crystallization age of 321.2 ± 5.7 Ma, which roughly overlaps in age with the younger mafic rocks of the Xiaohuangshan region, potentially indicating petrogenesis in an extensional setting (Li et al., 2012c; Wang, 2015). The (ultra-)mafic rocks exposed in the Jijitaizi region are generally considered to be part of the Shibanjing-Xiaohuangshan tectonic zone based on the spatial continuity of similar lithologies (Xiao et al., 2010b; Li et al., 2012c; Wang, 2015), but the >100 m.y. difference of crystallization ages signals that more data is needed to test this interpretation.

5.4.3. Hongliuhe-Niujuanzi-Baiyunshan-Yueyashan-Xichangjing Tectonic Zone

Ca. 528–516 Ma granitoids and ca. 414–405 Ma gabbro intruded the ophiolitic mélange in the Hongliuhe and Yushishan regions (Zhang and Guo, 2008; Cleven et al., 2015a; Shi et al., 2018), which suggests that an ocean closed sometime between 516 and 414 Ma. Results of whole-rock and isotopic geochemical analyses have been interpreted to reflect petrogenesis in a supra-subduction zone setting (Cleven et al., 2015a; Shi et al., 2018). From the Huoshishan, Niujuanzi, and Tongchangkou regions, zircon from gabbro, andesite, plagiogranite, and diabase yield U-Pb crystallization ages of 455–411 Ma and ca. 354 Ma (Wu et al., 2012; Tian et al., 2014; Wang et al., 2018a; Wang et al., 2020a). Results of whole-rock geochemical analyses have been interpreted to reflect petrogenesis in an island arc, mid-ocean ridge, or supra-subduction zone setting (Tian et al., 2014; Wang et al., 2018a). From the Baiyunshan region, zircons from mid-ocean-ride gabbro and plagiogranite yield U-Pb crystallization ages of 496.4 ± 2.2 Ma and 519.8 ± 2.1 Ma, respectively (Sun et al., 2017; Tian et al., 2020a). From the Yueyashan and Xichangjing regions, zircons from gabbro, altered pyroxenite, gabbroic diorite, and plagiogranite yield U-Pb crystallization ages of 542–527 Ma (Ao et al., 2012; Hou et al., 2012; Hu et al., 2015; Shi et al., 2018). Results from whole-rock geochemical and sedimentological analyses have been interpreted to reflect petrogenesis in a mature ocean to supra-subduction zone setting (Ao et al., 2012; Hu et al., 2015; Shi et al., 2018).

5.4.4. Cihai-Liuyuan-Zhangfangshan Tectonic Zone

For the Cihai region, zircons from a mafic dike yield U-Pb crystallization ages of 307–292 Ma (Chen et al., 2013; Wang et al., 2020b). Results from whole-rock geochemical analyses have been interpreted to reflect petrogenesis in intraplate extension tectonic (Chen et al., 2013; Wang et al., 2020b). In the Huitongshan region, several (ultra-)mafic intrusions (e.g., serpentine pyroxene peridotite, olivine gabbro, and gabbro) have been documented. Zircons from gabbro and mafic volcanic rocks yield U-Pb crystallization ages of ca. 451–420.7 Ma (Mao et al., 2012a; Yu et al., 2012; Li et al., 2015; this study). For the Ganquan, Liuyuan, and Yinaoxia regions, zircons from felsic intrusions and volcanic rocks, gabbro, mafic dikes, and ultramafic rocks yield U-Pb crystallization ages of 291–268 Ma and ca. 250.4 Ma, which are distinctly different ages compared to the (ultra-)mafic rocks of the Huitongshan region (Zhang et al., 2011b; Mao et al., 2012b; Zhang et al., 2015a; Wang et al., 2017a; Xu et al., 2019a; Gao et al., 2020; Sun et al., 2020b; Ma et al., 2022). Results of whole-rock geochemical and sedimentological analyses have been interpreted to reflect petrogenesis during lithospheric mantle delamination and mantle plume activity or in an intraplate-rift extension or supra-subduction zone setting (Zhao et al., 2004, 2006; Jiang et al., 2007; Zhang et al., 2011b; Mao et al., 2012b; Zhang et al., 2015a; Chen et al., 2016; Wang et al., 2017a; Xu et al., 2019a; Gao et al., 2020; Sun et al., 2020b; Ma et al., 2022). A mafic dike intruding Carboniferous–Early Permian (ultra-)mafic rocks has a crystallization age of ca. 227 Ma, and is interpreted to have been generated in a post-collisional extension setting (Wang et al., 2017a; Sun et al., 2020a). From these constraints, closure of the rift/ocean occurred prior to ca. 227 Ma. For the Zhangfangshan region, zircons from gabbro yield a U-Pb crystallization age of 362.6 ± 4 Ma, which is older than other ages from the Cihai-Zhangfangshan tectonic zone (Yu et al., 2012). For Jiujing and Jijiquan regions, zircons from gabbro yield U-Pb crystallization ages of 284–274 Ma, and is interpreted to have been generated in a supra-subduction zone or intraplate extension setting (Gao et al., 2018a, 2018b; Zheng et al., 2021).

6. DISCUSSION

Our U-Pb geochronology results combined with existing ages from the Beishan show that Cambrian to Triassic plutons intruded Paleozoic strata. We integrated our data with published results to better constrain the tectono-magmatic evolution of the Beishan orogen.

6.1. Magmatic Record of the Beishan Orogen

The primary results plotted in an age versus distance diagram clearly show three phases of magmatism (Fig. 13). One age cluster is distributed in the north flank of the Hongliuhe-Xichangjing tectonic zone, another cluster is focused in the southern Beishan in the Cihai-Zhangfangshan tectonic zone region, and the remaining ages are distributed across the whole Beishan region that young toward the north. To consider the effects of the strike-slip faulting, we divided the age data into east and west domains. We used the Hongliuhe-Xichangjing and Hongshishan-Pengboshan tectonic zones as reference lines to replot the age versus distance diagrams based on the primary results (Fig. 13).

U-Pb zircon ages of plutonic rocks in the Beishan orogen define five age clusters of

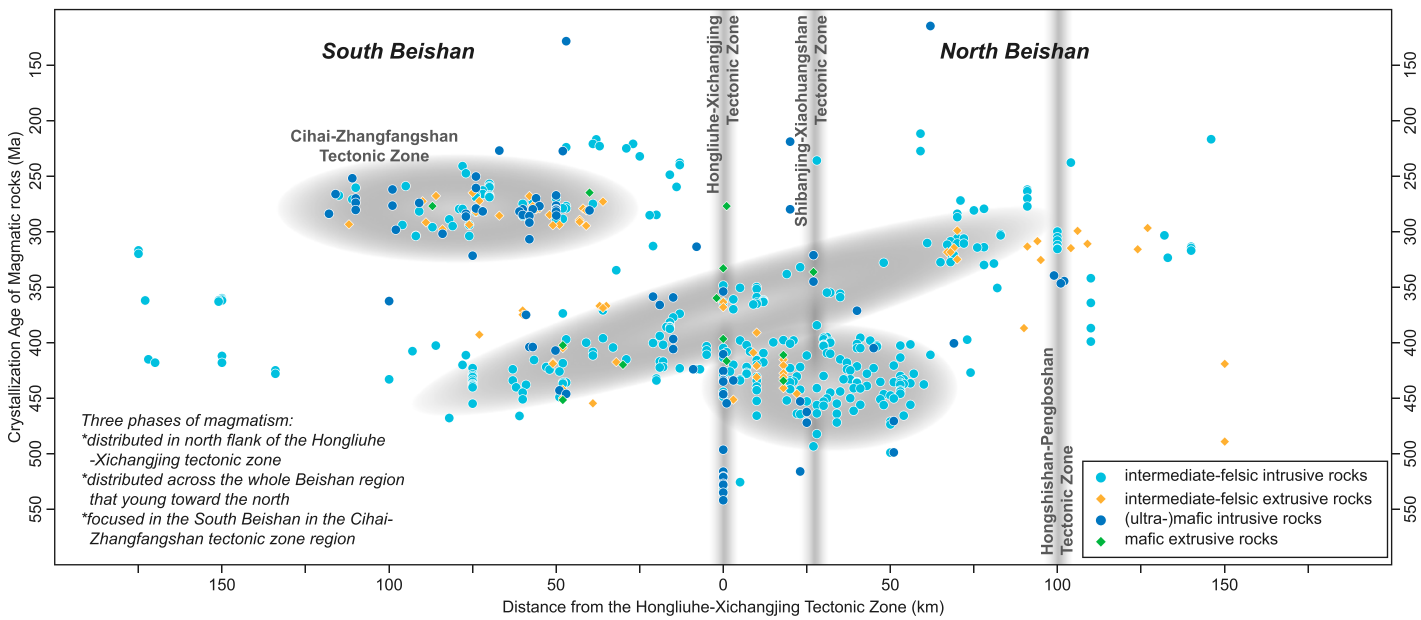

Figure 13. Preliminary result of crystallization ages versus distance from the Hongliuhe-Xichangjing tectonic zone across the Beishan region in central Asia.

1450–1395 Ma, 1024–867 Ma, 525–395 Ma, 468–212 Ma, and 300–212 Ma, with two prominent magmatic lulls at 1395–1024 Ma and 867–525 Ma (Fig. 14; Table S3). Mesoproterozoic granitic gneisses (1450–1395 Ma) only occur in the southern portion of the Hongliuhe-Xichangjing tectonic zone and are interpreted to be related to Mesoproterozoic magmatism across the southern Central Asian Orogenic System (e.g., Yili block, Central Tianshan arc, northern Alxa block, and Xilinhot block) (He et al., 2015; Yuan et al., 2019). Neoproterozoic granitic gneisses (1024–867 Ma) mostly occur in the southern portion of the Beishan orogen (e.g., Liu, et al., 2015; Yuan et al., 2015; Wang et al., 2017a; Soldner et al., 2020a; Wang et al., 2021b), whereas a ca. 885 Ma granitic gneiss is documented in the Hazhu area in the northern portion of the Beishan orogen (Figs. 2 and 14B; Table S3) (Niu et al., 2019). Here, according to the distribution of Proterozoic granitoids

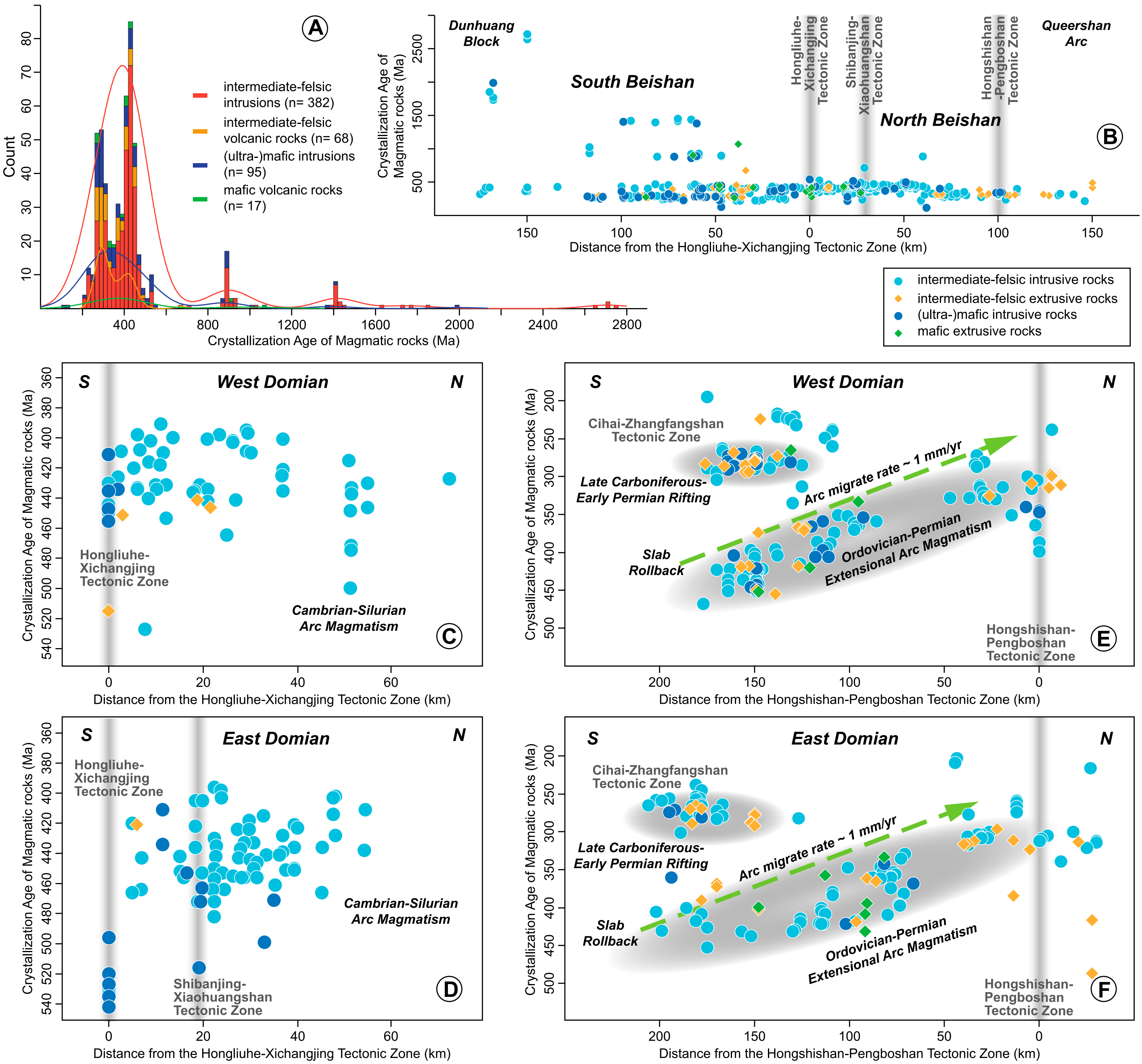

Figure 14. (A) Zircon crystallization age spectra of magmatic rocks exposed in the Beishan orogen of central Asia. (B) Crystallization ages of Proterozoic, Paleozoic, and Mesozoic plutons and volcanic rocks. (C and D) Crystallization ages versus the distance across the Hongliuhe-Xichangjing tectonic zone. (C) West domain, west of the Sanweishan-Shuangta fault. (D) East domain, east of the Sanweishan-Shuangta fault. (E and F) Crystallization ages versus the distance across the Hongshishan-Pengboshan tectonic zone. Note that the arc migrate rates in the diagrams are apparent under the consideration of Mesozoic crustal shortening deformation. (E) West domain. (F) East domain. Data are listed in Table S3 (see text footnote 1).

in the Beishan orogen (Fig. 14B), we divide the Beishan orogen into southern and northern parts along the Hongliuhe-Xichangjing tectonic zone. The geochemical composition of Neoproterozoic granitoids in the Beishan orogen suggest petrogenesis from reworked ancient crust during the assembly of Rodinia (Niu et al., 2019; Soldner et al., 2020a; Wang et al., 2021b). Cambrian–Silurian arc magmatic rocks (525–430 Ma) (e.g., Song et al., 2013b; Hu et al., 2015; Xiu et al., 2018; Yuan et al., 2018; Zhuan et al., 2018; Li et al., 2020a; Lv et al., 2021) and Silurian–Devonian syn/post-orogenic granitoids (430–395 Ma) (e.g., Zheng et al., 2012; Ding et al., 2015; Wang et al., 2018b; Zhang et al., 2018a; Bai et al., 2020; Li et al., 2020a) only occur north of the Hongliuhe-Xichangjing tectonic zone, suggesting the existence of a north-dipping early Paleozoic subduction zone along the Hongliuhe-Xichangjing tectonic zone (Figs. 14C and 14D; Table S3). Ordovician–Early Permian arc magmatic rocks (468–284 Ma) (e.g., Zhang et al., 2012a; Song et al., 2013b; Zheng et al., 2016b; Wang et al., 2017a; Cleven et al., 2018; Li et al., 2018a; Zhu et al., 2019; Yan et al., 2020; Yang et al., 2020; Zheng et al., 2021; this study) and Silurian–Triassic syn/post-orogenic granitoids (436–212 Ma) (e.g., Liu et al., 2006; Zhao et al., 2007; Feng et al., 2012; Zhang et al., 2012b; Li et al., 2013; Guo et al., 2018; Bu et al., 2019; Li et al., 2020c; Zhao et al., 2020a; this study) occurring throughout the Beishan orogen have a northward-younging trend, which is interpreted to reflect northward steepening of the subducting Paleo-Asian oceanic slab (Figs. 14E and 14F; Table S3). The minimum northward migration rate of this arc is ~1 mm/yr, similar to other documented continental arc migration rates commonly between ~1 and 5 mm/yr (Figs. 14E and 14F) (Gehrels et al., 2009; Cecil et al., 2012; Ducea et al., 2015). Late Carboniferous–Early Permian rifting/subduction-related granitoids (313–260 Ma) (e.g., Zhang et al., 2010, 2015b; Qin et al., 2011; Zhang et al., 2011b; Li et al., 2013; Zhang, 2013; Yi et al., 2017) and Early Permian–Triassic syn/post-collisional granitoids (260–217 Ma) (e.g., Li et al., 2012a; Zhang et al., 2015b; Zhu et al., 2015; Yuan et al., 2019; Yang et al., 2021c) occur in the southern Beishan orogen, which is attributed to closing in the Liuyuan region (Figs. 14E and 14F; Table S3).

U-Pb zircon ages of (ultra-)mafic rocks and their spatial relationships in the Beishan orogen mostly define four age groups of 1071–860 Ma, 542–433 Ma, 446–321 Ma, and 307–260 Ma (Fig. 14; Table S3). Neoproterozoic mafic rocks (1071–860 Ma) with an eclogite protolith and basalt in the southern Beishan orogen are interpreted to have been generated during the assembly of Rodinia (e.g., Yang et al., 2010a; Qu et al., 2011; Jiang et al., 2013; Soldner et al., 2020a; Wang et al., 2021b). The Cambrian–Early Silurian Hongliuhe-Xichangjing tectonic zone (542–433 Ma), which is characterized by a supra-subduction zone setting, may represent an ocean in the central Beishan orogen, which we refer to as the Beishan Ocean (e.g., Zhang and Guo, 2008; Wu et al., 2012; Tian et al., 2014; Cleven et al., 2015a; Hu et al., 2015; Shi et al., 2018; Wang et al., 2018a). In contrast, the Cambrian–Ordovician Shibanjing-Xiaohuangshan tectonic zone (516–453 Ma) (e.g., Zheng et al., 2013; Shi et al., 2018; Li et al., 2020a), which is characterized by a back-arc extension setting (Meng et al., 2021), may have been generated during north-dipping subduction of the Beishan oceanic slab. Silurian–Carboniferous (ultra-)mafic rocks (446–321 Ma), which include widespread exposures of incomplete ophiolite suites throughout the Beishan orogen (e.g., Li et al., 2012c; Wang, 2015; Wang et al., 2018a; Xie et al., 2018a; Niu et al., 2020b) may have been generated in an intracontinental extensional/island arc setting based on their geochemical signatures (e.g., Li et al., 2012c; Yu et al., 2012; Ma et al., 2018; Xie et al., 2018a; Yu et al., 2021). These Silurian–Carboniferous (ultra-)mafic rocks have a northward-younging trend (cf., Huitongshan ca. 446–420 Ma, Yu et al., 2012; this study; Heijianshan ca. 406–360 Ma, Yan et al., 2012; Xie et al., 2015; Ma et al., 2018; Yu et al., 2021; Cihai-Zhangfangshan ca. 375–363 Ma, Zheng et al., 2009; Yu et al., 2012; Niujuanzi-Xiaohuangshan ca. 410–345 Ma, Zheng et al., 2013; Tian et al., 2014; Wang et al., 2018a; Jijitaizi-Shibanjing ca. 371–321 Ma, Li et al., 2012c; Zhang et al., 2012c; and Hongshishan-Baiheshan ca. 346–340 Ma, Wang et al., 2014b; Xie et al., 2018a; Niu et al., 2020b; from south to north; Figs. 2, 14E, and 14F). Late Carboniferous–Permian (ultra-)mafic rocks (307–260 Ma) in the southern Beishan orogen are interpreted to have been generated in an intracontinental rift setting based on their geochemical characteristics and nearby evidence of sedimentation in a rift basin (e.g., Qin et al., 2011; Chen et al., 2013; Zheng et al., 2014; Wang et al., 2017a; Niu et al., 2021a).

Reconstructions of the Beishan orogen have used its suture zones, discontinuous ophiolite and mélange complexes, arc plutons, and high-pressure metamorphic rocks as evidence for the Paleozoic collision of multiple arcs along several sutures (Fig. 4) (Xiao et al., 2010b; Mao et al., 2012b; Saktura et al., 2017; Tian et al., 2014; Wang et al., 2017a; He et al., 2018; Shi et al., 2018; Wang et al., 2018a; Tian et al., 2020c). However, our findings show that multiple sutures and magmatic arcs overlap in time and space, which provides a more complex picture of the tectono-magmatic evolution of the Beishan orogen. Any viable model for the development of the Beishan orogen must include the following key findings: (1) progressive northward-younging Ordovician–Early Permian magmatism across the Beishan orogen and Cambrian–Silurian arc magmatism north of the Hongliuhe-Xichangjing tectonic zone (Fig. 14); (2) Cambrian–Early Silurian supra-subduction zone ophiolite and mélange material dispersed along the Hongliuhe-Xichangjing tectonic zone; (3) Silurian–Carboniferous intracontinental extensional (ultra-)mafic rocks scattered throughout the Beishan orogen (Fig. 2); and (4) the spatial and temporal overlap between arc magmatism and high-pressure metamorphism (Figs. 2 and 5).

In light of these considerations, we interpret that both a north-dipping subduction system along the Hongliuhe-Xichangjing tectonic zone and a south-dipping subduction system operated along the northern margin of Queershan arc/terrane or farther north. The Cambrian–Silurian strata and ophiolites along the northern margin of the South Beishan continent may have been emplaced via complex mélange/ophiolite obduction or ophiolite underthrusting (Fig. 2) (Cleven et al., 2015a; Song et al., 2014, 2015). In the North Beishan continent, the ~70-km-wide belt of arc plutons located north of the Hongliuhe-Xichangjing tectonic zone (Figs. 14C and 14D) (e.g., Song et al., 2013b; Hu et al., 2015; Xiu et al., 2018; Yuan et al., 2018; Zhuan et al., 2018; Li et al., 2020a) can be explained by north-dipping subduction of the early Paleozoic Beishan oceanic slab. The Silurian–Carboniferous extensional (ultra-)mafic rocks throughout the Beishan orogen may have been generated during lithospheric thinning and mantle upwelling. Across the Beishan orogen, the ~200-km-wide belts of arc plutons mixed with (ultra-)mafic magmatic rocks that generally young to the north (Figs. 14E and 14F) (e.g., Li et al., 2012c; Zhang et al., 2012c; Song et al., 2013b; Wang et al., 2017a; Cleven et al., 2018; Li et al., 2018a; Xie et al., 2018a; Zhu et al., 2019; Niu et al., 2020b; Zheng et al., 2021) can be explained by northward rollback of the south-dipping Paleo-Asian oceanic slab. The high-pressure metamorphic rocks in the southern margin of the Beishan orogen developed within this subduction system. The ca. 467–453 Ma zircon U-Pb and Lu-Hf and Sm-Nd garnet ages from eclogite record an Ordovician high-pressure metamorphism event, and the younger Early and Late Silurian cooling ages record retrograde metamorphism or exhumation (Qu et al., 2011; Saktura et al., 2017; Soldner et al., 2020b).

6.2. Neoproterozoic–Triassic Tectonic Evolution of the Beishan Orogen

As both the timing and magnitude of the Mesozoic and Cenozoic intracontinental deformation have yet to be systematically quantified, our reconstruction should be viewed as preliminary. The Neoproterozoic, passive-margin, continental-shelf, and/or continental slope sediments were deposited along the northern edge of the South Beishan continent that faced the Beishan Ocean (Figs. 2 and 15). The sediments contain ca. 2.5 Ga, 1.7–1.8 Ga, 1.4–1.5 Ga, and 0.8–1.0 Ga detrital zircon grains derived from the linked North Tarim-North China craton

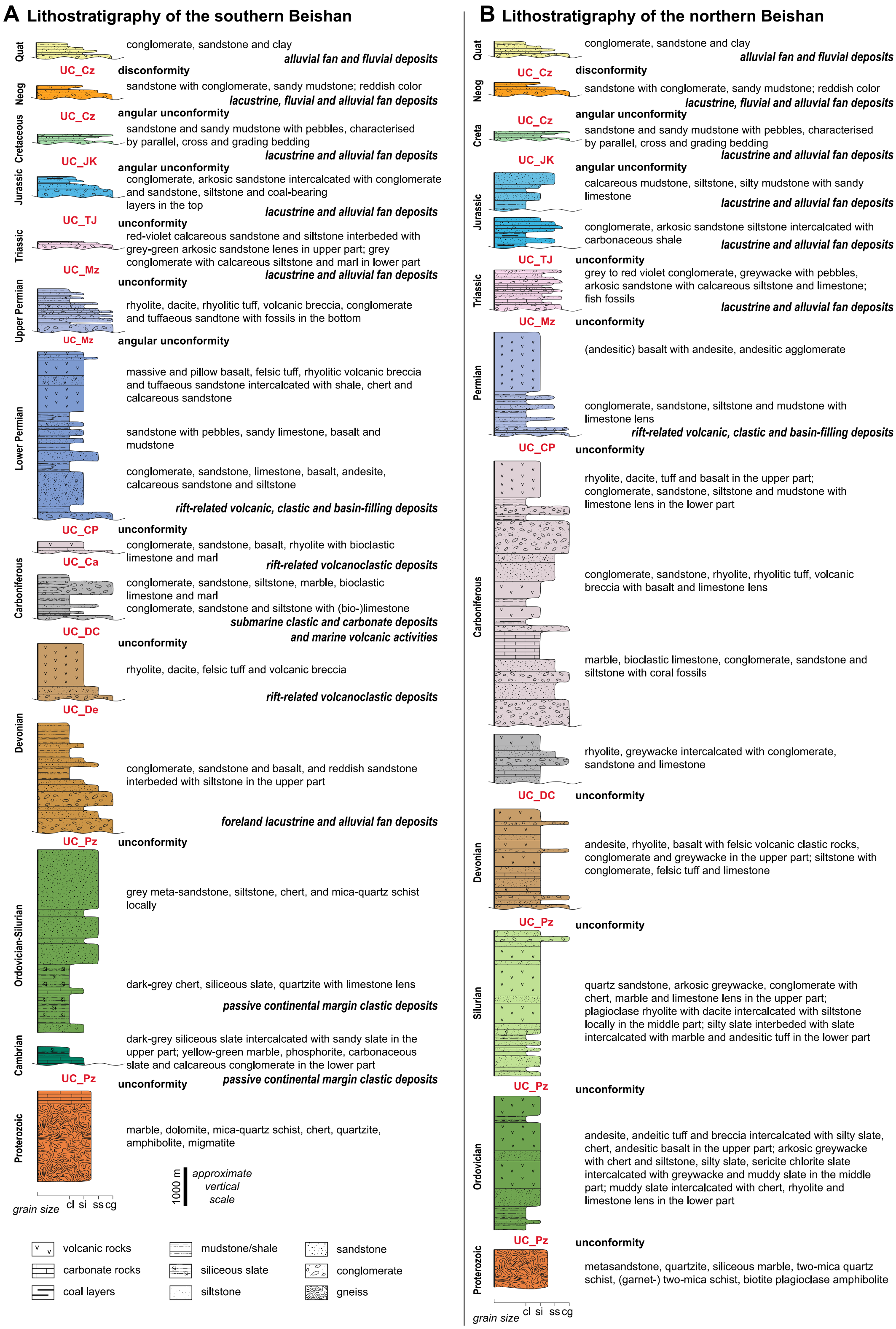

Figure 15. Lithostratigraphy of the southern and northern Beishan orogen in central Asia (Gansu BGMR, 1996). Quat—Quaternary; Neog—Neogene; Creta—Cretaceous; cl—claystone; si—siltstone; ss—sandstone; cg—conglomerate.

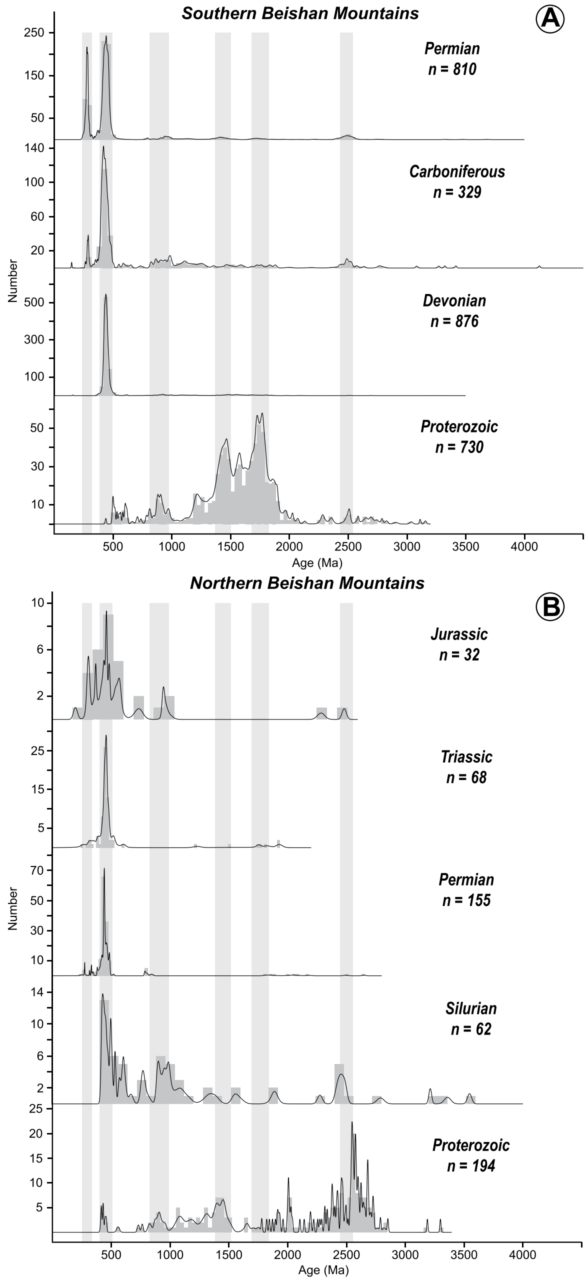

Figure 16. Proterozoic–Mesozoic relative probability plot of detrital zircon data from the southern and northern Beishan orogen in central Asia. Data are from Song et al., 2013c, 2014, 2016; Tian et al., 2013, 2015; Liang et al., 2014; Yang et al., 2016a; Zheng et al., 2018a, 2021; Cleven et al., 2018; Xu et al., 2018b; Yu et al., 2018; Niu et al., 2021b.

(Fig. 16A) (Song et al., 2013c; Zheng et al., 2018a, 2021; Yu et al., 2018). In the North Beishan continent, the sediments contain zircon grains of similar age clusters (Fig. 16B) (Song et al., 2013c; Yang et al., 2016a; Xu et al., 2018b). Based on similar ages of Proterozoic sedimentary rocks located north and south of the Hongliuhe-Xichangjing tectonic zone, we interpret that opening of the Beishan Ocean between the South and North Beishan continents likely occurred within the Greater North China craton (Fig. 17A) (Zuza and Yin, 2017). Proterozoic structures were overprinted during Phanerozoic magmatism and tectonism. In the Cambrian, the Beishan Ocean reached its maximum extent and subduction initiated along its northern boundary. Following subduction initiation, arc magmatic rocks were generated (530–430 Ma) north of the Beishan orogen and the Shibanjing-Xiaohuangshan ocean basin (516–453 Ma) opened in a back-arc extension setting (Figs. 15B and 17B). During Cambrian–Early Silurian oceanic subduction, passive continental margin sediments were deposited on the northern edge of South Beishan continent (Figs. 2 and 15). In the Ordovician–Early Silurian, volcanic arc magmatism initiated as the Beishan Ocean subducted beneath the North Beishan continent. Ordovician–Early Silurian strata were deposited in back-arc and forearc settings to the south and north of the magmatic arc, respectively, along the southern edge of North Beishan continent (Fig. 17C). By ca. 430 Ma, the South Beishan continent collided with the North Beishan continent. The timing of collision is not well constrained, but 430–395 Ma granitoids and volcanic rocks with syn/post-collisional geochemical characteristics were generated shortly afterwards (Fig. 17D) (e.g., Zheng et al., 2012; Ding et al., 2015; Wang et al., 2018b; Li et al., 2020a; Pan et al., 2022). Early Devonian orogenic foreland strata were deposited in lacustrine and alluvial fan environments at this time (e.g., Zuo et al., 1995; Liang et al., 2014, 2020; Niu et al., 2020a). During this collision, passive continental margin strata of the South Beishan continent were juxtaposed against the accretionary wedge, tectonic mélange rocks, and ophiolite complex of the magmatic arc (Fig. 17D).

During Paleo-Asian oceanic subduction, abundant Ordovician–Permian arc magmatic rocks (470–280 Ma) and Silurian–Carboniferous (ultra-)mafic rocks (446–320 Ma) were generated throughout the Beishan orogen. In the $\varepsilon_{Nd}(t)$ and zircon $\varepsilon_{Hf}(t)$ versus crystallization age diagram, Beishan felsic magmatic rocks show a descending trend from 540 to 450 Ma and an ascending trend from 450 to 310 Ma and a further descending trend after ca. 310 Ma (Figs. 12B and 12C). Similarly, in the paleo-crustal thickness versus crystallization age diagram (Sundell et al., 2021), felsic magmatic rocks show a thickening trend from ~40 to ~60⁺ km in the from 540 Ma to 450 Ma, which supports early Paleozoic Beishan oceanic subduction and crustal thickening via magmatic and deformational processes that may reflect more crustal melting and assimilation (Fig. 12), and a thinning trend from ~80 to ~30 km from 450 to 310 Ma, which supports northward rollback of the Paleo-Asian oceanic slab and extensional thinning that may reflect thinner crust and/or more mantle input in the melts (Fig. 12), and a slight thickening trend after ca. 310 Ma, which may be the response of the activity of the Liuyuan Ocean that perhaps was driven by more assimilation and crustal melting (Fig. 12). Northward slab rollback at the south-dipping Paleo-Asian Ocean subduction zone can explain three key observations: (1) the northward-younging trend of arc magmatism throughout the Beishan orogen (Figs. 2, 14E, and 14F); (2) the northward-younging trend of (ultra-)mafic intrusions throughout the Beishan orogen (Figs. 2, 14E, and 14F); and (3) the position of high-pressure rocks within the arc (Fig. 2). Under extension, the upper plate develops basins/rifts that can occur from the backarc to the forearc regions, with crustal thickness

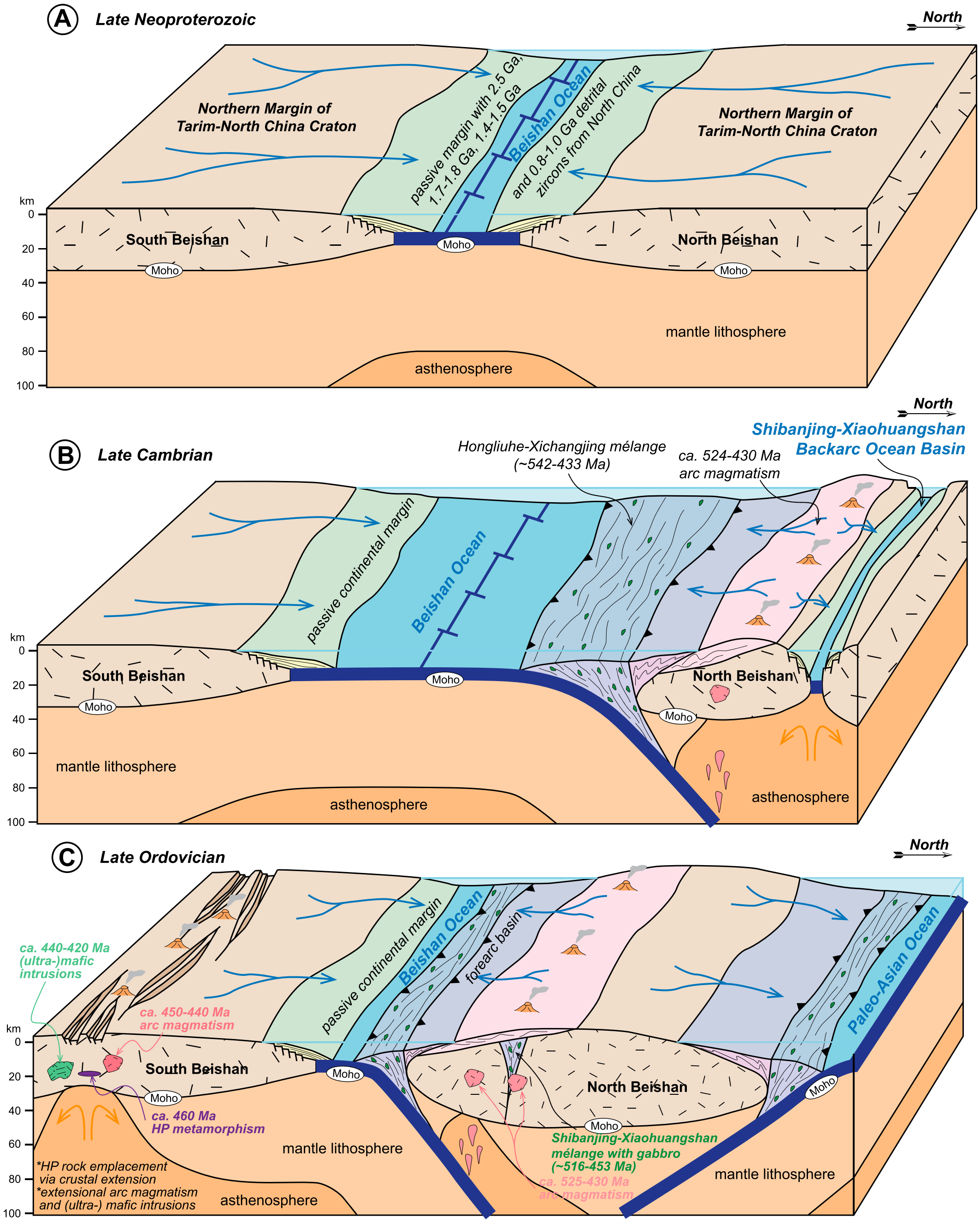

Figure 17. Block models showing the tectonic evolution of the Beishan orogen in central Asia from the late Neoproterozoic through the Early Triassic. Note that the north arrow points to the north in the present-day coordinate system. See text for the details. HP—high pressure.

remaining relatively thin (~30 km) (Ducea et al., 2015). This interpretation is supported by the presence of Late Devonian strata in the south and Permian strata in the north across the Beishan orogen that were deposited in rift basins (Figs. 2 and 15). Protracted extension may have led to the exhumation of the Ordovician high-pressure metamorphic rocks in the Silurian (e.g., Kapp et al., 2000; Yin et al., 2007).

In the Late Carboniferous (ca. 310 Ma), rifting of the South Beishan continent initiated, resulting in the opening of the Liuyuan Ocean along the Cihai-Zhangfangshan tectonic zone (Figs. 2 and 17E). Regionally, coeval volcanic eruptions are exposed extensively along the southern margin of Central Asian Orogenic System from the northern margin of the Tarim block to the northern flanks of the Alxa block and the northern North China craton. Bimodal volcanism and rift-basin development occurred at 310–260 Ma and was followed by subduction and closure (e.g., Chen et al., 2013; Zheng et al., 2014; Wang et al., 2017a). During rift extension, doleritic dike swarms (285–282 Ma) were generated in the South Beishan continent (Fig. 5). The Early Carboniferous–Early Permian strata record a transition in sedimentary environment from a marine tidal flat to continental braided stream, which indicate the presence of a marine rift basin setting (Figs. 8 and 15A) (e.g., Xu et al., 2019a; Niu et al., 2021b). Permian strata show two major detrital zircon age peaks at 250–300 Ma and 400–500 Ma, and two minor age peaks at 800–1000 Ma and ca. 2500 Ma (Fig. 16), reflecting provenance from the local Beishan orogen, although we acknowledge that recycling of older strata may have resulted in this age distribution. The limited unconformity outcrops between Triassic strata and Permian,

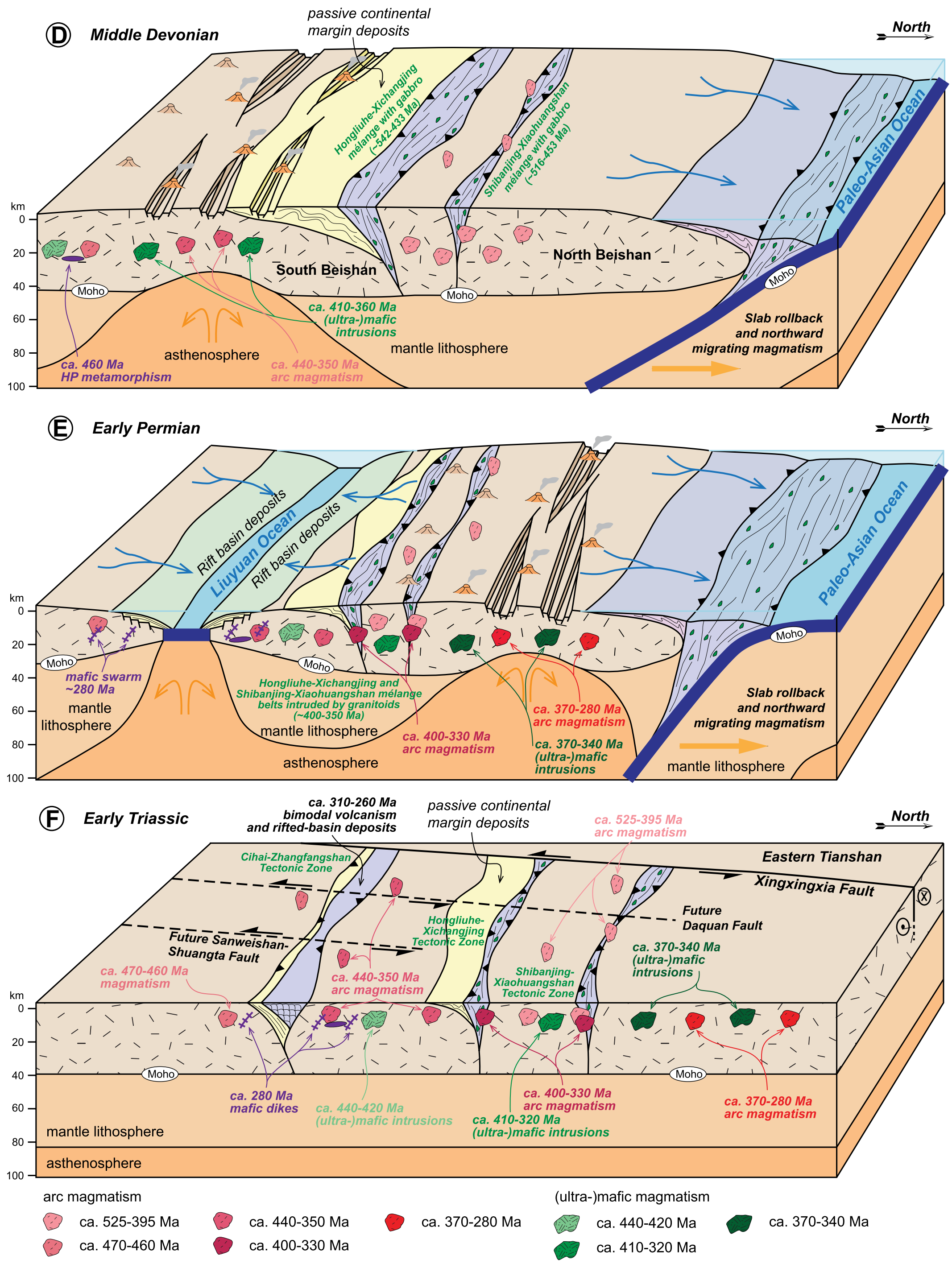

Figure 17. (Continued)

and Triassic lacustrine and alluvial sedimentary environments in southern Beishan indicate the rift was closed (Fig. 17F) (Gansu BGMR, 1989). Meanwhile, folds and faults in Devonian-Permian strata suggest a north-dipping subduction of the Liuyuan Ocean along the Gubaoquan-Hongliuyuan fault (Fig. 6).

After the Permian–Triassic, the Beishan orogen experienced intracontinental deformation associated with the final closure of the Paleo-Asian Ocean in the north and closure of the Tethyan tectonic domain in the south (Fig. 17F) (Zuo et al., 1991; Zheng et al., 1996; Yin and Harrison, 2000; Zhang and Cunningham, 2012; Zuza and Yin, 2017). Middle Jurassic continuous north-south-directed contraction mixed with strike-slip faulting resulted in the exposures of Paleozoic and Precambrian plutons and (meta-) sedimentary rocks and the strong deformation of Mesozoic strata across the Beishan (Zheng et al., 1996; Zhang and Cunningham, 2012; Tian et al., 2013), which is similar to southern Mongolia. Late Jurassic–Early Cretaceous extension affected and controlled the distribution and deformation of Cretaceous deposits across the Beishan and Alxa block. Due to the lack of Cenozoic tectonic activities, the exhumation of the Beishan region is extremely slow, with low relief topography modulated by climate (e.g., Jepson et al., 2021).

In summary, the early Paleozoic history of the Beishan involved a north-dipping subduction system along the Hongliuhe-Xichangjing tectonic zone, which resulted in the formation of early Paleozoic arc magmatic records and back-arc extension in the North Beishan. Later southward subduction of the Paleo-Asian Ocean and northward rollback led to an extensional arc setting with thinning crust and mixed crust-mantle magma petrogenesis. Our model suggests that the final closure site of the southern Paleo-Asian Ocean was the northern extent of the Beishan, also supported by geophysical data evidence (Guy et al., 2015; Comeau et al., 2020).

7. CONCLUSIONS

In this study, we collected new field, geochemical, and geochronological data from the Beishan area. Our new data, when combined with the existing work, led us to propose a tectonics model that involves the following five phases of deformation: (1) Proterozoic rifting that separated the North Beishan block from the Greater North China craton that led to the opening of the Beishan Ocean; (2) Early Paleozoic north-dipping subduction (ca. 530–430 Ma) of the Beishan oceanic plate associated with back-arc extension followed by collision between the North and South Beishan microcontinental blocks; (3) Northward slab rollback of the south-dipping subducting Paleo-Asian oceanic plate at ca. 450–440 Ma along the northern margin of the North Beishan block that led to the formation of a northward-younging extensional continental arc (ca. 470–280 Ma) associated with bimodal igneous activity, which indicates that the westward extension of the Solonker suture is located north of the Hongshishan-Pengboshan tectonic zone; (4) Late Carboniferous opening and Permian north-dipping subduction of the Liuyuan Ocean in the southern Beishan orogen; and (5) Mesozoic-Cenozoic intracontinental deformation induced by the final closure of the Paleo-Asian Ocean system in the north and the Tethyan Ocean system in the south.

ACKNOWLEDGMENTS

This research was supported by grants from the China Geological Survey (nos. DD20160083 and DD20190011), the Basic Science Center for Tibetan Plateau Earth System (no. 41988101-01), the Second Tibetan Plateau Scientific Expedition and Research Program (no. 2019QZKK0708), and the Tectonics Program of the National Science Foundation (Division of Earth Sciences 1914501 and 1914503). Dr. Luojuan Wang, Dr. Yanfei Chen, Dr. Hongxu Chen, and Dr. Ye Wang from Chinese Academy of Geological Sciences are thanked for assistance in the field. We are grateful to Dr. Yahui Yue for her assistance with zircon U-Pb analysis. We appreciate Science Editor Brad Singer, Associate Editor Timothy Kusky, and three Reviewers for their critical, careful, and very constructive reviews that have helped improve the clarity and interpretations of the original manuscript draft.

REFERENCES CITED

An, Y., 2018, Geochemical and tectonic implications of bimodal volcanic rocks in the eastern Beishan Area, Gansu [Masters thesis]: Lanzhou, China, Lanzhou University, 64 p.

Andersen, T., 2002, Correction of common lead in U-Pb analyses that do not report ^{204}Pb: Chemical Geology, v. 192, p. 59–79, https://doi.org/10.1016/S0009-2541(02)00195-X.

Ao, S.J., Xiao, W.J., Han, C.M., Mao, Q.G., and Zhang, J.E., 2010, Geochronology and geochemistry of Early Permian mafic–ultramafic complexes in the Beishan area, Xinjiang, NW China: Implications for late Paleozoic tectonic evolution of the southern Altaids: Gondwana Research, v. 18, no. 2–3, p. 466–478, https://doi.org/10.1016/j.gr.2010.01.004.

Ao, S.J., Xiao, W.J., Han, C.M., Li, X.H., Qu, J.F., Zhang, J.E., Guo, Q.Q., and Tian, Z.H., 2012, Cambrian to early Silurian ophiolite and accretionary processes in the Beishan collage, NW China: Implications for the architecture of the Southern Altaids: Geological Magazine, v. 149, no. 4, p. 606–625, https://doi.org/10.1017/S0016756811000884.

Ao, S.J., Xiao, W.J., Windley, B.F., Mao, Q.G., Han, C.M., Zhang, J.E., Yang, L.K., and Geng, J.Z., 2016, Paleozoic accretionary orogenesis in the eastern Beishan orogen: Constraints from zircon U-Pb and ^{40}Ar/^{39}Ar geochronology: Gondwana Research, v. 30, p. 224–235, https://doi.org/10.1016/j.gr.2015.03.004.

Bai, R.L., Liu, X.F., and Zhou, H.L., 2020, Genesis and tectonic setting of granite in the central region of the Beishan orogenic belt (Gansu section, China) [in Chinese with English abstract]: Acta Petrologica Sinica (Yanshi Xuebao), v. 36, no. 6, p. 1731–1754.

Briggs, S.M., Yin, A., Manning, C.E., Chen, Z.L., Wang, X.F., and Grove, M., 2007, Late Paleozoic tectonic history of the Ertix Fault in the Chinese Altai and its implications for the development of the Central Asian Orogenic System: Geological Society of America Bulletin, v. 119, no. 7–8, p. 944–960, https://doi.org/10.1130/B26044.1.

Briggs, S.M., Yin, A., Manning, C.E., Chen, Z.L., and Wang, X.F., 2009, Tectonic development of the southern Chinese Altai Range as determined by structural geology, thermobarometry, ^{40}Ar/^{39}Ar thermochronology, and Th/Pb ion-microprobe monazite geochronology: Geological Society of America Bulletin, v. 121, no. 9–10, p. 1381–1393, https://doi.org/10.1130/B26385.1.

Bu, T., Yu, J.Y., Guo, L., Wang, G.Q., Guo, L., and Ji, B., 2019, Petrogenesis of the Late Permian granodiorite in southern Dahuoluo area, Beishan, Gansu: Constraints from zircon U-Pb geochronology and geochemistry [in Chinese with English abstract]: Geological Bulletin of China, v. 38, no. 2–3, p. 254–265.

Cecil, M., Rotberg, G.L., Ducea, M.N., Saleeby, J.B., and Gehrels, G.E., 2012, Magmatic growth and batholithic root development in the northern Sierra Nevada, California: Geosphere, v. 8, p. 592–606, https://doi.org/10.1130/GES00729.1.

Charvet, J., Shu, L.S., and Laurent-Charvet, S., 2007, Paleozoic structural and geodynamic evolution of eastern Tianshan (NW China): Welding of the Tarim and Junggar plates: Episodes, v. 30, no. 3, p. 162–186.

Chen, C., Xiu, D., Pan, Z.L., Zhang, H., Zhang, J.L., Li, Q.Z., and Zhuan, S.P., 2017a, Early Paleozoic crustal extensional tectonic regime in the central part of Beishan orogenic belt: new evidence from geochronology and geochemistry of gabbro in Shibanjing [in Chinese with English abstract]: Acta Geologica Sinica, v. 91, no. 8, p. 1661–1673.

Chen, C., Pan, Z.L., Xiu, D., Wei, W.T., Zhang, J.L., Zhang, H., Wang, S., Chang, Z.K., and Wang, R.X., 2017b, Analysis on sedimentary period, depositional environment, and provenance tectonic setting of Hongliuyuan Formation in Beishan area [in Chinese with English abstract]: Chenji Xuebao, v. 35, no. 3, p. 470–479.

Chen, C., Teng, X.J., Pan, Z.L., Xiu, D., He, J.Y., Zhao, H.P., Zhang, H., Zhang, J.L., and Yang, J., 2020a, LA-ICP-MS zircon U-Pb age of A-type granite from the Shibanjing area of middle Beishan orogenic belt, Inner Mongolia, and its constraint on closure time of Beishan Ocean [in Chinese with English abstract]: Geological Bulletin of China, v. 39, no. 9, p. 1448–1460.

Chen, H.D., Wang, Z.L., Jing, Y.Z., Gao, Y., Hao, Z.Y., and Lu, N., 2017c, Geochemical characteristics and age of rhyolite LA-ICP-MS zircon U-Pb in Fengleishan area of Beishan, Inner Mongolia [in Chinese with English abstract]: Geological Survey of China, v. 4, no. 5, p. 48–54.

Chen, H.D., Gao, Y., He, G.Q., Qiu, J.X., and Lu, N., 2020c, LA-ICP-MS zircon U-Pb ages and geochemical characteristics of Sangejing gabbro in Beishan area of Inner Mongolia [in Chinese with English abstract]: Geological Survey of China, v. 7, no. 1, p. 53–59.

Chen, J.P., Liao, Q.A., Luo, T., Zhang, X.H., Guo, D.B., Zhu, H.L., and Liu, X.M., 2013, Zircon U-Pb geochronology and genesis study on the mafic complex from diabase-type iron deposit in Cihai, Beishan area [in Chinese with English abstract]: Geological Science and Technology Information, v. 32, no. 4, p. 76–83.

Chen, S., Guo, Z.J., Qi, J.F., Zhang, Y.Y., Pe-Piper, G., and Piper, D.J.W., 2016, Early Permian volcano-sedimentary successions, Beishan, NW China: Peperites demonstrate an evolving rift basin: Journal of Volcanology and Geothermal Research, v. 309, p. 31–44, https://doi.org/10.1016/j.jvolgeores.2015.11.004.

Chen, X., Wu, Y.S., Zhao, K.D., Zhou, K.F., and Chen, Y.J., 2020b, Age, sediment source and tectonic setting of the ore-hosting Jinwozi Formation at the Jinwozi gold deposit in Beishan Orogen, NW China: Evidence from detrital zircon U-Pb ages and Lu-Hf isotopes: Ore Geology Reviews, v. 117, https://doi.org/10.1016/j.oregeorev.2019.103296.

Chen, X.H., Dong, S.W., Shi, W., Ding, W.C., Zhang, Y.P., Li, B., Shao, Z.G., and Wang, Y., 2022, Construction of the continental Asia in Phanerozoic: A review [English edition]: Acta Geologica Sinica, v. 96, no. 1, p. 26–51, https://doi.org/10.1111/1755-6724.14867.

Chen, Y.Y., Li, J., Bai, C.D., Li, D., Zhang, Z.X., and Lin, Y.M., 2019, Geochemical characteristics and zircon U-Pb age of the intermediate and acid volcanic rocks from Yuanbaoshan area in the northern part of Beishan orogenic belt [in Chinese with English abstract]: Geological Bulletin of China, v. 38, no. 2–3, p. 266–275.

Cheng, H.F., Xu, X.M., Liu, G., Duan, B.X., Xu, C., and Guan, G., 2017, LA-ICP-MS U-Pb geochronology of detrital zircons from the Gudongjing complex group in Pantuoshan area of Beishan region within Inner Mongolia during Changchengian Period and its geological significance [in Chinese with English abstract]: Geological Bulletin of China, v. 36, no. 8, p. 1385–1392.

Cheng, H.F., Xin, H.T., Liang, G.Q., Zhang, Z.P., Zhang, Y., Feng, Y.P., Zhu, W., Ti, Z.H., and Su, P.T., 2018, Geochemical characteristics and LA-ICP-MS zircon U-Pb age of porphyritic granodiorite in Heihongshan area of Beishan region, Inner Mongolia, and their geological significance [in Chinese with English abstract]: Geological Bulletin of China, v. 37, no. 10, p. 1895–1904.

Cheng, X.Y., Teng, X.J., Tian, J., and Duan, X.L., 2020, Geochemical characteristics, isotopic ages and tectonic environment of Sangejing Formation in Beishan orogenic belt, Inner Mongolia [in Chinese with English abstract]: Geological Bulletin of China, v. 39, no. 9, p. 1461–1473.

Clemens, J.D., and Stevens, G., 2016, Melt segregation and magma interactions during crustal melting: Breaking out of the matrix: Earth-Science Reviews, v. 160, p. 333–349, https://doi.org/10.1016/j.earscirev.2016.07.012.

Cleven, N., Lin, S.F., Guilmette, C., Xiao, W.J., and Davis, B., 2015a, Petrogenesis and implications for tectonic setting of Cambrian suprasubduction-zone ophiolitic rocks in the central Beishan orogenic collage, Northwest China: Journal of Asian Earth Sciences, v. 113, p. 369–390, https://doi.org/10.1016/j.jseaes.2014.10.038.

Cleven, N.R., Lin, S.F., and Xiao, W.J., 2015b, The Hongliuhe fold-and-thrust belt: Evidence of terminal collision and suture-reactivation after the Early Permian in the Beishan orogenic collage, Northwest China: Gondwana Research, v. 27, no. 2, p. 796–810, https://doi.org/10.1016/j.gr.2013.12.004.

Cleven, N.R., Lin, S.F., Xiao, W.J., Davis, D.W., and Davis, B., 2018, Successive arc accretion in the southern Central Asian orogenic belt, NW China: Evidence from two Paleozoic arcs with offset magmatic periods: Geological Society of America Bulletin, v. 130, no. 3–4, p. 537–557, https://doi.org/10.1130/B31434.1.

Comeau, M.J., Becken, M., Käufl, J.S., Grayver, A.V., Kuvshinov, A.V., Tserendug, S., Batmagnai, E., and Demberel, S., 2020, Evidence for terrane boundaries and suture zones across Southern Mongolia detected with a 2-dimensional magnetotelluric transect: Earth, Planets, and Space, v. 72, no. 1, https://doi.org/10.1186/s40623-020-1131-6.

Cunningham, D., 2013, Mountain building processes in intracontinental oblique deformation belts: Lessons from the Gobi Corridor, Central Asia: Journal of Structural Geology, v. 46, p. 255–282, https://doi.org/10.1016/j.jsg.2012.08.010.

Cunningham, D., 2017, Folded basinal compartments of the southern Mongolian borderland: A structural archive of the final consolidation of the Central Asian Orogenic Belt: Geosciences, v. 7, no. 1, https://doi.org/10.3390/geosciences7010002.

Ding, J.X., Han, C.M., Xiao, W.J., Wang, Z.M., and Yang, X.M., 2015, Geochemistry and U-Pb geochronology of tungsten deposit of Huaniushan island arc in the Beishan Orogenic Belt, and its geodynamic background [in Chinese with English abstract]: Acta Petrologica Sinica (Yanshi Xuebao), v. 31, no. 2, p. 594–616.

Ding, J.X., Han, C.M., Xiao, W.J., Wang, Z.M., and Song, D.F., 2017, Geochronology, geochemistry and Sr-Nd isotopes of the granitic rocks associated with tungsten deposits in Beishan district, NW China, Central Asian Orogenic Belt: Petrogenesis, metallogenic and tectonic implications: Ore Geology Reviews, v. 89, p. 441–462, https://doi.org/10.1016/j.oregeorev.2017.06.018.

Dong, H.K., Meng, Q.T., Liu, G., Duan, X.L., Ti, Z.H., Zhu, W., Xue, P.Y., Chen, H.F., and Ji, T.Y., 2018, Geochemical characteristics of early Silurian granite from Biaoshan Area in Beishan, Inner Mongolia and their tectonic implications [in Chinese with English abstract]: Northwest Geology, v. 51, no. 1, p. 159–174.

Duan, L.F., Niu, W.C., Zhang, Y., Zhao, Z.L., Zhang, G.Z., Ren, B.F., Li, C.D., and Tu, J.R., 2020, The petrogenesis of quartz diorite (350 Ma) from the Baiheshan area of the Beishan orogenic belt, and its chronological constraint on Hongshishan-Baiheshan Ocean's subduction initiation [in Chinese with English abstract]: Geological Bulletin of China, v. 39, no. 9, p. 1330–1340.

Ducea, M.N., Saleeby, J.B., and Bergantz, G., 2015, The architecture, chemistry, and evolution of continental magmatic arcs: Annual Review of Earth and Planetary Sciences, v. 43, no. 1, p. 299–331, https://doi.org/10.1146/annurev-earth-060614-105049.

Eby, G.N., 1990, The A-type granitoids: A review of their occurrence and chemical characteristics and speculations on their petrogenesis: Lithos, v. 26, p. 115–134, https://doi.org/10.1016/0024-4937(90)90043-Z.

Eby, G.N., 1992, Chemical subdivision of the A-type granitoids: Petrogenetic and tectonic implications: Geology, v. 20, no. 7, p. 641–644, https://doi.org/10.1130/0091-7613(1992)020<0641:CSOTAT>2.3.CO;2.

Eizenhöfer, P.R., Zhao, G., Zhang, J., and Sun, M., 2014, Final closure of the Paleo-Asian Ocean along the Solonker Suture Zone: Constraints from geochronological and geochemical data of Permian volcanic and sedimentary rocks: Tectonics, v. 33, no. 4, p. 441–463, https://doi.org/10.1002/2013TC003357.

Feng, J.C., Zhang, W., Wu, T.R., Zheng, R.G., Luo, H.L., and He, Y.K., 2012, Geochronology and geochemistry of granite pluton in the north of Qiaowan, Beishan Mountain, Gansu Province, China, and its geological significance [in Chinese with English abstract]: Acta Scientiarum Naturalium Universitatis Pekinensis, v. 48, no. 1, p. 61–70.

Fu, P.F., Xia, D., Gong, X.P., Sun, Q.L., Yang, Y., Wei, J., and Zhao, Q., 2020b, LA-ICP-MS zircon U-Pb age, geochemical characteristics and geological significance of Qingbaishan granite in Beishan area, Xinjiang [in Chinese with English abstract]: Xinjiang Geology, v. 38, no. 1, p. 25–31.

Fu, Y.G., Cai, Y.W., Ma, S.M., Xi, M.J., Gao, J.W., and Wang, Z.L., 2020a, Discovery of ~338 Ma Shibanjing plagiogranite in the Beishan Area, NW China, and its geological significance [English edition]: Acta Geologica Sinica, v. 94, no. 2, p. 577–579, https://doi.org/10.1111/1755-6724.14520.

Gansu BGMR, (Gansu Bureau of Geology and Mineral Resources), 1989, Regional geology of Gansu Province [in Chinese with English abstract]: Beijing, China, Geological Publishing House.

Gansu BGMR, (Gansu Bureau of Geology and Mineral Resources), 1996, Stratigraphy (lithostratic) of Gansu Province [in Chinese]: Wuhan, China, China University of Geosciences Press.

Gao, F., Jian, K.K., He, Y.F., Li, N., Yi, P.F., Liu, X.W., and Tang, L., 2018b, Genesis and metallogenic epoch constraints of Luzuizi antimony deposit of Beishan, Inner Mongolia [in Chinese with English abstract]: Mineral Exploration, v. 9, no. 9, p. 1644–1654.

Gao, F., Jian, K.K., Li, N., Du, B., Zhao, D.C., and Yi, P.F., 2018a, Zircon U-Pb dating and geochemistry of Jijiquan pluton in the eastern section of Beishan orogenic belt and their tectonic implications [in Chinese with English abstract]: Northwest Geology, v. 51, no. 3, p. 1644–1654.

Gao, W.B., Qian, Z.Z., Xu, G., Duan, J., Shi, Z., Ma, B.P., and Yang, T., 2020, Geochemical characteristics of Gubaoquan dolerite dykes in Beishan area of Gansu, China and their geological significance [in Chinese with English abstract]: Diqiu Kexue Yu Huanjing Xuebao, v. 42, no. 5, p. 622–636.

Gao, Y., Ding, H.L., Guo, R.J., Liu, Y.Y., and Wang, J.B., 2016, Structural deformation of Gonglujing-Sangejing ductile shear zone in the Beishan orogenic belt, and its geological significance [in Chinese with English abstract]: Geological Survey of China, v. 3, no. 1, p. 26–34.

Gehrels, G.E., Rushmore, M., Woodsworth, G., Crawford, M., Andronicos, C., Hollister, L., Patchett, J., Ducea, M., Butler, R., Klepeis, K., Davidson, C., Friedman, R., Haggart, J., Mahoney, B., Crawford, W., Pearson, D., and Girardi, J., 2009, U-Pb geochronology of the Coast Mountains batholith in north-coastal British Columbia: Constraints on age tectonic evolution: Geological Society of America Bulletin, v. 121, no. 9–10, p. 1341–1361, https://doi.org/10.1130/B26404.1.

Gillespie, J., Glorie, S., Xiao, W.J., Zhang, Z.Y., Collins, A.S., Evans, N., Mclnnes, B., and de Grave, J., 2017, Mesozoic reactivation of the Beishan, southern Central Asian Orogenic Belt: Insights from low-temperature thermochronology: Gondwana Research, v. 43, p. 107–122, https://doi.org/10.1016/j.gr.2015.10.004.

Guan, S., Ren, E.F., Zhao, H.B., Zhu, X.L., Cheng, L., and Wang, H.Y., 2019, LA-ICP-MS zircon U-Pb age and geochemical characteristics of granodiorite in Beishan area, Gansu Province [in Chinese with English abstract]: Journal of Qinghai University, v. 37, no. 2, p. 92–99.

Guo, F., Wang, H.J., Liu, J., and Wang, W.H., 2020, Geochronology, geochemistry of the Shenjing syenitegranite in Mazongshan area, Beishan Mountain, and its geological significance [in Chinese with English abstract]: Modern Mining, v. 36, no. 12, p. 24–30.

Guo, L., Wang, G.Q., Guo, L., and Bu, T., 2018, Petrogenesis of Early Triassic felsic dikes in the Lucaogou area of southern Beishan Orogenic Belt [in Chinese with English abstract]: Bulletin of Mineralogy: Petrology and Geochemistry, v. 37, no. 3, p. 502–512.

Guo, Q.Q., Xiao, W.J., Hou, Q.L., Windley, B.F., Han, C.M., Tian, Z.H., and Song, D.F., 2014, Construction of Late Devonian Dundunshan arc in the Beishan orogen and its implication for tectonics of southern Central Asian Orogenic Belt: Lithos, v. 184–187, p. 361–378, https://doi.org/10.1016/j.lithos.2013.11.007.

Guo, Q.Q., Chung, S.L., Xiao, W.J., Hou, Q.L., and Li, S., 2017, Petrogenesis and tectonic implications of Late Devonian arc volcanic rocks in southern Beishan orogen, NW China: Geochemical and Nd-Sr-Hf isotopic constraints: Lithos, v. 278–281, p. 84–96, https://doi.org/10.1016/j.lithos.2017.01.017.

Guo, Z.J., Zhang, Z.C., Zhang, C., Liu, C., Zhang, Y., Wang, J., and Chen, W.M., 2008, Lateral growth of the Altyn Tagh strike-slip fault at the north margin of the Qinghai-Tibet Plateau: Late Cenozoic strike-slip faults and the crustal stability in the Beishan area, Gansu, China [in Chinese with English abstract]: Geological Bulletin of China, v. 27, no. 10, p. 1678–1686.

Guy, A., Schulmann, K., Janoušek, V., Štípská, P., Armstrong, R., Belousova, E., Dolgopolova, A., Seltmann, R., Lexa, O., Jiang, Y.D., and Hanžl, P., 2015, Geophysical and geochemical nature of relaminated arc-derived lower crust underneath oceanic domain in southern Mongolia: Tectonics, v. 34, p. 1030–1053, https://doi.org/10.1002/2015TC003845.

Hao, Z.Y., Gao, J., Wang, C., Liu, X.D., Li, D.C., and Wang, X.L., 2020, LA-ICP-MS zircon U-Pb dating and tectonic setting of the monzogranites in the Fengleishan area of Beishan orogenic belt, Inner Mongolia [in Chinese with English abstract]: Geology in China, v. 47, no. 4, p. 1204–1219.

He, Z.Y., Zhang, Z.M., Zong, K.Q., and Dong, X., 2013, Paleoproterozoic crustal evolution of the Tarim Craton: Constrained by zircon U-Pb and Hf isotopes of meta-igneous rocks from Korla and Dunhuang: Journal of Asian Earth Sciences, v. 78, p. 54–70, https://doi.org/10.1016/j.jseaes.2013.07.022.

He, Z.Y., Zong, K.Q., Jiang, H.Y., Xiang, H., and Zhang, Z.M., 2014, Early Paleozoic tectonic evolution of the southern Beishan orogenic collage: Insights from the granitoids [in Chinese with English abstract]: Acta Petrologica Sinica (Yanshi Xuebao), v. 30, no. 8, p. 2324–2338.

He, Z.Y., Sun, L.X., Mao, L.J., Zong, K.Q., and Zhang, Z.M., 2015, Zircon U-Pb and Hf isotopic study of gneiss and granodiorite from the southern Beishan orogenic collage: Mesoproterozoic magmatism and crustal growth [in Chinese with English abstract]: Chinese Science Bulletin, v. 60, p. 389–399, https://doi.org/10.1360/N972014-00898.

He, Z.Y., Klemd, R., Yan, L.L., and Zhang, Z.M., 2018, The origin and crustal evolution of microcontinents in the Beishan orogen of the southern Central Asian Orogenic Belt: Earth-Science Reviews, v. 185, p. 1–14, https://doi.org/10.1016/j.earscirev.2018.05.012.

Heubeck, C., 2001, Assembly of central Asia during the middle and late Paleozoic, *in* Hendrix, M.S., and Davis, G.A., eds., Paleozoic and Mesozoic Tectonic Evolution of Central and Eastern Asia: From Continental Assembly to Intracontinental Deformation: Geological Society of America Memoir 194, p. 1–22, https://doi.org/10.1130/0-8137-1194-0.1.

Hou, Q.Y., Wang, Z., Liu, J.B., Wang, J., and Li, D.P., 2012, Geochemistry characteristics and SHRIMP dating of Yueyashan ophiolite in Beishan Orogen [in Chinese with English abstract]: Geoscience, v. 26, no. 5, p. 1008–1018.

Hou, T., Zhang, Z., Santosh, M., Encarnacion, J., and Wang, M., 2013, The Cihai diabase in the Beishan region, NW China: Isotope geochronology, geochemistry and implications for Cornwall-style iron mineralization: Journal of Asian Earth Sciences, v. 70–71, p. 231–249, https://doi.org/10.1016/j.jseaes.2013.03.016.

Hsü, K.J., and Chen, H., 1999, Geologic atlas of China: An application of the tectonic facies concept to the geology of China: New York, USA, Elsevier, 262 p.

Hu, X.Z., Zhao, G.C., Hu, X.Y., Liao, Y.F., and Cheng, H.F., 2015, Geological characteristics, formation epoch and geotectonic significance of the Yueyashan ophiolitic tectonic mélange in Beishan area, Inner Mongolia [in Chinese with English abstract]: Geological Bulletin of China, v. 34, no. 2–3, p. 425–436.

Huang, B.T., Wang, G.Q., Bu, T., Guo, L., Dong, Z.C., Wang, J.L., and He, Z.Y., 2021, Petrogenesis and tectonic significance of the Silurian granites in Yemadaquan area, Beishan, Gansu Province [in Chinese with English abstract]: Earth Science, v. 46, no. 11, p. 3993–4005.

Huang, H., Wang, T., Tong, Y., Qin, Q., Ma, X.X., and Yin, J.Y., 2020, Rejuvenation of ancient micro-continents during accretionary orogenesis: Insights from the Yili Block and adjacent regions of the SW Central Asian Orogenic Belt: Earth-Science Reviews, v. 208, https://doi.org/10.1016/j.earscirev.2020.103255.

Huang, Z.B., and Jin, X., 2006, Tectonic environment of basic volcanic rocks in the Hongshishan ophiolite mélange zone, Beishan Mountains, Gansu [in Chinese with English abstract]: Geology in China, v. 33, no. 5, p. 1030–1037.

Hui, W.D., Zhu, J., Deng, J., Lv, X.B., Mo, Y.L., and Li, C.C., 2013, U-Pb geochronology and geochemical characteristics of rhyolite porphyry in the Baishantang mine, Beishan, Gansu and their geological implications [in Chinese with English abstract]: Geology and Exploration, v. 49, no. 3, p. 484–495.

Huppert, H.E., and Sparks, R.S.J., 1988, The generation of granitic magmas by intrusion of basalt into continental crust: Journal of Petrology, v. 29, p. 599–624, https://doi.org/10.1093/petrology/29.3.599.

Jackson, S.E., Pearson, N.J., Griffin, W.L., and Belousova, E.A., 2004, The application of laser ablation-inductively coupled plasma-mass spectrometry to in situ U-Pb zircon geochronology: Chemical Geology, v. 211, p. 47–69, https://doi.org/10.1016/j.chemgeo.2004.06.017.

Jahn, B.M., Wu, F.Y., and Hong, D.W., 2000, Important crustal growth in the Phanerozoic: Isotopic evidence of granitoids from east-central Asia: Journal of Earth System Science, v. 109, p. 5–20, https://doi.org/10.1007/BF02719146.

Jepson, G., Carrapa, B., Gillespie, J., Feng, R., DeCelles, P.G., Kapp, P., Tabor, C.R., and Zhu, J., 2021, Climate as the great equalizer of continental-scale erosion: Geophysical Research Letters, v. 48, no. 20, https://doi.org/10.1029/2021GL095008.

Jia, Y.Q., Zhao, Z.X., Xu, H., Wang, X.L., Liu, Q., and Wang, J.R., 2016, Zircon LA-ICP-MS U-Pb dating of and tectonic setting of rhyolites from Baishan Formation in Fengleishan area of the Beishan orogenic belt [in Chinese with English abstract]: Geology in China, v. 43, no. 1, p. 91–98.

Jia, Y.Y., Sun, J.M., Lü, L.X., Pang, J.Z., and Wang, Y., 2020, Late Oligocene-Miocene intra-continental mountain building of the Harke Mountains, southern Chinese Tian Shan: Evidence from detrital AFT and AHe analysis: Journal of Asian Earth Sciences, v. 191, https://doi.org/10.1016/j.jseaes.2019.104198.

Jiang, C.Y., Cheng, S.L., Ye, S.F., Xia, M.Z., Jiang, H.B., and Dai, Y.C., 2006, Lithogeochemistry and petrogenesis of Zhongposhanbei mafic rock body, at Beishan region, Xinjiang [in Chinese with English abstract]: Acta Petrologica Sinica (Yanshi Xuebao), v. 22, no. 1, p. 115–126.

Jiang, C.Y., Xia, M.Z., Yu, X., Lu, D.X., Wei, W., and Ye, S.F., 2007, Liuyuan trachybasalt belt in the northeastern Tarim Plate: Products of asthenosphere mantle decompressional melting [in Chinese with English abstract]: Acta Petrologica Sinica (Yanshi Xuebao), v. 23, no. 7, p. 1765–1778.

Jiang, H.Y., He, Z.Y., Zong, K.Q., Zhang, Z.M., and Zhao, Z.D., 2013, Zircon U-Pb dating and Hf isotopic studies on the Beishan complex in the southern Beishan orogenic belt [in Chinese with English abstract]: Acta Petrologica Sinica (Yanshi Xuebao), v. 29, no. 11, p. 3949–3967.

Jin, Y.H., Chang, L., Ji, G., Jia, Y.M., Zhang, P., and Yan, D.H., 2020, Chemical characteristics and metallogenic indications of intrusive rocks in Hongliudaquan area of Beishan [in Chinese with English abstract]: Mineral Exploration, v. 11, no. 1, p. 10–20.

Kang, W.B., Li, W., Kang, L., Dong, Y.P., Jiang, D.Z., Liang, J.W., and Dong, H.Q., 2020, Metamorphism and geochronology of garnet amphibolite from the Beishan Orogen, southern Central Asian Orogenic Belt: Constraints from P-T path and zircon U-Pb dating: Geoscience Frontiers, v. 11, no. 4, p. 1189–1201, https://doi.org/10.1016/j.gsf.2019.10.007.

Kapp, P., Yin, A., Manning, C.E., Murphy, M., Harrison, T.M., Spurlin, M., Ding, L., Deng, X.G., and Wu, C.M., 2000, Blueschist-bearing metamorphic core complexes in the Qiangtang block reveal deep crustal structure of northern Tibet: Geology, v. 28, p. 19–22, https://doi.org/10.1130/0091-7613(2000)28<19:BMCCIT>2.0.CO;2.

Keto, L.S., and Jacobsen, S.B., 1987, Nd and Sr isotopic variations of Early Paleozoic oceans: Earth and Planetary Science Letters, v. 84, p. 27–41, https://doi.org/10.1016/0012-821X(87)90173-7.

Khain, E.V., Bibikova, E.V., Kröner, A., Zhuravlev, D.Z., Sklyarov, E.V., Fedotova, A.A., and Kravchenko-Berezhnoy, I.R., 2002, The most ancient ophiolite of the Central Asian fold belt: U-Pb and Pb-Pb zircon ages for the Dunzhugur Complex, Eastern Sayan, Siberia, and geodynamic implications: Earth and Planetary Science Letters, v. 199, p. 311–325, https://doi.org/10.1016/S0012-821X(02)00587-3.

Kröner, A., Windley, B.F., Badarch, G., Tomurtogoo, O., Hegner, E., Jahn, B.M., Gruschka, S., Khain, E.V., Demoux, A., and Wingate, M.T.D., 2007, Accretionary growth and crust formation in the Central Asian Orogenic Belt and comparison with the Arabian-Nubian shield: Geological Society of America, v. 200, p. 181–209, https://doi.org/10.1130/2007.1200(11).

Kröner, A., Kovach, V., Belousova, E., Hegner, E., Armstrong, R., Dolgopolova, A., Seltmann, R., Alexeiev, D.V., Hoffmann, J.E., Wong, J., Sun, M., Cai, K., Wang, T., Tong, Y., Wilde, S.A., Degtyarev, K.E., and Rytsk, E., 2014, Reassessment of continental growth during the accretionary history of the Central Asian Orogenic Belt: Gondwana Research, v. 25, no. 1, p. 103–125, https://doi.org/10.1016/j.gr.2012.12.023.

Le Maitre, R.W., 1989, A Classification of Igneous Rocks and Glossary of Terms (second edition): Recommendations of the IUGS Commission on the Systematics of Igneous Rocks: Oxford, UK, Blackwell Scientific Publications, 193 p.

Li, J.Y., 2004, Late Neoproterozoic and Paleozoic tectonic framework and evolution of Eastern Xinjiang, NW China [in Chinese with English abstract]: Dizhi Lunping, v. 50, no. 3, p. 304–322.

Li, C.F., Li, X.H., Li, Q.L., Guo, J.H., Li, X.H., and Yang, Y.H., 2012b, Rapid and precise determination of Sr and Nd isotopic ratios in geological samples from the same filament loading by thermal ionization mass spectrometry employing a single-step separation scheme: Analytica Chimica Acta, v. 727, p. 54–60, https://doi.org/10.1016/j.aca.2012.03.040.

Li, J., Tian, Y., Ban, C.Y., Feng, Y.P., Chen, Y.Y., and Li, J.H., 2019a, Geochemical characteristics and chronology of early Late Carboniferous granites in Yuanbaoshan area, Beishan region [in Chinese with English abstract]: Acta Petrologica et Mineralogica, v. 38, no. 2, p. 145–159.

Li, M., Ren, B.F., Teng, X.J., Zhang, Y., Duan, X.L., Niu, W.C., and Duan, L.F., 2018a, Geochemical characteristics, zircon U-Pb age and Hf isotope and geological significance of granitoid in Beishan orogenic belt [in Chinese with English abstract]: Earth Science, v. 43, no. 12, p. 4586–4605.

Li, M., Xin, H.T., Tian, J., Meng, X.F., Pan, Z.L., Chen, C., and Liang, G.Q., 2020a, Composition, age and polarity of Gongpoquan arc and its tectonic significance in Beishan Orogen [in Chinese with English abstract]: Earth Science, v. 45, no. 7, p. 2393–2412.

Li, M., Xin, H.T., Ren, B.F., Ren, Y.W., and Liu, W.G., 2020b, Early–Middle Permian post-collisional granitoids in the northern Beishan orogen, northwestern China: Evidence from U-Pb ages and Sr-Nd-Hf isotopes: Canadian Journal of Earth Sciences, v. 57, no. 6, p. 681–697, https://doi.org/10.1139/cjes-2019-0088.

Li, M., Ren, B.F., Duan, X.L., Tian, J., Duan, L.F., and Niu, W.C., 2020c, Petrogenesis of Triassic granites in Xiaohongshan area, Beishan orogenic belt: Constraints from zircon U-Pb ages and Hf isotopes [in Chinese with English abstract]: Geological Bulletin of China, v. 39, no. 9, p. 1422–1435.

Li, S., Wang, T., Tong, Y., Hong, D.W., and Ou Yang, Z.X., 2009, Identification of the Early Devonian Shuangfengshan A-type granites in Liuyuan area of Beishan and its implications to tectonic evolution [in Chinese with English abstract]: Acta Petrologica et Mineralogica, v. 28, no. 5, p. 407–422.

Li, S., Wang, T., Tong, Y., Wang, Y.B., Hong, D.W., and Ou Yang, Z.X., 2011a, Zircon U-Pb age, origin and its tectonic significances of Huitongshan Devonian K-feldspar granites from Beishan orogen, NW China [in Chinese with English abstract]: Acta Petrologica Sinica (Yanshi Xuebao), v. 27, no. 10, p. 3055–3070.

Li, S., Wang, T., Wilde, S.A., Tong, Y., Hong, D.W., and Guo, Q.Q., 2012a, Geochronology, petrogenesis and tectonic implications of Triassic granitoids from Beishan, NW China: Lithos, v. 134–135, p. 123–145, https://doi.org/10.1016/j.lithos.2011.12.005.

Li, S., Wilde, S.A., and Wang, T., 2013, Early Permian post-collisional high-K granitoids from Liuyuan area in southern Beishan orogen, NW China: Petrogenesis and tectonic implications: Lithos, v. 179, p. 99–119, https://doi.org/10.1016/j.lithos.2013.08.002.

Li, W.C., Zhao, P.B., Luo, Q.Z., Peng, H.L., Zhou, D., Gao, F., and Zhao, D.C., 2018b, Geological characteristics and mineralization age constraint of the Wangxushan tungsten deposit in Beishan, Inner Mongolia [in Chinese with English abstract]: Geology and Exploration, v. 54, no. 4, p. 659–673.

Li, X.F., 2013, Age, geochemical and geological implications of Paleozoic granitoids in the Mazongshan region [Master thesis]: Xi'an, China, Northwest University, 57 p.

Li, X.F., Zhang, C.L., Li, L., Bao, Z.A., Zhang, B.L., and Wei, Q., 2015, Formation age, geochemical characteristics of the Mingshujing pluton in Beishan area of Gansu Province and its geological significance [in Chinese with English abstract]: Acta Petrologica Sinica (Yanshi Xuebao), v. 31, no. 9, p. 2521–2538.

Li, X.M., Yu, J.Y., Wang, G.Q., Wu, P., and Zhou, Z.Q., 2011b, LA-ICP-MS zircon U-Pb dating of Devonian Sangejing Formation and Dundunshan Group in Hongliuyuan, Beishan area, Gansu Province [in Chinese with English abstract]: Geological Bulletin of China, v. 30, no. 10, p. 1501–1507.

Li, X.M., Yu, J.Y., Wang, G.Q., and Wu, P., 2012c, Geochronology of Jijitaizi ophiolite in Beishan area, Gansu Province, and its geological significance [in Chinese with English abstract]: Geological Bulletin of China, v. 31, no. 12, p. 2025–2031.

Li, Z., Zhu, W.B., and Wu, H.L., 2019b, Structural characteristics and chronological constraints on the Yemaquan-Lebaquan ductile shear zone in Mazongshan area, Beishan [in Chinese with English abstract]: Gaoxiao Dizhi Xuebao, v. 25, no. 6, p. 932–942.

Liang, G.B., Ding, S.P., Li, Z.C., Li, R.B., Wang, M., Chen, Y.X., and Pei, X.Z., 2017, Geochronology and geochemistry of Early Devonian-Late Silurian mylonitized quartz diorites from the southern Xiaoxigong in the Beishan area of Gansu Province and their geologic implications [in Chinese with English abstract]: Northwest Geology, v. 50, no. 1, p. 249–260.

Liang, J.W., Chen, Y.L., Zhang, W.Q., Wang, G.Q., Yu, J.Y., and Li, X.M., 2014, Detrital zircon dating of Devonian and geological significance of the Devonian Sangejing Formation in Beishan area, Gansu Province [in Chinese with English abstract]: Geological Science and Technology Information, v. 33, no. 3, p. 1–9.

Liang, J.W., Feng, T.W., Ding, J.G., Ma, X.J., Tao, W.X., Liu, Y.L., Yu, Z.K., Jiang, L.Q., and Chang, X.B., 2020, Research on sedimentary characteristics and tectonic setting of Devonian Sangejing Formation in Beishan, Gansu Province [in Chinese with English abstract]: Chinese Journal of Geology, v. 55, no. 4, p. 1012–1024.

Liu, M.Q., and Zhu, Y.X., 2018, Zircon LA-ICP-MS U-Pb dating of the porphyritic monzonitic granite from southwest Hongyanjing in Beishan area, Gansu Province and its significance [in Chinese with English abstract]: Northwest Geology, v. 51, no. 1, p. 23–33.

Liu, M.Q., Wang, J.J., and Dai, W.J., 2006, The U-Pb age of single-grained zircon from Maanshanbei granite in Hongshishan area of the Beishan orogenic belt, Gansu Province [in Chinese with English abstract]: Acta Petrologica et Mineralogica, v. 25, no. 6, p. 473–479.

Liu, Q., Zhao, G.C., Sun, M., Eizenhöfer, P.R., Han, Y.G., Hou, W.Z., Zhang, X.R., Wang, B., Liu, D.X., and Xu, B., 2015, Ages and tectonic implications of Neoproterozoic ortho- and paragneisses in the Beishan Orogenic Belt, China: Precambrian Research, v. 266, p. 551–578, https://doi.org/10.1016/j.precamres.2015.05.022.

Liu, Q., Zhao, Z.X., Jia, Y.Q., Xu, H., Wang, X.L., and Gao, J., 2019, Geochemical characteristics and LA-ICP-MS zircon U-Pb age of the gabbro in Xiaoheishan of Beishan area, Inner Mongolia [in Chinese with English abstract]: Geological Survey of China, v. 6, no. 1, p. 41–47.

Liu, X.C., Chen, B.L., Jahn, B., Wu, G.G., and Liu, Y.S., 2011, Early Paleozoic (ca. 465 Ma) eclogites from Beishan (NW China) and their bearing on the tectonic evolution of the southern Central Asian Orogenic Belt:

Journal of Asian Earth Sciences, v. 42, p. 715–731, https://doi.org/10.1016/j.jseaes.2010.10.017.
Liu, X.M., Chen, Y.L., Li, D.P., Wang, Z., and Liu, J.B., 2010, The U-Pb ages and Hf isotopes of zircons in the metadiabase and gneissic granite, Beishan orogenic belt, Inner Mongolia, China and its significance [in Chinese with English abstract]: Geological Bulletin of China, v. 29, no. 4, p. 518–529.
Liu, X.Y., and Wang, Q., 1995, Tectonics of orogenic belts in Beishan Mts., western China and their evolution [in Chinese with English abstract]: Dixue Yanjiu, v. 28, p. 37–48.
Liu, Y.S., Gao, S., Yuan, H.L., Zhou, L., Liu, X.M., Wang, X.C., Hu, Z.C., and Wang, L.S., 2004, U-Pb zircon ages and Nd, Sr, and Pb isotopes of lower crustal xenoliths from North China Craton: Insights on evolution of lower continental crust: Chemical Geology, v. 211, p. 87–109, https://doi.org/10.1016/j.chemgeo.2004.06.023.
Lu, J.C., Niu, Y.Z., Wei, X.Y., Chen, G.C., and Li, Y.H., 2013, LA-ICP-MS zircon U-Pb dating of the Late Paleozoic volcanic rocks from the Hongshishan area of the Beishan orogenic belt and its tectonic significances [in Chinese with English abstract]: Acta Petrologica Sinica (Yanshi Xuebao), v. 29, no. 8, p. 2685–2694.
Ludwig, K.R., 2003, User's Manual for Isoplot 3.00: A Geochronological Toolkit for Microsoft Excel: Berkeley Geochronology Center Special Publication, v. 4, 70 p.
Lv, C.L., Yang, F.Q., Luo, J.S., Ma, W.F., Liu, W.X., and Shi, W.M., 2021, Isotopic age of rock mass in Gongpoquan mining area in Beishan of Gansu and its geological significance [in Chinese with English abstract]: Mineral Resources and Geology, v. 35, no. 1, p. 83–89.
Ma, B., Qian, Z., Keays, R.R., Xu, G., Duan, J., Zhang, J., and Gao, W., 2022, Petrogenesis of the Permian Luotuoshan sulfide-bearing mafic-ultramafic intrusion, Beishan Orogenic Belt, NW China: Evidence from whole-rock Sr-Nd-Pb and zircon Hf isotopic geochemistry: Journal of Geochemical Exploration, v. 233, https://doi.org/10.1016/j.gexplo.2021.106920.
Ma, L., Wei, H.F., Wang, H.T., Yang, J., Huo, Y.H., and Zhai, X.W., 2018, Geochemistry, zircon U-Pb chronology and tectonic significance of gabbro in the Hongliugou area in Gansu Province [in Chinese with English abstract]: Journal of Lanzhou University: Natural Sciences, v. 54, no. 1, p. 59–67.
Maniar, P.D., and Piccoli, P.M., 1989, Tectonic discrimination of granitoids: Geological Society of America Bulletin, v. 101, p. 635–643, https://doi.org/10.1130/0016-7606(1989)101<0635:TDOG>2.3.CO;2.
Mao, Q.G., Xiao, W.J., Han, C.M., Sun, M., Yuan, C., Zhang, J.E., Ao, S.J., and Li, J.L., 2010, Discovery of Middle Silurian adakite granite and its tectonic significance in Liuyuan area, Beishan Mountains, NW China [in Chinese with English abstract]: Acta Petrologica Sinica (Yanshi Xuebao), v. 26, no. 2, p. 584–596.
Mao, Q.G., Xiao, W.J., Fang, T.H., Wang, J.B., Han, C.M., Sun, M., and Yuan, C., 2012a, Late Ordovician to early Devonian adakites and Nb-enriched basalts in the Liuyuan area, Beishan, NW China: Implications for early Paleozoic slab-melting and crustal growth in the southern Altaids: Gondwana Research, v. 22, p. 534–553, https://doi.org/10.1016/j.gr.2011.06.006.
Mao, Q.G., Xiao, W.J., Windley, B.F., Han, C.M., Qu, J.F., Ao, S.J., Zhang, J.E., and Guo, Q.Q., 2012b, The Liuyuan complex in the Beishan, NW China: A Carboniferous–Permian ophiolitic fore-arc sliver in the southern Altaids: Geological Magazine, v. 149, no. 3, p. 483–506, https://doi.org/10.1017/S0016756811000811.
Mei, H.L., Yu, H.F., Li, Q., Lu, S.N., Li, H.M., Zuo, Y.C., Zuo, G.C., Ye, D.J., and Liu, J.C., 1999, The first discovery of eclogite and Palaeoproterozoic granitoids in the Beishan area, northwestern Gansu Province, China: Chinese Science Bulletin, v. 44, no. 4, p. 356–361, https://doi.org/10.1007/BF02885491.
Meng, Q.T., Zhang, Z.P., Dong, H.K., and Xu, C., 2021, Chronology, geochemical characteristics and tectonic significance of Aminwusu ophiolite in the Beishan area, Inner Mongolia [in Chinese with English abstract]: Geology and Exploration, v. 57, no. 1, p. 122–135.
Middlemost, E.A.K., 1994, Naming materials in the magma/igneous rock system: Earth-Science Reviews, v. 37, p. 215–224, https://doi.org/10.1016/0012-8252(94)90029-9.
Niu, W.C., Ren, B.F., Ren, Y.W., Duan, X.L., Duan, L.F., Sun, L.X., Li, M., and Zhang, J.H., 2019, Neoproterozoic magmatic records in the North Beishan Orogenic Belt: Evidence of the gneissic granites from the Hazhu area, Inner Mongolia [in Chinese with English abstract]: Earth Science, v. 44, no. 1, p. 284–297.
Niu, W.C., Xin, H.T., Duan, L.F., Zhao, Z.L., Zhang, G.Z., Ren, B.F., and Zhang, Y., 2020b, Geochemical characteristics, zircon U-Pb age of SSZ ophiolite in the Baiheshan area of the Beishan orogenic belt, Inner Mongolia, and its indication for the evolution of the Paleo-Asian Ocean [in Chinese with English abstract]: Geological Bulletin of China, v. 39, no. 9, p. 1317–1329.
Niu, Y.Z., Wei, J.S., Shi, J.Z., and Chen, G.C., 2013, LA-ICP-MS zircon U-Pb dating of the Upper Carboniferous volcanic rocks from northern Beishan region in Gansu Province and its tectonic significance [in Chinese with English abstract]: Geological Bulletin of China, v. 32, no. 11, p. 1720–1727.
Niu, Y.Z., Lu, J.C., Wei, J.S., Chen, G.C., Shi, J.Z., and Wu, J., 2014, Chronology of the Lvtiaoshan Formation in the Beishan area and its tectonic significances [in Chinese with English abstract]: Dizhi Lunping, v. 60, no. 3, p. 567–575, https://doi.org/10.16509/j.georeview.2014.03.009.
Niu, Y.Z., Lu, J.C., Liu, C.Y., Xu, W., Shi, J.Z., and Song, B., 2018a, Geochronology and distribution of the Upper Carboniferous-Lower Permian Ganquan Formation in the Beishan Region, northwestern China and its tectonic implication [in Chinese with English abstract]: Dizhi Lunping, v. 64, no. 4, p. 1131–1148.
Niu, Y.Z., Lu, J.C., Liu, C.Y., Song, B., Shi, J.Z., and Xu, W., 2018b, Chronostratigraphy and regional comparison of marine Permian System in the Beishan Region, North China [in Chinese with English abstract]: Acta Geologica Sinica, v. 92, no. 6, p. 1131–1148.
Niu, Y.Z., Song, B., Zhou, J.L., Xu, W., Shi, J.Z., Zhang, Y.X., and Lu, J.C., 2020a, Lithofacies and chronology of volcano-sedimentary sequence in the southern Beishan Region, Central Asian Orogenic Belt and its paleogeographical implication [in Chinese with English abstract]: Acta Geologica Sinica, v. 94, no. 2, p. 615–633.
Niu, Y.Z., Shi, G.R., Ji, W.H., Zhou, J.L., Wang, J.Q., Wang, K., Bai, J.K., and Yang, B., 2021a, Paleogeographic evolution of a Carboniferous–Permian sea in the southernmost part of the Central Asian Orogenic Belt, NW China: Evidence from microfacies, provenance and paleobiogeography: Earth-Science Reviews, v. 220, https://doi.org/10.1016/j.earscirev.2021.103738.
Niu, Y.Z., Shi, G.R., Wang, J.Q., Liu, C.Y., Zhou, J.L., Lu, J.C., Song, B., and Xu, W., 2021b, The closing of the southern branch of the Paleo-Asian Ocean: Constraints from sedimentary records in the southern Beishan Region of the Central Asian Orogenic Belt, NW China: Marine and Petroleum Geology, v. 124, https://doi.org/10.1016/j.marpetgeo.2020.104791.
Pan, Z.L., Zhang, H., Chen, C., Wang, S., Zhang, J.L., Tian, F.Y., Liu, C., Zhang, L.G., and Li, Q.Z., 2017a, Zircon U-Pb geochronology and Lu-Hf isotope compositions of porphyritic syenite granite from Aobaohuturen in Beishan, Inner Mongolia and its tectonic implication [in Chinese with English abstract]: Chinese Journal of Geology, v. 52, no. 1, p. 301–316.
Pan, Z.L., Wang, S., Qiu, Z., Zhang, H., Zhang, J.L., Tian, F.Y., Li, Q.Z., and Ji, H., 2017b, Geochemistry, zircon U-Pb ages and Hf isotopes of the Early Carboniferous Hongliuyuan volcanic rocks in Xianshuigou, Beishan area, Inner Mongolia [in Chinese with English abstract]: Geological Survey and Research, v. 40, no. 2, p. 99–108.
Pan, Z.L., Wang, S., Zhang, L.G., Zhang, H., Zhang, J.L., and Hou, D.H., 2022, Early Silurian magma evolution in the eastern Beishan orogenic belt: Geochemical and geochronological constraints from the Jidong granodiorite [in Chinese with English abstract]: Journal of Hebei Geo University, v. 44, no. 6, p. 1–10.
Pearce, J.A., Harris, N.W., and Tindle, A.G., 1984, Trace element discrimination diagrams for the tectonic interpretation of granitic rocks: Journal of Petrology, v. 25, p. 956–983, https://doi.org/10.1093/petrology/25.4.956.
Pearce, T.H., Gorman, B.E., and Birkett, T.C., 1975, The TiO_2-K_2O-P_2O_5 diagram: A method of discriminating between oceanic and non-oceanic basalts: Earth and Planetary Science Letters, v. 24, p. 419–426, https://doi.org/10.1016/0012-821X(75)90149-1.
Profeta, L., Ducea, M.N., Chapman, J.B., Paterson, S.R., Henriquez Gonzales, S.M., Kirsch, M., Petrescu, L., and DeCelles, P.G., 2016, Quantifying crustal thickness over time in magmatic arcs: Scientific Reports, v. 5, https://doi.org/10.1038/srep17786.
Qi, Q., Wang, Y.H., Yu, J.Y., Liu, D.M., Guo, L., Ji, B., Feng, M.X., Yang, J.G., and Wang, L., 2017, Geochronology, geochemistry and tectonic significance of diabase dike swarms in Beishan, Gansu [in Chinese with English abstract]: Xinjiang Geology, v. 35, no. 1, p. 99–106.
Qin, K.Z., Su, B.X., Sakyi, P.A., Tang, D.M., Li, X.H., Sun, H., Xiao, Q.H., and Liu, P.P., 2011, SIMS zircon U-Pb geochronology and Sr-Nd isotopes of Ni-Cu-bearing mafic-ultramafic intrusions in eastern Tianshan and Beishan in correlation with flood basalts in Tarim Basin (NW China): Constraints on a ca. 280 Ma mantle plume: American Journal of Science, v. 311, p. 237–260, https://doi.org/10.2475/03.2011.03.
Qu, C.X., Yang, X.K., He, H.J., Gao, P., and Song, H.Y., 2013, Geochemical features and ages of the intrusive rocks from Yantan belt in Beishan area of Xinjiang and their geological implications [in Chinese with English abstract]: Geology in China, v. 40, no. 5, p. 1409–1420.
Qu, J.F., Xiao, W.J., Windley, B.F., Han, C.M., Mao, Q.G., Ao, S.J., and Zhang, J.E., 2011, Ordovician eclogites from the Chinese Beishan: Implications for the tectonic evolution of the southern Altaids: Journal of Metamorphic Geology, v. 29, p. 803–820, https://doi.org/10.1111/j.1525-1314.2011.00942.x.
Ren, B.F., Ren, Y.W., Niu, W.C., Duan, L.F., Sun, L.X., Li, M., Tian, J., Duan, X.L., and Zhang, Y.Q., 2019b, Zircon U-Pb ages and Hf isotope characteristics of the volcanic rocks from Queershan Group in the Hazhudongshan area of Beishan, Inner Mongolia and their geological significance [in Chinese with English abstract]: Earth Science, v. 44, no. 1, p. 298–311.
Ren, Y.W., Ren, B.F., Niu, W.C., Sun, L.X., Li, M., Zhang, K., Zhang, J.H., and Duan, L.F., 2019a, Carboniferous volcanics from the Beishan formation in the Hazhu area, Inner Mongolia: Implications for the Late Paleozoic active continental margin magmatism in the Northern Beishan [in Chinese with English abstract]: Earth Science, v. 44, no. 1, p. 312–327.
Saktura, W.M., Buckman, S., Nutman, A.P., Belousova, E.A., Yan, Z., and Aitchison, J.C., 2017, Continental origin of the Gubaoquan eclogite and implications for evolution of the Beishan Orogen, Central Asian Orogenic Belt, NW China: Lithos, v. 294–295, p. 20–38, https://doi.org/10.1016/j.lithos.2017.10.004.
Şengör, A.M.C., 1984, The Cimmeride orogenic system and the tectonics of Eurasia: Geological Society of America Special Papers, v. 195, 74 p., https://doi.org/10.1130/SPE195-p1.
Şengör, A.M.C., and Natal'in, B.A., 1996, Turkic-type orogeny and its role in the making of the continental crust: Annual Review of Earth and Planetary Sciences, v. 24, p. 263–337, https://doi.org/10.1146/annurev.earth.24.1.263.
Şengör, A.M.C., Natal'in, B.A., and Burtman, V.S., 1993, Evolution of the Altaid tectonic collage and Palaeozoic crustal growth in Eurasia: Nature, v. 364, p. 299–307, https://doi.org/10.1038/364299a0.
Şengör, A.M.C., Natal'in, B.A., Sunal, G., and van der Voo, R., 2018, The tectonics of the Altaids: Crustal growth during the construction of the continental lithosphere of central asia between ∼750 and ∼130 Ma ago: Annual Review of Earth and Planetary Sciences, v. 46, no. 1, p. 439–494, https://doi.org/10.1146/annurev-earth-060313-054826.
Shaanxi, I.G.S., (Shaanxi Institute of Geological Survey), 2014, Geological map of Xingxingxia sheet People's Republic of China, scale 1:250,000 [in Chinese].
Shan, L., Xu, R.K., Zheng, Y.Y., Zhang, Y.L., Cao, L., and Pang, Y.C., 2013, Zircon LA-ICP-MS U-Pb chronology of magmatic rock in the Baishantang copper polymetal-

lic deposit of Beishan area, Northwest China [in Chinese with English abstract]: Geology in China, v. 40, no. 5, p. 1600–1611.
Shi, Y.R., Zhang, W., Kröner, A., Li, L.L., and Jian, P., 2018, Cambrian ophiolite complexes in the Beishan area, China, southern margin of the Central Asian Orogenic Belt: Journal of Asian Earth Sciences, v. 153, p. 193–205, https://doi.org/10.1016/j.jseaes.2017.05.021.
Soldner, J., Yuan, C., Schulmann, K., Štípská, P., Jiang, Y., Zhang, Y., and Wang, X., 2020a, Grenvillean evolution of the Beishan Orogen, NW China: Implications for development of an active Rodinian margin: Geological Society of America Bulletin, v. 132, no. 7–8, p. 1657–1680, https://doi.org/10.1130/B35404.1.
Soldner, J., Štípská, P., Schulmann, K., Yuan, C., Anczkiewicz, R., Sala, D., Jiang, Y.D., Zhang, Y.Y., and Wang, X.Y., 2020b, Coupling of P-T-t-D histories of eclogite and metagreywacke: Insights to late Ordovician–Silurian crustal folding events recorded in the Beishan Orogen (NW China): Journal of Metamorphic Geology, v. 38, no. 6, p. 555–591, https://doi.org/10.1111/jmg.12531.
Song, D.F., Xiao, W.J., Han, C.M., Li, J.L., Qu, J.F., Guo, Q.Q., Li, L.N., and Wang, Z.M., 2013a, Progressive accretionary tectonics of the Beishan orogenic collage, southern Altaids: Insights from zircon U-Pb and Hf isotopic data of high-grade complexes: Precambrian Research, v. 227, p. 368–388, https://doi.org/10.1016/j.precamres.2012.06.011.
Song, D.F., Xiao, W.J., Han, C.M., and Tian, Z.H., 2013b, Geochronological and geochemical study of gneiss-schist complexes and associated granitoids, Beishan Orogen, southern Altaids: International Geology Review, v. 55, no. 14, p. 1705–1727, https://doi.org/10.1080/00206814.2013.792515.
Song, D.F., Xiao, W.J., Han, C.M., Tian, Z.H., and Wang, Z.M., 2013c, Provenance of metasedimentary rocks from the Beishan orogenic collage, southern Altaids: Constraints from detrital zircon U-Pb and Hf isotopic data: Gondwana Research, v. 24, no. 3–4, p. 1127–1151, https://doi.org/10.1016/j.gr.2013.02.002.
Song, D.F., Xiao, W.J., Han, C.M., and Tian, Z.H., 2014, Polyphase deformation of a Paleozoic forearc–arc complex in the Beishan orogen, NW China: Tectonophysics, v. 632, p. 224–243, https://doi.org/10.1016/j.tecto.2014.06.030.
Song, D.F., Xiao, W.J., Windley, B.F., Han, C.M., and Tian, Z.H., 2015, A Paleozoic Japan-type subduction-accretion system in the Beishan orogenic collage, southern Central Asian Orogenic Belt: Lithos, v. 224–225, p. 195–213, https://doi.org/10.1016/j.lithos.2015.03.005.
Song, D.F., Xiao, W.J., Windley, B.F., Han, C.M., and Yang, L., 2016, Metamorphic complexes in accretionary orogens: Insights from the Beishan collage, southern Central Asian Orogenic Belt: Tectonophysics, v. 688, p. 135–147, https://doi.org/10.1016/j.tecto.2016.09.012.
Sun, H.R., Lv, Z.C., Yu, X.F., Li, Y.S., Du, Z.Z., Lv, X., Du, Y.L., and Gong, F.Y., 2020a, Early Mesozoic tectonic evolution of Beishan Orogenic Belt: Constraints from chronology and geochemistry of the Late Triassic diabase dyke in Liuyuan area, Gansu Province [in Chinese with English abstract]: Acta Petrologica Sinica (Yanshi Xuebao), v. 36, no. 6, p. 1755–1768.
Sun, H.R., Lv, Z.C., Yu, X.F., Li, Y.S., Du, Z.Z., Lv, X., and Gong, F.Y., 2020b, Late Paleozoic tectonic evolution of Beishan orogenic belt: chronology and geochemistry constraints of Early Permian syenogranitic porphyry dyke in Liuyuan area, Gansu Province [in Chinese with English abstract] [Earth Science edition]: Journal of Jilin University, v. 50, no. 5, p. 1433–1449.
Sun, L.X., Zhang, J.H., Ren, B.F., Niu, W.C., Ren, Y.W., and Zhang, K., 2017, Geochemical characteristics and U-Pb age of Baiyunshan ophiolite mélange in the Beishan orogenic belt and their geological implications [in Chinese with English abstract]: Acta Petrologica et Mineralogica, v. 36, no. 2, p. 131–147.
Sun, Q.L., Xia, D., and Gong, X.P., 2020c, Genesis and tectonic environment of Qingbaishan granite in Beishan, Xinjiang [in Chinese with English abstract]: Xinjiang Geology, v. 38, no. 3, p. 298–304.
Sun, S.S., and McDonough, W.F., 1989, Chemical and isotopic systematics of oceanic basalts: implications for mantle composition and processes, *in* Saunders, A.D., and Norry, M.J., eds., Magmatism in the Ocean Basins: Geological Society of London, Special Publications, v. 42, no. 1, p. 313–345, https://doi.org/10.1144/GSL.SP.1989.042.01.19.
Sun, X.C., Wang, H.T., Li, T.G., Wei, H.F., Xu, L., and Wang, X.W., 2021, LA-ICP-MS zircon U-Pb ages of the granodiorites from Shuangfengshan in Beishan Mountain, Gansu Province, and its tectonic significance [in Chinese with English abstract]: Acta Petrologica et Mineralogica, v. 40, no. 2, p. 171–184.
Sundell, K.E., Laskowski, A.K., Kapp, P.A., Ducea, M.N., and Chapman, J.B., 2021, Jurassic to Neogene quantitative crustal thickness estimates in southern Tibet: GSA Today, v. 31, no. 6, p. 4–10, https://doi.org/10.1130/GSATG461A.1.
Tao, G.H., Li, X.F., Chen, W.L., Chen, W., Lu, G., Hao, C., Pan, S., and Wu, K.N., 2022, The geochemical characteristics and tectonic of Devonian bimodal volcanic rocks in Yemaquan area, Beishan area, Inner Mongolia and their implications for early Paleozoic tectonic evolution in Beishan [in Chinese with English abstract]: Geological Bulletin of China, (in press).
Tian, J., Teng, X.J., Xin, H.T., Duan, X.L., Cheng, X.Y., Zhang, Y., and Ren, B.F., 2020a, Structure, composition and ages of ophiolitic mélanges in the Baiyunshan area, Beishan Orogenic Belt [in Chinese with English abstract]: Acta Petrologica Sinica (Yanshi Xuebao), v. 36, no. 12, p. 3741–3756.
Tian, J., Xin, H.T., Teng, X.J., Duan, X.L., Cheng, X.Y., Zhang, Y., and Ren, B.F., 2020b, The determination of volcanic rocks in Upper Devonian Dundunshan formation in the Baiyunshan area of Beishan orogenic belt, Inner Mongolia [in Chinese with English abstract]: Acta Petrologica Sinica (Yanshi Xuebao), v. 36, no. 2, p. 509–525.
Tian, J., Xin, H.T., Teng, X.J., Duan, X.L., Cheng, X.Y., Zhang, Y., and Ren, B.F., 2020c, The tectonic implication of Hongliuhe-Xichangjing ophiolitic mélanges belt in the central of Beishan Orogen, NW China: Constraints by the U-Pb ages of detrital zircons of the metasandstones: Acta Geologica Sinica-English Edition, v. 94, no. 4, p. 1256–1275, https://doi.org/10.1111/1755-6724.14571.
Tian, Y., Li, J., Ban, C.Y., Yang, J.Y., and Zhou, J., 2020d, Petrogeochemistry of Late Permian calc-alkaline intrusive rocks in Tamusu area of Alxa and its significances [in Chinese with English abstract]: China Mining Magazine, v. 29, p. 251–255.
Tian, Z.H., Xiao, W.J., Shan, Y.H., Windley, B., Han, C.H., Zhang, J.E., and Song, D.F., 2013, Mega-fold interference patterns in the Beishan orogen (NW China) created by change in plate configuration during Permo-Triassic termination of the Altaids: Journal of Structural Geology, v. 52, p. 119–135, https://doi.org/10.1016/j.jsg.2013.03.016.
Tian, Z.H., Xiao, W.J., Windley, B.F., Lin, L.N., Han, C.M., Zhang, J.E., Wan, B., Ao, S.J., Song, D.F., and Feng, J.Y., 2014, Structure, age, and tectonic development of the Huoshishan–Niujuanzi ophiolitic mélange, Beishan, southernmost Altaids: Gondwana Research, v. 25, p. 820–841, https://doi.org/10.1016/j.gr.2013.05.006.
Tian, Z.H., Xiao, W.J., Sun, J.M., Windley, B.F., Glen, R., Han, C.M., Zhang, Z.Y., Zhang, J.E., Wan, B., Ao, S.J., and Song, D.F., 2015, Triassic deformation of Permian Early Triassic arc-related sediments in the Beishan (NW China): Last pulse of the accretionary orogenesis in the southernmost Altaids: Tectonophysics, v. 662, p. 363–384, https://doi.org/10.1016/j.tecto.2015.01.009.
Tian, Z.H., Xiao, W.J., Zhang, Z.Y., and Lin, X., 2016, Fission-track constrains on superposed folding in the Beishan orogenic belt, southernmost Altaids: Geoscience Frontiers, v. 7, no. 2, p. 181–196, https://doi.org/10.1016/j.gsf.2015.11.007.
Tian, Z.H., Xiao, W.J., Windley, B.F., Huang, P., Zhang, J.E., Ao, S.J., Zhang, Z.Y., Song, D.F., and Liu, F.L., 2021, Two key switches in regional stress field during multi-stage deformation in the Carboniferous−Triassic southernmost Altaids (Beishan, NW China): Response to orocline-related roll-back processes: Geological Society of America Bulletin, v. 133, no. 11–12, p. 2591–2611, https://doi.org/10.1130/B35898.1.
Turner, S.P., Foden, J.D., and Morrison, R.S., 1992, Derivation of some A-type magmas by fractionation of basaltic magma: An example from the Padthaway Ridge, South Australia: Lithos, v. 28, p. 151–179, https://doi.org/10.1016/0024-4937(92)90029-X.
Wang, B.R., Yang, X.S., Li, S.C., Teng, C., Yang, X.J., Huang, F.Y., Cao, J., Yang, B., Zhang, X.F., and Zhou, Y., 2021a, Age, depositional environment, and tectonic significance of an Early Neoproterozoic volcano-sedimentary sequence in the eastern Beishan orogenic belt, southern Central Asian Orogenic Belt: Geological Journal, v. 56, no. 3, p. 1346–1357, https://doi.org/10.1002/gj.3985.
Wang, B.R., Yang, X.S., Li, S.C., Teng, C., Yang, X.J., Huang, F.Y., Zhang, X.F., Cao, J., Zhou, Y., Zhang, H.C., and Li, J., 2021b, Geochronology, geochemistry, and tectonic implications of early Neoproterozoic granitic rocks from the eastern Beishan Orogenic Belt, southern Central Asian Orogenic Belt: Precambrian Research, v. 352, https://doi.org/10.1016/j.precamres.2020.106016.
Wang, G.Q., 2015, The research of the Paleozoic ophiolites and volcanic rocks and the tectonic evolution in the Beishan area (Northwest China) [Ph.D. thesis]: Xi'an, China, Chang'an University, 139 p.
Wang, G.Q., Li, X.M., Xu, X.Y., Yu, J.Y., and Wu, P., 2014b, Zircon U-Pb chronological study of the Hongshishan ophiolite in the Beishan area and their tectonic significance [in Chinese with English abstract]: Acta Petrologica Sinica (Yanshi Xuebao), v. 30, no. 6, p. 1685–1694.
Wang, H., Zhang, H., Pan, Z.L., Wang, S., He, J.Y., Zhang, J.L., Hou, D.H., Ma, M.L., and Liu, Y.F., 2021c, Geochemistry and geochronology of Hariama island arc granitoids in Beishan area of Inner Mongolia: Geological implication [in Chinese with English abstract]: Geology and Resources, v. 30, no. 2, p. 103–117.
Wang, H.J., Guo, F., Zhao, H.B., Liu, J., and Wang, W.H., 2020d, Determination of Silurian intrusive rocks in Mazongshan area, Beishan, Gansu and its tectonic significance [in Chinese with English abstract]: Gansu Geology, v. 29, no. 3–4, p. 13–21.
Wang, H.J., Guo, F., Zhao, H.B., Liu, J., and Wang, W.H., 2021d, Determination of Silurian granites in Beishan, Gansu and its tectonic significance [in Chinese with English abstract]: Modern Mining, v. 37, no. 3, p. 1–5.
Wang, J.T., Dong, Y.P., Zeng, Z.C., Yang, Z., Sun, S.S., Zhang, F.F., Zhou, B., and Sun, J.P., 2016, Geochronology, geochemistry and geological significance of the Huangcaotan pluton in the southern Beishan Orogenic Belt [in Chinese with English abstract]: Geoscience, v. 30, no. 5, p. 937–949.
Wang, J.X., Zhang, K.X., Windley, B.F., Song, B.W., Kou, X.H., Wang, S.D., and Wang, L.J., 2020a, A mid-Palaeozoic ocean-continent transition in the Mazongshan subduction-accretion complex, Beishan, NW China: New structural, chemical and age data constrain the petrogenesis and tectonic evolution: Geological Magazine, v. 157, no. 11, p. 1877–1897, https://doi.org/10.1017/S0016756820000114.
Wang, L., Yang, J.G., Wang, X.H., Qi, Q., and Xie, X., 2017b, SHRIMP zircon U-Pb age of the Dashantounan granodiorite from Beishan Mountains in Gansu Province and its significance [in Chinese with English abstract]: Northwest Geology, v. 50, no. 4, p. 41–50.
Wang, L.S., Yang, J.G., Xie, C.L., Lei, Y.X., Wang, Y.X., Cao, H.X., Yang, P.F., Qi, Y.L., and Jin, S.L., 2009a, Geochronology and geochemistry of Haergentoukoubu granites in the Beishan area, Gansu, China and their geological significance [in Chinese with English abstract]: Acta Geologica Sinica, v. 83, no. 3, p. 377–387.
Wang, L.S., Yang, J.G., Wang, Y.X., Lei, Y.X., Xie, C.L., Cao, H.X., Yang, P.F., Qi, Y.L., and Gao, M., 2009b, Isotopic dating of basalt from Gongpoquan Group in Yingmaotuo area of the Beishan Mountain, Gansu Province, and its geological significance [in Chinese with English abstract]: Acta Geoscientica Sinica, v. 30, no. 3, p. 363–368.
Wang, S.D., Zhang, K.X., Song, B.W., Li, S.C., Li, M., and Zhou, J., 2018a, Geochronology and geochemistry of

the Niujuanzi ophiolitic mélange, Gansu Province, NW China: Implications for tectonic evolution of the Beishan Orogenic Collage: International Journal of Earth Sciences, v. 107, no. 1, p. 269–289, https://doi.org/10.1007/s00531-017-1489-2.

Wang, S.D., Zhang, K.X., Song, B.W., Li, S.C., Li, J.X., Yu, J.Y., and Bu, J.J., 2018d, Detrital zircon U-Pb Geochronology from greywackes in the Niujuanzi ophiolitic mélange, Beishan Area, NW China: Provenance and tectonic implications: Journal of Earth Science, v. 29, no. 1, p. 103–113, https://doi.org/10.1007/s12583-018-0824-2.

Wang, S.D., Zhang, K.X., Chen, F.N., Wang, J.X., Song, B.W., Li, J.X., Wang, W., and Dai, P., 2021e, Recognition of a Permian to Triassic foreland basin in the central Beishan Orogen, NW China: Provenance variations and their constraints on latest Palaeozoic orogeny: Palaeogeography, Palaeoclimatology, Palaeoecology, v. 565, https://doi.org/10.1016/j.palaeo.2020.110168.

Wang, X.Y., Yuan, C., Long, X.P., Zhang, Y.Y., and Lin, Z.F., 2018c, Geochronological, geochemical, and geological significance of Jianshan and Shibanjing granites in the Gongpoquan Arc, Beishan Orogenic Belt [in Chinese with English abstract]: Geochimica, v. 47, no. 1, p. 63–78.

Wang, X.Y., Yuan, C., Zhang, Y.Y., Long, X.P., Sun, M., Wang, L.X., Soldner, J., and Lin, Z.F., 2018b, S-type granite from the Gongpoquan arc in the Beishan Orogenic Collage, southern Altaids: Implications for the tectonic transition: Journal of Asian Earth Sciences, v. 153, p. 206–222, https://doi.org/10.1016/j.jseaes.2017.07.037.

Wang, Y., Sun, G.H., and Li, J.Y., 2010, U-Pb (SHRIMP) and $^{40}Ar/^{39}Ar$ geochronological constraints on the evolution of the Xingxingxia shear zone, NW China: A Triassic segment of the Altyn Tagh fault system: Geological Society of America Bulletin, v. 122, no. 3–4, p. 487–505, https://doi.org/10.1130/B26347.1.

Wang, Y., Luo, Z.H., Santosh, M., Wang, S.Z., and Wang, N., 2017a, The Liuyuan Volcanic Belt in NW China revisited: Evidence for Permian rifting associated with the assembly of continental blocks in the Central Asian Orogenic Belt: Geological Magazine, v. 154, no. 2, p. 265–285, https://doi.org/10.1017/S0016756815001077.

Wang, Y.H., Zhang, F.F., Li, B.C., Xue, C.J., Liu, J.J., Zhao, Y., and Zhang, W., 2020b, Geology and genesis of the Cihai mafic intrusions in Beishan Terrane, Xinjiang, Northwest China: Implication for iron mineralization and tectonic setting: Ore Geology Reviews, v. 121, https://doi.org/10.1016/j.oregeorev.2020.103573.

Wang, Y.X., Hou, L., Zhou, Q.H., Quan, S.C., Li, W.M., and Yang, S.F., 2014a, The discussion of the granite genesis in Gansu Beishan Shibanjing Area [in Chinese with English abstract]: Xinjiang Geology, v. 32, no. 3, p. 377–385.

Wei, Z.J., Huang, Z.B., Jin, X., Sun, Y.J., and Huo, J.C., 2004, Geological characteristics of ophiolite migmatitic complex of Hongshishan region, Gansu [in Chinese with English abstract]: Northwest Geology, v. 37, no. 2, p. 13–18.

Whalen, J.B., Currie, K.L., and Chappell, B.W., 1987, A-type granites: Geochemical characteristics, discrimination and petrogenesis: Contributions to Mineralogy and Petrology, v. 95, p. 407–419, https://doi.org/10.1007/BF00402202.

Wilhem, C., Windley, B.F., and Stampfli, G.M., 2012, The Altaids of Central Asia: A tectonic and evolutionary innovative review: Earth-Science Reviews, v. 113, no. 3–4, p. 303–341, https://doi.org/10.1016/j.earscirev.2012.04.001.

Windley, B.F., and Xiao, W.J., 2018, Ridge subduction and slab windows in the Central Asian Orogenic Belt: Tectonic implications for the evolution of an accretionary orogen: Gondwana Research, v. 61, p. 73–87, https://doi.org/10.1016/j.gr.2018.05.003.

Windley, B.F., Alexeiev, D., Xiao, W., Kröner, A., and Badarch, G., 2007, Tectonic models for accretion of the Central Asian Orogenic Belt: Journal of the Geological Society, v. 164, no. 1, p. 31–47, https://doi.org/10.1144/0016-76492006-022.

Wood, D.A., 1980, The application of a Th-Hf-Ta diagram to problems of tectonomagmatic classification and to establishing the nature of crustal contamination of basaltic lavas of the British Tertiary volcanic province: Earth and Planetary Science Letters, v. 50, p. 11–30, https://doi.org/10.1016/0012-821X(80)90116-8.

Wu, C., Yin, A., Zuza, A.V., Zhang, J.Y., Liu, W.C., and Ding, L., 2016a, Pre-Cenozoic geologic history of the central and northern Tibetan Plateau and the role of Wilson cycles in constructing the Tethyan orogenic system: Lithosphere, v. 8, no. 3, p. 254–292, https://doi.org/10.1130/L494.1.

Wu, C., Liu, C.F., Zhu, Y., Zhou, Z.G., Jiang, T., Liu, W.C., Li, H.Y., Wu, C., and Ye, B.Y., 2016b, Early Paleozoic magmatic history of central Inner Mongolia, China: implications for the tectonic evolution of the Southeast Central Asian Orogenic Belt: International Journal of Earth Sciences, v. 105, no. 5, p. 1307–1327, https://doi.org/10.1007/s00531-015-1250-7.

Wu, C., Zuza, A.V., Li, J., Haproff, P.J., Yin, A., Chen, X.H., Ding, L., and Li, B., 2021, Late Mesozoic-Cenozoic cooling history of the northeastern Tibetan Plateau and its foreland derived from low-temperature thermochronology: Geological Society of America Bulletin, v. 133, no. 11–12, p. 2393–2417, https://doi.org/10.1130/B35879.1.

Wu, P., Wang, G.Q., Li, X.M., Yu, J.Y., and Kang, L., 2012, The age of Niujuanzi ophiolite in Beishan area of Gansu Province and its geological significance [in Chinese with English abstract]: Geological Bulletin of China, v. 31, no. 12, p. 2032–2037.

Xiao, P.X., You, W.F., Dong, Z.C., Xie, C.R., and Li, P., 2010c, The re-definition of formation age of Xiaocaohu volcanic rocks in Beishan area, Gansu Province, China [in Chinese with English abstract]: Geological Bulletin of China, v. 29, no. 9, p. 1268–1274.

Xiao, W.J., Windley, B.F., Hao, J., and Zhai, M.G., 2003, Accretion leading to collision and the Permian Solonker suture, Inner Mongolia, China: Termination of the central Asian orogenic belt: Tectonics, v. 22, no. 6, https://doi.org/10.1029/2002TC001484.

Xiao, W.J., Windley, B.F., Huang, B.C., Han, C.M., Yuan, C., Chen, H.L., Sun, M., Sun, S., and Li, J.L., 2009a, End-Permian to mid-Triassic termination of the accretionary processes of the southern Altaids: Implications for the geodynamic evolution, Phanerozoic continental growth, and metallogeny of Central Asia: International Journal of Earth Sciences, v. 98, no. 6, p. 1189–1217, https://doi.org/10.1007/s00531-008-0407-z.

Xiao, W.J., Windley, B.F., Yuan, C., Sun, M., Han, C.M., Lin, S.F., Chen, H.L., Yan, Q.R., Liu, D.Y., Qin, K.Z., Li, J.L., and Sun, S., 2009b, Paleozoic multiple subduction-accretion processes of the southern Altaids: American Journal of Science, v. 309, p. 221–270, https://doi.org/10.2475/03.2009.02.

Xiao, W.J., Han, C.M., Yuan, C., Sun, M., Zhao, G.C., and Shan, Y.H., 2010a, Transitions among Mariana-, Japan-, Cordillera- and Alaska-type arc systems and their final juxtapositions leading to accretionary and collisional orogenesis, *in* Kusky, T.M., Zhai, M.-G., and Xiao, W., eds., The Evolving Continents: Understanding Processes of Continental Growth: Geological Society of London, Special Publications, v. 338, no. 1, p. 35–53, https://doi.org/10.1144/SP338.3.

Xiao, W.J., Mao, Q.G., Windley, B.F., Han, C.M., Qu, J.F., Zhang, J.E., Ao, S.J., Guo, Q.Q., Cleven, N.R., Lin, S.F., Shan, Y.H., and Li, J.L., 2010b, Paleozoic multiple accretionary and collisional processes of the Beishan orogenic collage: American Journal of Science, v. 310, p. 1553–1594, https://doi.org/10.2475/10.2010.12.

Xiao, W.J., Windley, B.F., Allen, M.B., and Han, C.M., 2013, Paleozoic multiple accretionary and collisional tectonics of the Chinese Tianshan orogenic collage: Gondwana Research, v. 23, no. 4, p. 1316–1341, https://doi.org/10.1016/j.gr.2012.01.012.

Xiao, W.J., Han, C.M., Liu, W., Wan, B., Zhang, J.E., Ao, S.J., Zhang, Z.Y., Song, D.F., Tian, Z.H., and Luo, J., 2014, How many sutures in the southern Central Asian Orogenic Belt: Insights from East Xinjiang-West Gansu (NW China)?: Geoscience Frontiers, v. 5, no. 4, p. 525–536, https://doi.org/10.1016/j.gsf.2014.04.002.

Xiao, W.J., Windley, B.F., Han, C.M., Liu, W., Wan, B., Zhang, J.E., Ao, S.J., Zhang, Z.Y., and Song, D.F., 2018, Late Paleozoic to early Triassic multiple roll-back and oroclinal bending of the Mongolia collage in Central Asia: Earth-Science Reviews, v. 186, p. 94–128, https://doi.org/10.1016/j.earscirev.2017.09.020.

Xiao, W.J., Song, D.F., Windley, B.F., Li, J.L., Han, C.M., Wan, B., Zhang, J.E., Ao, S.J., and Zhang, Z.Y., 2020, Accretionary processes and metallogenesis of the Central Asian Orogenic Belt: Advances and perspectives: Science China. Earth Sciences, v. 63, no. 3, p. 329–361, https://doi.org/10.1007/s11430-019-9524-6.

Xiao, X.C., Tang, Y.Q., Feng, Y.M., Zhu, B.Q., Li, J.Y., and Zhao, M., 1992, Tectonic evolution of northern Xinjiang and its adjacent regions [in Chinese]: Beijing, China, Geological Publishing House, p. 1–169.

Xie, J.Q., Di, P.F., Yang, J., Chen, W.F., Wei, H.F., and Zhai, X.W., 2018b, LA-ICP-MS zircon U-Pb age, geochemistry and tectonic implications of metamorphic dacite from Huaniushan Group in Beishan area, Gansu, China [in Chinese with English abstract]: Northwest Geology, v. 51, no. 1, p. 54–64.

Xie, L.W., Zhang, Y.B., Zhang, H.H., Sun, J.F., and Wu, F.Y., 2008, In situ simultaneous determination of trace elements, U-Pb and Lu-Hf isotopes in zircon and baddeleyite: Chinese Science Bulletin, v. 53, p. 1565–1573.

Xie, X., Yang, J.G., Wang, X.H., Wang, L., Jiang, L., and Jiang, A.D., 2015, Zircon SHRIMP U-Pb dating of Hongliugou mafic-ultramafic complex in the Beishan area of Gansu Province and its geological significance [in Chinese with English abstract]: Geology in China, v. 42, no. 2, p. 396–405.

Xie, X., Zhao, G.B., Yang, H.Q., Yang, S.F., Ren, H.N., Jia, J., Sun, X.C., and Huang, Z.B., 2018a, LA-ICP-MS zircon U-Pb dating and geological significance of the Sunjialing scandium mineralized intrusion in the Beishan region, Gansu Province [in Chinese with English abstract]: Geology in China, v. 45, no. 3, p. 483–492.

Xiu, D., Chen, C., Zhuan, S.P., Shen, Z.Y., Wang, J.G., Chen, Z., Zhang, L.G., Wang, S., Yang, X.P., Hou, D.H., Shi, G.Y., and Zhang, P.C., 2018, Zircon U-Pb age and petrogenesis of tonalite-quartz diorite in the Shibanjing area, central Beishan orogenic belt, and its constraint on subduction of the ancient oceanic basin [in Chinese with English abstract]: Geological Bulletin of China, v. 37, no. 6, p. 975–986.

Xu, W., Xu, X.Y., Niu, Y.Z., Chen, G.C., Shi, J.Z., Wei, J.S., Song, B., and Zhang, Y.X., 2018c, Geochronology, petrogenesis and tectonic implications of Early Permian A-type rhyolite from southern Beishan orogen, NW China [in Chinese with English abstract]: Acta Petrologica Sinica (Yanshi Xuebao), v. 34, no. 10, p. 3011–3033.

Xu, W., Xu, X.Y., Niu, Y.Z., Song, B., Chen, G.C., Shi, J.Z., Zhang, Y.X., and Li, C.H., 2019a, Geochronology and petrogenesis of the Permian marine basalt in the southern Beishan region and their tectonic implications [in Chinese with English abstract]: Acta Geologica Sinica, v. 93, no. 8, p. 1928–1953.

Xu, W., Xu, X.Y., Lu, J.C., Niu, Y.Z., Chen, G.C., Shi, J.Z., Dang, B., Song, B., Zhang, Y.X., and Zhang, Q., 2019b, Geochronology, petrogenesis and tectonic Implications of Devonian high-K acid magmatic rocks from Yemajing area in Beishan Orogen [in Chinese with English abstract]: Earth Science, v. 44, no. 8, p. 2775–2793.

Xu, X.M., Lu, Y., Xin, H.T., Zhang, Y., Zhang, Z.P., and Feng, Y.P., 2018a, The constraint of closing time of Paleo-Asian Ocean in the north edge of Beishan, Inner Mongolia: Evidence from the Late Carboniferous quartz diorite in Heihongshan [in Chinese with English abstract]: Journal of Mineralogy and Petrology, v. 38, no. 4, p. 66–75.

Xu, X.M., Cheng, H.F., Duan, B.X., and Xue, P.Y., 2018b, The LA-ICP-MS U-Pb geochronology of detrital zircons from quartzite in the Beishan Complex-Group in Biaoshan area in Beishan region during Changchengian Period and its geologic significance [in Chinese with English abstract]: Xinjiang Geology, v. 36, no. 3, p. 393–398.

Yakubchuk, A., 2017, Evolution of the Central Asian Orogenic Supercollage since Late Neoproterozoic revised again: Gondwana Research, v. 47, p. 372–398, https://doi.org/10.1016/j.gr.2016.12.010.

Yan, H.Q., Zhao, H.Q., Ding, R.Y., Mi, S.H., Wang, Q., He, B.L., Fan, M.C., and Ren, J.M., 2012, Zircon SHRIMP

U-Pb dating of the Dashantou basic complex and its geological significance in Beishan area, Gansu Province [in Chinese with English abstract]: Northwest Geology, v. 45, no. 4, p. 216–228.

Yan, T., Xin, H.T., Wei, Y.S., Yang, W.B., and Li, Z.Y., 2020, A new thinking on the process of ocean-continent transition in Beishan orogenic belt of Inner Mongolia: Evidence from the Devonian arc granite in the south of Dahong Mountain [in Chinese with English abstract]: Geological Bulletin of China, v. 39, no. 9, p. 1341–1366.

Yang, F.L., Zhao, Z.X., Jia, W.Y., Yang, L., Xu, H., Jia, Y.Q., and Gao, Y., 2016a, Discussion on the forming age of the Beishan Group in the Beishan area, Inner Mongolia [in Chinese with English abstract]: Geological Survey and Research, v. 39, no. 2, p. 90–94.

Yang, F.L., Zou, Y.X., Cao, X., Yang, L., Ma, G., and Gao, J., 2017, Zircon LA-ICPMS U-Pb dating for the quartz diorite in the south Pengboshan of Beishan area, Inner Mongolia [in Chinese with English abstract]: Geological Survey and Research, v. 40, no. 2, p. 109–118.

Yang, H.B., Yang, X.P., Zhan, Y., Cunningham, D., Zhao, L.Q., Sun, X.Y., Hu, Z.K., Huang, X.N., Huang, W.L., and Miao, S.Q., 2019a, Quaternary activity of the Beihewan Fault in the southeastern Beishan Wrench Belt, Western China: Implications for crustal stability and intraplate earthquake hazards north of Tibet: Journal of Geophysical Research. Solid Earth, v. 124, no. 12, p. 13,286–13,309, https://doi.org/10.1029/2018JB017209.

Yang, H.B., Cunningham, D., and Yang, X.P., 2021a, Quaternary crustal reactivation of the southwestern Beishan, NW China: The Liuyuan sinistral transpressional duplex: Tectonophysics, v. 803, https://doi.org/10.1016/j.tecto.2021.228758.

Yang, H.Q., Li, Y., Zhao, G.B., Li, W.Y., Wang, X.H., Jiang, H.B., Tan, W.J., and Sun, N., 2010a, Character and structural attitude of the Beishan ophiolite [in Chinese with English abstract]: Northwest Geology, v. 43, no. 1, p. 26–36.

Yang, J.G., Zhai, J.Y., Yang, H.W., Wang, C.F., Xie, C.L., Wang, X.H., and Lei, Y.X., 2010b, LA-ICP-MS zircon U-Pb dating of basalt and its geological significance in Huaniushan Pb-Zn deposit, Beishan area, Gansu, China [in Chinese with English abstract]: Geological Bulletin of China, v. 29, no. 7, p. 1017–1023.

Yang, J.G., Wang, L., Wang, X.H., Xie, X., and Jiang, A.D., 2015, SHRIMP zircon U-Pb dating of the Xiaohongshan vanadium-titanium magnetite deposit, Ejin Banner, Beishan, Inner Mongolia, and its geological implications [in Chinese with English abstract]: Geological Bulletin of China, v. 34, no. 9, p. 1699–1705.

Yang, J.G., Wang, L., Xie, X., Wang, X.H., Qi, Q., Jiang, A.D., and Zhang, Z.Y., 2016b, SHRIMP zircon U-Pb age and its signification of Guaishishan mafic-ultramafic complex in Beishan Mountains, Gansu Province [in Chinese with English abstract]: Geotectonica et Metallogenia, v. 40, no. 1, p. 98–108.

Yang, Q.P., Ren, E.F., Zhao, H.B., Guan, S., Zhu, X.L., and Cheng, L., 2019b, The LA-ICP-MS zircon U-Pb age of rhyolite in the Erdaoquan area of Beishan, Gansu, and its geological significance [in Chinese with English abstract]: Journal of Qinghai University, v. 37, no. 1, p. 94–98.

Yang, W.B., Yan, T., Zhang, Y., Wei, Y.S., and Li, Z.Y., 2020, Zircon U-Pb age and geochemistry of TTG rocks in Xiaohongshan area of the Beishan orogenic belt, Inner Mongolia, and their constraints on the properties of the Baihe Mountain tectonic belt [in Chinese with English abstract]: Geological Bulletin of China, v. 39, no. 9, p. 1404–1421.

Yang, Y.Q., Lv, B., Meng, G.X., Yan, J.Y., Zhao, J.H., Wang, S.G., Jia, L.L., and Han, J.G., 2013, Geochemistry, SHRIMP zircon U-Pb dating and formation environment of Dongqiyishan Granite, Inner Mongolia [in Chinese with English abstract]: Acta Geoscientica Sinica, v. 34, no. 2, p. 163–175.

Yang, Z.X., Ding, S.H., Zhang, J., Fan, X.X., Kong, W.Q., Zhao, J.C., and Jing, D.L., 2021b, The discovery of Early Devonian adakites in Beishan orogenic belt and its geological significance [in Chinese with English abstract]: Acta Petrologica Mineralogica, v. 40, no. 2, p. 185–201.

Yang, Z.X., Zhao, J.C., Jing, D.L., Zhao, Q.H., Zhang, J., and Fan, X.X., 2021c, Chronological and geochemical characteristics of the porphyritic granodiorite in the Qianhongquan area, Beishan region, Gansu Province [in Chinese with English abstract]: Bulletin of Mineralogy: Petrology and Geochemistry, v. 40, no. 1, p. 228–241.

Ye, X.F., Zong, K.Q., Zhang, Z.M., He, Z.Y., Liu, Y.S., Hu, Z.C., and Wang, W., 2013, Geochemistry of Neoproterozoic granite in Liuyuan area of southern Beishan orogenic belt and its geological significance [in Chinese with English abstract]: Geological Bulletin of China, v. 32, no. 2–3, p. 307–317.

Yi, P.F., Li, N., Gao, F., Feng, W.H., Tang, L., Gao, Y.P., Li, Q., Liu, W., and Song, D.Y., 2017, LA-ICP-MS zircon U-Pb ages of the granites from Mashan of Inner Mongolia and their geological significances [in Chinese with English abstract]: Geological Bulletin of China, v. 36, no. 2–3, p. 331–341.

Yin, A., 2010, Cenozoic tectonic evolution of Asia: A preliminary synthesis: Tectonophysics, v. 488, no. 1–4, p. 293–325, https://doi.org/10.1016/j.tecto.2009.06.002.

Yin, A., and Harrison, T.M., 2000, Geologic Evolution of the Himalayan-Tibetan Orogen: Annual Review of Earth and Planetary Sciences, v. 28, p. 211–280, https://doi.org/10.1146/annurev.earth.28.1.211.

Yin, A., and Nie, S.Y., 1996, A Phanerozoic palinspastic reconstruction of China and its neighboring regions, *in* Yin, A., and Harrison, T.M., eds., The Tectonic Evolution of Asia: New York, USA, Cambridge University Press, p. 442–485.

Yin, A., Manning, C.E., Lovera, O., Menold, C.A., Chen, X.H., and Gehrels, G.E., 2007, Early Paleozoic tectonic and thermomechanical evolution of ultrahigh-pressure (UHP) metamorphic rocks in the northern Tibetan Plateau, northwest China: International Geology Review, v. 49, no. 8, p. 681–716, https://doi.org/10.2747/0020-6814.49.8.681.

Yu, F.S., Li, J.B., and Wang, T., 2006, The U-Pb isotopic age of zircon from Hongliuhe ophiolites in East Tianshan Mountains, Northwest China [in Chinese with English abstract]: Acta Geoscientica Sinica, v. 27, no. 3, p. 213–216.

Yu, H.F., Lu, S.N., Mei, H.L., Zhao, F.Q., Li, H.K., and Li, H.M., 1999, Characteristics of Neoproterozoic eclogite-granite zones and deep level ductile shear zone in western China and their significance for continental reconstruction [in Chinese with English abstract]: Acta Petrologica Sinica (Yanshi Xuebao), v. 15, no. 4, p. 532–538.

Yu, J.P., Wang, H.T., Wang, Y.X., Sun, X.C., Ren, W.X., Wei, H.F., and Wang, X.W., 2021, Geochronology and geochemistry of Tanshanzidong olivine-gabbro in Beishan area, Gansu Province, and its geological significance [in Chinese with English abstract]: Acta Petrologica et Mineralogica, v. 40, no. 2, p. 202–216.

Yu, J.Y., Guo, L., Li, J.X., Li, Y.G., Smithies, R.H., Wingate, M.T.D., Meng, Y., and Chen, S.F., 2016, The petrogenesis of sodic granites in the Niujuanzi area and constraints on the Paleozoic tectonic evolution of the Beishan region, NW China: Lithos, v. 256–257, p. 250–268, https://doi.org/10.1016/j.lithos.2016.04.003.

Yu, J.Y., Ji, B., Guo, L., Guo, L., and Bu, T., 2018, Geological characteristics and age determination of the Palaeoproterozoic Gudongjing Group complex in the Beishan Mountain, Gansu Province [in Chinese with English abstract]: Geological Bulletin of China, v. 37, no. 4, p. 704–715.

Yu, J.Y., Li, X.M., Wang, G.Q., Wu, P., and Yan, Q.J., 2012, Zircon U-Pb ages of Huitongshan and Zhangfangshan ophiolite in Beishan of Gansu-Inner Mongolia border area and their significance [in Chinese with English abstract]: Geological Bulletin of China, v. 31, no. 12, p. 2038–2045.

Yu, L.D., Zhang, J., Wang, Q.S., Wang, C.Y., and Lai, C., 2020, Geochronology and geochemistry of granodiorite at Jinwozi Au deposit: Tectonomagmatic evolution for Palaeozoic Beishan Orogen (Central Asian Orogenic Belt) in NW China: Geological Journal, v. 55, no. 10, p. 6779–6798, https://doi.org/10.1002/gj.3836.

Yue, Y., and Liou, J.G., 1999, Two-stage evolution model for the Altyn Tagh fault, China: Geology, v. 27, no. 3, p. 227–230, https://doi.org/10.1130/0091-7613(1999)027<0227:TSEMFT>2.3.CO;2.

Yuan, Y., Zong, K.Q., He, Z.Y., Klemd, R., Liu, Y.S., Hu, Z.C., Guo, J.L., and Zhang, Z.M., 2015, Geochemical and geochronological evidence for a former early Neoproterozoic microcontinent in the South Beishan Orogenic Belt, southernmost Central Asian Orogenic Belt: Precambrian Research, v. 266, p. 409–424, https://doi.org/10.1016/j.precamres.2015.05.034.

Yuan, Y., Zong, K.Q., He, Z.Y., Klemd, R., Jiang, H.Y., Zhang, W., Liu, Y.S., Hu, Z.C., and Zhang, Z.M., 2018, Geochemical evidence for Paleozoic crustal growth and tectonic conversion in the Northern Beishan Orogenic Belt, southern Central Asian Orogenic Belt: Lithos, v. 302–303, p. 189–202, https://doi.org/10.1016/j.lithos.2017.12.026.

Yuan, Y., Zong, K.Q., Cawood, P.A., Cheng, H., Yu, Y.Y., Guo, J.L., Liu, Y.S., Hu, Z.C., Zhang, W., and Li, M., 2019, Implication of Mesoproterozoic (~1.4 Ga) magmatism within microcontinents along the southern Central Asian Orogenic Belt: Precambrian Research, v. 327, p. 314–326, https://doi.org/10.1016/j.precamres.2019.03.014.

Yun, L., Zhang, J., Wang, J., Zhao, Z.T., Bao, Y.T., Zhuang, H.Y., Chen, S., Zhang, J.J., Zhang, J., Zhao, H., and Zhang, B.H., 2021, Discovery of active faults in the southern Beishan area, NW China: Implications for regional tectonics [in Chinese with English abstract]: Journal of Geometry, v. 27, no. 2, p. 195–207.

Zhang, D.Y., Fu, X., Wei, O.X., Ye, L.X., Jiang, H., Zhang, Y., and Xin, H.T., 2020c, Discovery of the Silurian andesitic porphyry in the Xiaohulishan Mo-polymetallic deposit, the Beishan district, Inner Mongolia, and its geological significance [in Chinese with English abstract]: Earth Science Frontiers, v. 27, no. 3, p. 222–238.

Zhang, H., Wang, H., Pan, Z.L., Wang, S., Chen, C., Zhang, J.L., Zhang, L.G., and Li, Q.Z., 2021, Geochronological constraints and deformation of the western section of Shibanjing ductile shear zone in Beishan, Inner Mongolia [in Chinese with English abstract]: Geological Bulletin of China, v. 40, no. 6, p. 930–941.

Zhang, H.D., Liu, J.C., Yang, J.K., Ge, J.K., Wang, J.Y., and Li, Z., 2020a, Testing final closure time of the Paleo-Asian Ocean along the Solonker suture by a transition of compressional and extensional setting: Geoscience Frontiers, v. 11, no. 6, p. 1935–1951, https://doi.org/10.1016/j.gsf.2020.05.020.

Zhang, J.J., 2014, The petrogenesis and mineralization potential of two types of mafic-ultramafic intrusions, Gansu Beishan, China [Ph.D. thesis]: Xi'an, China, Chang'an University, 104 p.

Zhang, J., and Cunningham, D., 2012, Kilometer-scale refolded folds caused by strike-slip reversal and intraplate shortening in the Beishan region, China: Tectonics, v. 31, no. 3, TC3009, https://doi.org/10.1029/2011TC003050.

Zhang, J.R., 2017, SHRIMP zircon U-Pb chronology and geological significance of Carboniferous Qingshuiquan complex in Beishan region across Gansu and Inner Mongolia [in Chinese with English abstract]: Gansu Geology, v. 26, no. 1, p. 32–39.

Zhang, S.M., He, Z.Y., Hu, E.H., Wang, Y.N., Wang, B., and Chen, Q., 2018b, The discovery of Mesozoic overthrust nappe tectonics and an analysis of its control of mineralization in Shapoquan area, Ejin Banner, Inner Mongolia [in Chinese with English abstract]: Geological Bulletin of China, v. 37, no. 2–3, p. 435–445.

Zhang, W., 2013, Late Paleozoic granitoids in Beishan-Northern Alxa area (NW China) and their tectonic implications [Ph.D. thesis]: Beijing, China, Peking University, 200 p.

Zhang, W., Wu, T.R., He, Y.K., Feng, J.C., and Zheng, R.G., 2010, LA-ICP-MS zircon U-Pb ages of Xijianquanzi alkali-rich potassium-high granites in Beishan, Gansu Province, and their tectonic significance [in Chinese with English abstract]: Acta Petrologica et Mineralogica, v. 29, no. 6, p. 719–731.

Zhang, W., Feng, J.C., Zheng, R.G., Wu, T.R., Luo, H.L., He, Y.K., and Jing, X., 2011a, LA-ICP MS zircon U-Pb ages of the granites from the south of Yin'aoxia and their tectonic significances [in Chinese with English abstract]: Acta Petrologica Sinica (Yanshi Xuebao), v. 27, no. 6, p. 1649–1661.

Zhang, W., Pease, V., Wu, T.R., Zheng, R.G., Feng, J.C., He, Y.K., Luo, H.L., and Xu, C., 2012a, Discovery of an adakite-like pluton near Dongqiyishan (Beishan, NW China): Its age and tectonic significance: Lithos, v. 142–143, p. 148–160, https://doi.org/10.1016/j.lithos.2012.02.021.

Zhang, W., Wu, T.R., Zheng, R.G., Feng, J.C., Luo, H.L., He, Y.K., and Xu, C., 2012b, Post-collisional Southeastern Beishan granites: Geochemistry, geochronology, Sr-Nd-Hf isotopes and their implications for tectonic evolution: Journal of Asian Earth Sciences, v. 58, p. 51–63, https://doi.org/10.1016/j.jseaes.2012.07.004.

Zhang, W., Pease, V., Meng, Q., Zheng, R., Thomsen, T.B., Wohlgemuth-Ueberwasser, C., and Wu, T., 2015b, Timing, petrogenesis, and setting of granites from the southern Beishan late Palaeozoic granitic belt, Northwest China and implications for their tectonic evolution: International Geology Review, v. 57, no. 16, p. 1975–1991, https://doi.org/10.1080/00206814.2015.1045944.

Zhang, W., Pease, V., Meng, Q.P., Zheng, R.G., and Wu, T.R., 2017a, Age and petrogenesis of Mingshui-Shuangjingzi granites from the northern Beishan area, northwest China, and their implications for tectonic evolution: Geosciences Journal, v. 21, no. 5, p. 667–682, https://doi.org/10.1007/s12303-017-0017-5.

Zhang, W., Pease, V., Meng, Q.P., Zheng, R.G., and Wu, T.R., 2018a, Recognition of a Devonian-early Mississippian plutonic belt in the eastern Beishan area, Northwest China, and its tectonic implications: Geological Journal, v. 53, p. 803–819, https://doi.org/10.1002/gj.2928.

Zhang, X.Q., Wei, Q.R., Wei, J.H., Sun, J., Hao, W., and Zhang, D.C., 2012c, Geochemical characteristics and significance of Late Devonian gabbros in Jidong area, Inner Mongolia [in Chinese with English abstract]: Geological Science and Technology Information, v. 31, no. 6, p. 80–87.

Zhang, Y.L., Xu, R.K., Shan, L., Jian, Q.Z., Song, Z.B., Chen, X.Y., Zhang, X.F., Chen, B., Li, Y.Z., and Quan, S.C., 2012d, Rock-forming and ore-forming ages of the Xiaohulishan molybdenum deposit in Beishan area, Inner Mongolia [in Chinese with English abstract]: Geological Bulletin of China, v. 31, no. 2–3, p. 469–475.

Zhang, Y.Y., and Guo, Z.J., 2008, Accurate constraint on formation and emplacement age of Hongliuhe ophiolite, boundary region between Xinjiang and Gansu Provinces and its tectonic implications [in Chinese with English abstract]: Acta Petrologica Sinica (Yanshi Xuebao), v. 24, no. 4, p. 803–809.

Zhang, Y.Y., Dostal, J., Zhao, Z.H., Liu, C., and Guo, Z.J., 2011b, Geochronology, geochemistry and petrogenesis of mafic and ultramafic rocks from southern Beishan area, NW China: Implications for crust-mantle interaction: Gondwana Research, v. 20, p. 816–830, https://doi.org/10.1016/j.gr.2011.03.008.

Zhang, Y.Y., Yuan, C., Sun, M., Long, X.P., Xia, X.P., Wang, X.Y., and Huang, Z.Y., 2015a, Permian doleritic dikes in the Beishan Orogenic Belt, NW China: Asthenosphere-lithosphere interaction in response to slab breakoff: Lithos, v. 233, p. 174–192, https://doi.org/10.1016/j.lithos.2015.04.001.

Zhang, Z.P., Duan, B.X., Meng, Q.T., Xu, C., Dong, H.K., Liu, G., and Ti, Z.H., 2017b, LA-ICP-MS zircon U-Pb dating of amphibolites of the Beishan group in the Beishan area, Inner Mongolia and its geological significance [in Chinese with English abstract]: Geology and Exploration, v. 53, no. 6, p. 1129–1139.

Zhang, Z.P., Xin, H.T., Cheng, H.F., Zhang, Y., Liang, G.Q., Ti, Z.H., Zhu, W., Su, P.T., Du, J.L., Wang, M., and Zhao, Q.Y., 2020b, The discovery of the Elegen ophiolite in Beishan orogenic belt, Inner Mongolia: Evidence for the east extension of the Hongshishan-Baiheshan ophiolite belt [in Chinese with English abstract]: Geological Bulletin of China, v. 39, no. 9, p. 1389–1403.

Zhao, H.G., Liang, J.W., Wang, J., Su, R., Jin, Y.X., Tian, X., and Luo, H., 2019b, Geochronology and geochemical characteristics of the Suanjingzi adakitic granites in the Beishan Mountains, Gansu Province, China, and their tectonic significance [in Chinese with English abstract]: Acta Geologica Sinica, v. 93, no. 2, p. 329–352.

Zhao, K.Q., Ma, S.M., Xi, M.J., Yang, J.Z., Cai, Y.W., and Gong, J.J., 2020c, The LA-ICP-MS Zircon U-Pb ages and geochemical characteristics of Late Paleozoic intermediate-acidic intrusive complexes in Shibanjing area, Beishan Mountains, Inner Mongolia, and their geological significance [in Chinese with English abstract]: Dizhi Lunping, v. 66, no. 1, p. 69–87.

Zhao, P.B., Zhang, J.J., Gao, Y.P., Zhu, H.P., Li, W.J., and He, Z.F., 2017a, Geochronology and geochemistry of northern Baiyunshan granites in the Beishan area, Inner Mongolia, China and their geological significance [in Chinese with English abstract]: Northwest Geology, v. 50, no. 3, p. 36–46.

Zhao, P.B., Li, W.C., Luo, Q.Z., Peng, H.L., Li, Y., Li, W.J., and Zhang, S.H., 2019a, Formation age and tectonic environment of Yingzuihongshan granite in Beishan, Inner Mongolia [in Chinese with English abstract]: Northwest Geology, v. 52, no. 4, p. 1–13.

Zhao, S., Liu, J., Zhang, Y., Zhang, J., Xu, W., and Li, J., 2021, Geochronology and petrogenesis of the Yuanbaoshan leucogranite in southeast Inner Mongolia: Implications for the collision between the Sino-Korean and Siberian paleo-plates: Lithos, v. 384–385, https://doi.org/10.1016/j.lithos.2021.105981.

Zhao, Y., Sun, Y., Diwu, C.R., Zhu, T., Ao, W.H., Zhang, H., and Yan, J.H., 2017b, Paleozoic intrusive rocks from the Dunhuang tectonic belt, NW China: Constraints on the tectonic evolution of the southernmost Central Asian Orogenic Belt: Journal of Asian Earth Sciences, v. 138, p. 562–587, https://doi.org/10.1016/j.jseaes.2017.02.037.

Zhao, Z.H., Guo, Z.J., Han, B.F., Wang, Y., and Liu, C., 2006, Comparative study on Permian basalts from eastern Xinjiang-Beishan area of Gansu province and its tectonic implications [in Chinese with English abstract]: Acta Petrologica Sinica (Yanshi Xuebao), v. 22, no. 5, p. 1279–1293.

Zhao, Z.H., Guo, Z.J., and Wang, Y., 2007, Geochronology, geochemical characteristics and tectonic implications of the granitoids from Liuyuan area, Beishan, Gansu province, northwest China [in Chinese with English abstract]: Acta Petrologica Sinica (Yanshi Xuebao), v. 23, no. 8, p. 1847–1860.

Zhao, Z.H., Guo, Z.J., Zhang, Z.C., Shi, H.Y., and Tian, J., 2004, The geochemical characteristics and tectonic setting of the Lower Permian basalts in Hongliuhe area at the border between Xinjiang and Gansu Provinces [in Chinese with English abstract]: Gaoxiao Dizhi Xuebao, v. 10, no. 4, p. 545–553.

Zhao, Z.N., Yang, J.K., Wei, M., Wang, Z.L., and Guo, S.E., 2020a, Geological significance and characteristics of geochemistry and geochronology of Baiyunshan granodiorite in the Beishan area of Inner Mongolia [in Chinese with English abstract]: Mineralogy and Petrology, v. 40, no. 3, p. 53–66.

Zhao, Z.X., Jia, Y.Q., Xu, H., Wang, J.R., Wang, X.L., and Liu, Q., 2015, LA-ICP-MS zircon U-Pb age of quartz diorite from the Jiaochagou area in Beishan orogenic belt, Inner Mongolia, and its tectonic significance [in Chinese with English abstract]: Acta Geologica Sinica, v. 89, no. 7, p. 1210–1218.

Zhao, Z.X., Xu, H., Jia, Y.Q., Gao, Y., Chen, H.D., and Gao, J., 2016, Geochemistry and LA-ICP-MS zircon U-Pb age of porphyritic granodiorite in the Beishan orogenic belt in Inner Mongolia and their geological significance [in Chinese with English abstract]: East China Geology, v. 37, no. 4, p. 252–258.

Zhao, Z.X., Xiong, Y., Jia, Y.Q., Wang, J.R., Xu, H., Gao, J., Wang, X.L., and Liu, Q., 2018, The continental arcs magmatic at the Dulongbao Area in Beishan orogenic belt in Late Carboniferous: Evidences from zircon U-Pb dating and geochemistry of the granodiorite [in Chinese with English abstract]: Dizhi Lunping, v. 64, no. 3, p. 597–609.

Zheng, R.G., Wu, T.R., Zhang, W., Xu, C., and Meng, Q.P., 2012, Early Devonian tectono-magmatic events in the middle Beishan, Gansu Province: Evidence from chronology and geochemistry of Gongpoquan granite [in Chinese with English abstract]: Acta Scientiarum Naturalium Universitatis Pekinensis, v. 48, no. 4, p. 603–616.

Zheng, R.G., Wu, T.R., Zhang, W., Xu, C., and Meng, Q.P., 2013, Late Paleozoic subduction system in the southern Central Asian Orogenic Belt: Evidences from geochronology and geochemistry of the Xiaohuangshan ophiolite in the Beishan orogenic belt: Journal of Asian Earth Sciences, v. 62, p. 463–475, https://doi.org/10.1016/j.jseaes.2012.10.033.

Zheng, R.G., Wu, T.R., Zhang, W., Meng, Q.P., and Zhang, Z.Y., 2014, Geochronology and geochemistry of late Paleozoic magmatic rocks in the Yinwaxia area, Beishan: Implications for rift magmatism in the southern Central Asian Orogenic Belt: Journal of Asian Earth Sciences, v. 91, p. 39–55, https://doi.org/10.1016/j.jseaes.2014.04.022.

Zheng, R.G., Wang, Y.P., Zhang, Z.Y., Zhang, W., Meng, Q.P., and Wu, T.R., 2016a, Geochronology and geochemistry of Yinwaxia acidic volcanic rocks in the southern Beishan: New evidence for Permian continental rifting [in Chinese with English abstract]: Geotectonica et Metallogenia, v. 40, no. 5, p. 1031–1048.

Zheng, R.G., Wu, T.R., Xiao, W.J., Meng, Q.P., and Zhang, W., 2016b, Geochronology, geochemistry and tectonic implications of the Shuangjizi composite pluton in the northern Beishan [in Chinese with English abstract]: Acta Geologica Sinica, v. 90, no. 11, p. 3153–3172.

Zheng, R.G., Li, J.Y., Xiao, W.J., and Zhang, J., 2018a, Nature and provenance of the Beishan Complex, southernmost Central Asian Orogenic Belt: International Journal of Earth Sciences, v. 107, no. 2, p. 729–755, https://doi.org/10.1007/s00531-017-1525-2.

Zheng, R.G., Xiao, W.J., Li, J.Y., Wu, T.R., and Zhang, W., 2018b, A Silurian-early Devonian slab window in the southern Central Asian Orogenic Belt: Evidence from high-Mg diorites, adakites and granitoids in the western Central Beishan region, NW China: Journal of Asian Earth Sciences, v. 153, p. 75–99, https://doi.org/10.1016/j.jseaes.2016.12.008.

Zheng, R.G., Li, J.Y., and Xiao, W.J., 2019, Mid-Paleozoic ridge subduction in the Central Beishan of the southern Altaids: Evidence from geochemical, Sr-Nd and zircon U-Pb-Hf-O isotopic data of Gongpoquan volcanic rocks: Journal of the Geological Society, v. 176, p. 755–770, https://doi.org/10.1144/jgs2018-231.

Zheng, R.G., Li, J.Y., Zhang, J., Xiao, W.J., and Wang, Q.J., 2020, Permian oceanic slab subduction in the southmost of Central Asian Orogenic Belt: Evidence from adakite and high-Mg diorite in the southern Beishan: Lithos, v. 358–359, https://doi.org/10.1016/j.lithos.2020.105406.

Zheng, R.G., Li, J.Y., Zhang, J., and Xiao, W.J., 2021, A prolonged subduction-accretion in the southern Central Asian Orogenic Belt: Insights from anatomy and tectonic affinity for the Beishan complex: Gondwana Research, v. 95, p. 88–112, https://doi.org/10.1016/j.gr.2021.02.022.

Zheng, Y., Chen, J., Pang, J.C., and Wang, J.L., 2009, Basic rock SHRIMP dating & its geologic value in Heishanling region of Beishan area, Xinjiang [in Chinese with English abstract]: Xinjiang Geology, v. 27, no. 4, p. 320–324.

Zheng, Y.D., Zhang, Q., Wang, Y., Liu, R., Wang, S.G., Zuo, G., Wang, S.Z., Lkaasuren, B., Badarch, G., and Badamgarav, Z., 1996, Great Jurassic thrust sheets in Beishan (North Mountains): Gobi areas of China and southern Mongolia: Journal of Structural Geology, v. 18, no. 9, p. 1111–1126, https://doi.org/10.1016/0191-8141(96)00038-7.

Zhou, H., Chen, L., and Sun, Y., 2018, Zircon U-Pb chronology and Hf isotope study on the Mesoproterozoic metasedimentary rocks: Insight into the evolution of Precambrian materials in the south section of Beishan Orogen [in Chinese with English abstract]: Acta Geologica Sinica, v. 92, no. 5, p. 928–945.

Zhu, J., Lv, X.B., Peng, S.G., Gong, Y.J., Qiu, X.F., and Xiao, G.L., 2015, LA-ICP-MS zircon U-Pb geochronology and geochemical characteristics of the quartz syenite porphyry in the Xiaoxigong gold deposit and their geological implications [in Chinese with English abstract]: Geological Bulletin of China, v. 34, no. 8, p. 1460–1469.

Zhu, J., Lv, X.B., and Peng, S.G., 2016, U-Pb zircon geochronology, geochemistry and tectonic implications of the early Devonian granitoids in the Liuyuan area, Beishan, NW China: Geosciences Journal, v. 20, no. 5, p. 609–625, https://doi.org/10.1007/s12303-016-0004-2.

Zhu, W., Zhang, Z.P., Sun, Y.S., Cheng, H.F., Ti, Z.H., Du, J.L., Su, P.T., Feng, Y.P., and Liang, G.Q., 2019, Time

constraint on the closing of the Paleo-Asian Ocean in northern Beishan of Inner Mongolia: Evidence from Heihongshan admellite [in Chinese with English abstract]: Geological Bulletin of China, v. 38, no. 11, p. 1846–1857.
Zhuan, S.P., Chen, C., Shen, Z.Y., Pan, Z.L., Zhang, Y.Q., Zhao, H.P., Chen, H.Q., Yang, R., and Xiu, D., 2018, Early Paleozoic subduction of the ocean in Beishan region: Zircon U-Pb geochronological and geochemical evidence from the high-Mg diorite in the Shibanjing area [in Chinese with English abstract]: Acta Petrologica et Mineralogica, v. 37, no. 4, p. 533–546.
Zonenshain, L.P., Kuz'min, M.I., and Natapov, L.M., 1990, Geology of the USSR: A plate-tectonic synthesis: Washington, D.C., American Geophysical Union, v. 21, 242 p., https://doi.org/10.1029/GD021.
Zong, K.Q., Liu, Y.S., Zhang, Z.M., He, Z.Y., Hu, Z.C., Guo, J.L., and Chen, K., 2013, The generation and evolution of Archean continental crust in the Dunhuang block, northeastern Tarim craton, northwestern China: Precambrian Research, v. 235, p. 251–263, https://doi.org/10.1016/j.precamres.2013.07.002.
Zong, K.Q., Klemd, R., Yuan, Y., He, Z.Y., Guo, J.L., Shi, X.L., Liu, Y.S., Hu, Z.C., and Zhang, Z.M., 2017, The assembly of Rodinia: The correlation of early Neoproterozoic (ca. 900 Ma) high-grade metamorphism and continental arc formation in the southern Beishan Orogen, southern Central Asian Orogenic Belt (CAOB): Precambrian Research, v. 290, p. 32–48, https://doi.org/10.1016/j.precamres.2016.12.010.
Zuo, G.C., and Li, S.X., 2011, Early Paleozoic tectonic framework and evolution in the northeast margin of Tarim Basin [in Chinese with English abstract]: Geology in China, v. 38, no. 4, p. 945–960.
Zuo, G.C., Zhang, S.L., He, G.Q., and Zhang, Y., 1991, Plate tectonic characteristics during the early Paleozoic in Beishan near the Sino-Mongolian border region, China: Tectonophysics, v. 188, p. 385–392, https://doi.org/10.1016/0040-1951(91)90466-6.
Zuo, G.C., Liu, C.Y., Bai, W.C., and Feng, Y.Z., 1995, Volcano-molasse geological structure and geochemical signature in Devonian period collision orogenic in Beishan, Gansu in Mongolia [in Chinese with English abstract]: Acta Geologica Gansu, v. 4, no. 1, p. 35–43.
Zuo, G.C., Liu, Y.K., and Li, S.X., 2011, Tectonic framework, fold styles and fault systems of Luoyachushan-Dahongshan area in Beishan region of Gansu Province [in Chinese with English abstract]: Gansu Geology, v. 20, no. 1, p. 6–15.
Zuza, A.V., and Yin, A., 2017, Balkatach hypothesis: A new model for the evolution of the Pacific, Tethyan, and Paleo-Asian oceanic domains: Geosphere, v. 13, no. 5, p. 1664–1712, https://doi.org/10.1130/GES01463.1.
Zuza, A.V., Wu, C., Reith, R.C., Yin, A., Li, J.H., Zhang, J.Y., Zhang, Y.X., Wu, L., and Liu, W.C., 2018, Tectonic evolution of the Qilian Shan: An early Paleozoic orogen reactivated in the Cenozoic: Geological Society of America Bulletin, v. 130, no. 5-6, p. 881–925, https://doi.org/10.1130/B31721.1.
Zuza, A.V., Cheng, X., and Yin, A., 2016, Testing models of Tibetan Plateau formation with Cenozoic shortening estimates across the Qilian Shan–Nan Shan thrust belt: Geosphere, v. 12, no. 2, p. 501–532, https://doi.org/10.1130/GES01254.1.

Science Editor: Brad S. Singer
Associate Editor: Timothy Kusky

Manuscript Received 10 January 2022
Revised Manuscript Received 10 March 2022
Manuscript Accepted 2 April 2022

Printed in the USA